NOTICE

The quality of this microform is heavily dependent upon the quality of the original thesis submitted for microfilming. Every effort has been made to ensure the highest quality of reproduction possible.

If pages are missing, contact the university which granted the degree.

Some pages may have indistinct print especially if the original pages were typed with a poor typewriter ribbon or if the university sent us an inferior photocopy.

Reproduction in full or in part of this microform is governed by the Canadian Copyright Act, R.S.C. 1970, c. C-30, and subsequent amendments.

AVIS

La qualité de cette microforme dépend grandement de la qualité de la thèse soumise au microfilmage. Nous avons tout fait pour assurer une qualité supérieure de reproduction.

S'il manque des pages, veuillez communiquer avec l'université qui a conféré le grade.

La qualité d'impression de certaines pages peut laisser à désirer, surtout si les pages originales ont été dactylographiées à l'aide d'un ruban usé ou si l'université nous a fait parvenir une photocopie de qualité inférieure.

La reproduction, même partielle, de cette microforme est soumise à la Loi canadienne sur le droit d'auteur, SRC 1970, c. C-30, et ses amendements subséquents.

THE MECHANICAL BEHAVIOUR OF SOFT CLAYS UNDER VIBRATION LOADING FROM VEHICLE TRAFFIC

Mustafa Z. Emir

A Thesis
in
The Department of Civil Engineering

Presented in Partial Fulfillment of the Requirements
for the Degree of Doctor of Philosophy
at
Concordia University
Montreal, Quebec, Canada

April 1991

ISBN 0-315-68733-9

Canada

CONCORDIA UNIVERSITY

DIVISION OF GRADUATE STUDIES

This is to certify that the thesis prepared

By: MUSTAFA EMIR

Entitled: THE MECHANICAL BEHAVIOUR OF SOFT CLAYS UNDER VIBRATION LOADING FROM VEHICLE TRAFFIC

and submitted in partial fulfillment of the requirements for the degree of

Doctor of Philosophy (Civil Engineering)

complies with the regulations of the University and meets the accepted standards with respect to originality and quality.

Signed by the final examining committee:

Dr. M. Kusy — Chair and Associate Dean of Graduate Studies

Dr. G. Lefebvre — External Examiner

Dr. V. Ramachandran — External to Program

Dr. M.S. Troitsky — Examiner

Dr. S. Sarraf — Examiner

Dr. M.M. Douglass — Examiner

Dr. H.B. Poorooshasb — Thesis Co-Supervisor

Dr T. Adachi — Thesis Co-Supervisor

Approved by _____
Chair of Department or Graduate Program Director

July 30 1991

_____
Dean of Faculty

ABSTRACT

The Mechanical Behaviour of Soft Clays Under Vibration Loading from Vehicle Traffic

Mustafa Z. Emir, Ph. D.
Concordia University, 1991

The proliferation of land reclamation projects around the world has increased the need for advanced studies on the mechanical behavior of soft clays. One of the most important aspects of soft clay behaviour is the time dependent deformation characteristics.

The behavioral characteristics of soft clays suggest that an overstress type soil model is suitable for the analysis of such deposits. A model initially proposed by P. Perzyna has been extended with the addition of a Cam Clay type yield criterion and implemented in a finite element code to analyze geotechnical problems in two dimensions. In addition to describing the monotonic loading behavior, the model is used for the analysis of soft clays under vibrational loads from vehicle traffic.

In order to investigate the effects of vibrations on the rate dependent behaviour of soft clays, a new vibrational slump test has been devised. The results are used to explain the processes involved during the deformation of a clay sample under its own weight. It is seen that the variations of the parameters used in the soil model exhibit a marked resemblance to the variations of the fundamental material state variables such as the flow volume, activation energy, and entropy. In the light of this observation, the possible relationships between the material parameters used in the present viscoplasticity model and the thermodynamic variables from rate process theory are discussed.

The conclusions drawn from the vibrational slump test results as well as the careful examination of the constitutive model have been implemented in a Finite Element computer code. The predictive abilities of this program have been established by comparison with field measurements and the behavior of a soft clay foundation under the effect of surface vibrations is simulated. It is found that vehicle traffic during and after the construction of landfills (or embankments) noticeably retards the consolidation process and creates prolonged periods of quasi-undrained conditions.

"If a phenomenon admits of a complete mechanical explanation, it will admit of an infinity of others which will account equally well for all the peculiarities disclosed by experiment."

Poincaré

"If solid ground cannot be found, but the place proves to be nothing but a heap of loose earth to the very bottom, or a marsh, then it must be dug up and cleared out and set with piles made of charred alder or olive wood or oak, and these must be driven down by machinery, very closely together like bridge piles, and the intervals between them filled in with charcoal, and finally the foundations are to be laid on them in the most solid form of construction."

Vitruvius, Book III, Ch. IV

ACKNOWLEDGEMENTS

I would like to express my sincerest gratitude to my parents who have provided me with every imaginable tool in life. Without their foresight and love, none of this would have been possible.

Thanks to Dr. Hormoz Poorooshasb and Dr. Matthew Douglass for changing my life with their trust, guidance and leadership. Thanks also to Dr. Toshihisa Adachi who has enriched me with his insight and integrity. I am honored to have known them.

The financial support of the Natural Sciences and Engineering Research Council of Canada, the Ministry of Education of the Japanese Government, and of Concordia University are gratefully acknowledged. I am also thankful for the many facilities and resources offered to all Graduate Students by the Department of Civil Engineering at Concordia University.

TABLE OF CONTENTS

CHAPTER 3

CHAPTER 4

CHAPTER 5

CHAPTER 6

CHAPTER 7

LIST OF TABLES

LIST OF FIGURES

NOMENCLATURE

CHAPTER 2

c_u ..... undrained shear strength
e ..... voids ratio
ε_{11} ..... vertical strain
K_o ..... coefficient of earth pressure at rest
LI ..... liquidity index
OCR ..... over consolidation ratio
PI ..... plasticity index
σ'_{11} ..... vertical effective stress
σ'_m ..... mean effective stress
v ..... specific volume (v = 1+e)

CHAPTER 3

C^e_{ijkl} ..... elastic compliance tensor
C^{ep}_{ijkl} ..... elasto-plastic compliance tensor
C^p_{ijkl} ..... plastic compliance tensor
$d\varepsilon^e_{ij}$ ..... increment of elastic strain
$d\varepsilon_{ij}$ ..... increment of total strain
$d\varepsilon^p_{ij}$ ..... increment of plastic strain
df ..... total derivative of the yield function
δ_{ij} ..... Kronecker delta
$d\lambda$ ..... scalar of proportionality
$d\sigma'_{ij}$ ..... tensor of effective stress increment
ε_n ..... normal strain (= $\varepsilon_{ij}n_in_j$)
ε_{nt} ..... shear strain (= $\varepsilon_{ij}n_jt_i$)
$f(\sigma_{ij})$ ..... yield function
G ..... elastic shear modulus

g.....plastic potential function
G_{ij}.....a symmetric tensor
h.....hardening rule function
I_1.....first invariant of the stress tensor
I_2.....second invariant of the stress tensor
I_3.....third invariant of the stress tensor
J_1.....first invariant of the stress deviator tensor
J_2.....second invariant of the stress deviator tensor
J_3.....third invariant of the stress deviator tensor
K.....elastic bulk modulus
k.....hardening parameter
n_i..... unit normal to the plane
σ_1.....maximum principal stress
σ_2.....intermediate principal stress
σ_3.....minimum principal stress
σ_n..... ..... normal stress (= $\sigma_{ij} n_j n_i$)
s^2_n.....shear stress (= $T_i T_i - \sigma^2_n$)
s_{ij}.....stress deviator tensor
σ_{ij}.....stress tensor
T_i..... stress vector (= $\sigma_{ij} n_j$)
t_i..... tangent to the unit normal to the plane

CHAPTER 4

C..... value of σ'_m at $\eta^*=0$
δe..... increment of shear strain
du..... increment of pore water pressure
δv..... increment of volumetric strain
e..... voids ratio
ε_a ..... axial strain
e_a ..... voids ratio at $\sigma'_{me}=1$
e_{ij} ..... second invariant of the strain deviator tensor
ε^p_{ij} ..... plastic strain tensor
e^p_{ij} ..... second invariant of the plastic strain deviator tensor

ε_v ..... volumetric strain

Γ ..... value of v at $p'=1$

η^* ..... stress ratio

I_2 ..... second invariant of the increment of strain deviator tensor

I^p_2 ..... second invariant of the increment of plastic strain deviator tensor

J_2 ..... second invariant of the stress deviator tensor

κ ..... a soil parameter

λ ..... a soil parameter

M ..... a soil parameter

M^* ..... stress ratio at critical state

p' ..... $(\sigma'_1 + 2\,\sigma'_2)/3$

p'_e ..... mean effective stress

q ..... $\sigma'_1 - \sigma'_2$

σ'_1 ..... vertical effective stress (triaxial)

σ'_2 ..... confining effective stress (triaxial)

σ'_{ij} ..... total effective stress tensor

σ'_{me} ..... mean effective stress on the virgin compression line equivalent to the current specific volume

σ'_{my} ..... size of the current yield locus (hardening parameter)

s_{ij} ..... deviator stress tensor

u ..... pore water pressure

v ..... specific volume

W_{ex} ..... external work

W_{in} ..... internal work

ψ^* ..... ratio of plastic volumetric strain to plastic deviatoric strain

CHAPTER 5

$\mathcal{D}$ ..... plane *state* domain in (σ,ε)

de^e_{ij} ..... elastic deviatoric strain rate

de_{ij} ..... total deviatoric strain rate

de^{vp}_{ij} ..... viscoplastic deviatoric strain rate

δ_{ij} ..... Kronecker delta

E ..... Young's modulus

ε_{ij} ..... total strain tensor
ε^{vp}_{ij} ..... viscoplastic strain tensor
F ..... overstress function
f ..... yield function
$\Phi(F)$ ..... dynamic property function
f_d ..... dynamic yield function
f_s ..... static yield function
G ..... elastic shear modulus
γ ..... viscosity coefficient
η ..... viscosity coefficient
$\varphi(\sigma,\varepsilon)$ ..... material function
J_2 ..... second invariant of the deviatoric stress tensor
K ..... elastic bulk modulus
k ..... yield limit in shear
k_d ..... dynamic hardening parameter
k_{ij} ..... part of s_{ij} corresponding to plastic properties
k_s ..... static hardening parameter
Λ ..... scalar variable
s_{ij} ..... stress deviator tensor
σ_{ij} ..... total stress tensor
$\sigma_{ij\,y}$ ..... yield stress
$\psi(\sigma,\varepsilon)$ ..... material function

CHAPTER 6

α ..... constant describing the dilatation rate of the soil
C ..... rate dependent soil parameter
c_o ..... rate dependent soil parameter
δ ..... rate dependent soil parameter
δ_{ij} ..... Kronecker delta
e ..... voids ratio
ε_{ij} ..... total strain tensor
ε^{vp}_{ij} ..... viscoplastic strain tensor
$\Phi(F)$ ..... dynamic property function

f_d ..... dynamic yield function
f_s ..... static yield function
G ..... elastic shear modulus
γ ..... viscosity coefficient
η ..... stress ratio
J_2 ..... second invariant of the deviatoric stress tensor
K ..... elastic bulk modulus
κ ..... soil parameter
k_d ..... dynamic hardening parameter
k_s ..... static hardening parameter
λ ..... soil parameter
m' ..... rate dependent soil parameter
M^* ..... soil parameter
σ'_m ..... mean effective stress (first invariant of the effective stress tensor)
$\sigma'_{my\ (d)}$ ..... dynamic hardening parameter
$\sigma'_{my\ (s)}$ ..... static preconsolidation pressure
$\sigma'_{myi\ (s)}$ ..... rate dependent soil parameter
s_{ij} ..... stress deviator tensor
σ_{ij} ..... total stress tensor
ξ ..... rate dependent soil parameter

CHAPTER 7

A ..... a proportionality constant
β ..... flow volume
β/kT ..... stress factor
c ..... rate dependent soil parameter
de_{ij} ..... shear strain rate
ΔF ..... activation free enthalpy or bond energy
k ..... Boltzmann's constant (1.38×10^{-16} erg/^oK)
m' ..... rate dependent soil parameter
s_{ij} ..... deviatoric stress tensor
T ..... absolute temperature in ^oK

CHAPTER 9

c ..... rate dependent parameter
C ..... velocity of wave propagation
D_{ijkl} ..... tangential constitutive matrix
e ..... voids ratio
ε_{ij} ..... strain tensor
$f(\sigma,\varepsilon)$ ..... material function
G ..... elastic shear modulus
$g(\sigma,\varepsilon)$ ..... material function
g_i ..... acceleration component
J_2 ..... second invariant of the stress deviator tensor
κ ..... soil parameter
K_f ..... average bulk modulus of the fluid
k_{ij} ..... permeability tensor
K_s ..... average bulk modulus of solids
λ ..... soil parameter
λ_i ..... Eigenvalues
l_i ..... Eigenvectors
m' ..... rate dependent parameter
M^* ..... soil parameter
n ..... porosity
p ..... pore water pressure
p_o ..... preconsolidation pressure
ρ ..... density of the solid-fluid mixture
ρ_f ..... density of the fluid
σ'_{ij} ..... effective stress tensor
σ'_m ..... mean effective stress (first invariant of the stress tensor)
s_{ij} ..... stress deviator tensor
σ_{ij} ..... total stress tensor
u_i ..... average displacement of solids
w_i ..... average relative displacement of fluid
w_i/n ..... Pore fluid displacement

CHAPTER 10

B ..... strain-nodal displacement matrix
C' ..... volumetric strain-nodal displacement matrix
D ..... tangential material stiffness matrix
D^e ..... elastic tangential stiffness matrix
D^{vp} ..... viscoplastic tangential stiffness matrix
ε_{ij} ..... strain tensor
F ..... overstress function
F_b ..... body forces
γ_w ..... specific weight of water
I ..... identity matrix
K ..... global system stiffness matrix
k_h ..... horizontal coefficient of permeability
k_v ..... vertical coefficient of permeability
N ..... displacement interpolation functions
v_n ..... flow velocity
σ ..... stress matrix
σ'_{ij} ..... effective stress tensor
T ..... applied surface load
u ..... displacement
u_w ..... pore pressure

CHAPTER 1 : INTRODUCTION

1.1. Objective

The objective of the present research project has been the study of the mechanical behavior of very soft clays under vibration loads from vehicle traffic or machinery and to propose an analytical method whereby settlements, lateral deformations, and pore water pressure developments can be predicted. The mechanism by which surface vibrations cause a pore water pressure build-up in soft clay deposits is also studied in the light of the physical processes described by internal state variables.

1.2. Rationale

Soft and very soft clays are generally classified by Engineers as difficult or problematic soils. Highly plastic and sometimes sensitive, soft clays are also susceptible to creep deformations. Although this in itself would imply long term consequences, the problems associated with soft clays commonly arise during or shortly after construction. It is therefore worthwhile to consider the influence of time dependent mechanical characteristics of soft clay masses on the short term stability of foundations. From the point of view of settlements, loading of soft clays usually results in excessive horizontal displacements, indicating the retardation of the consolidation process. In this sense, the lateral flow of a soft clay deposit is a manifestation of this so called retardation, which is itself a consequence of the time dependency of the soil's mechanical behavior.

1.3. Relevance

The understanding of soft clay behavior is the keystone for the success of land reclamation projects and their subsequent development. The former will require the realization of short term stability, and the latter, the prediction of long term settlements.

1.4. Building on Soft Clay

The main driving force behind soft clay research, I think, is economics. Most major population centers in South East Asia are built on soft alluvial clay deposits. Due to rapid economic growth, these cities are fast becoming sprawling mega-cities, thus increasing the demand for real estate. Another common point between South East Asian cities is that their geography dictates the direction of their growth, hence making land reclamation from the sea a viable means of creating real estate for expanding businesses. Thus, a need to establish a rational basis for the mechanical behavior of soft clays under various loading conditions is very much warranted by the increasing number of constructions on soft clay deposits.

1.4.1. Asia

Bangkok, home for almost 6 million residents, is underlain by a thick layer of leached marine deposit with high compressibility and low shear strength. The layer extends deep into the country and is commonly known as Bangkok Clay or Chao Playa Clay. The city itself is currently growing at an alarming rate and the problem of excessive pumping of ground water has been added to the list of foundation problems in the area. Differential settlements of buildings and pavements are common to the area and the home of the Asian Institute of Technology is subsiding at a rate of almost 6.0 cm/year, rivalling Venice in this category.

The southern coast of Singapore is underlain by a soft marine clay up to 40 m. in depth. The deposit called the Kallang formation extends out into the shallow waters off the coast as well as inland, covering an area including the city and the swamp land surrounding it. The Changi International Airport has recently been expanded by reclaiming a surface of 700 ha. from the sea. The fill is composed of dredged marine clay and currently supports a runway and terminal buildings.

Taipei is another city battling with congestion and over population. In its efforts to relieve the metropolitan area, the city is considering the rezoning of surrounding agricultural land for industrial development. This area had once

been covered by marshlands and therefore is likely to be underlain by a soft clay layer and create foundation problems in the future.

The west coast of Hong Kong and Macau are built on thick alluvial clay deposits. It is a well known fact that much of what is flat in Hong Kong is reclaimed land. This practice has been an integral part of the city's booming economy and some of the world's most notable (not to mention costly) high rises have been built on reclaimed land. Despite the wide spread use of end-tipping to fill the sea in Hong Kong, the process seems to have left the greater part of the fills still underlain by very soft marine clays. To prevent the excessive settlements due to the consolidation of this layer, the use of deep piles has become routine but the method is not always effective. Reclamation has not stopped in Hong Kong, despite the imminent transfer of the city to Chinese authority. Pending approval from the Chinese Government, The Hong Kong Airport will undergo expansion towards the sea (it is already on a parcel of landfill) in order to accommodate increased travel volumes.

Other Asian cities built on soft alluvial clay deposits include Jakarta, Rangoon, Ho Chi Minh City, Seoul, Manila, and Bombay to name a few. Layers of soft marine clays are also found in the Gulf of Kutch, Gulf of Cambay in India, the Malaysian Peninsula, and mainland China under the cities such as Lianyungang, Tianjin and Shanghai.

1.4.2. Other Areas of the World

In general, soft clays are found in the deltaic regions of the rivers Nile, Euphrates, Tigris, Rhine, Elbe, and Mississippi. More specifically, soft clays are most common in the Nordic countries (except Denmark), Eastern Canada (Champlain Clays), and Northern United States (Chicago Clay, Boston Blue Clay). Almost a quarter of Norway is covered by late glacial marine clays of high sensitivity. The Swedish soft clays are of glacial and Quaternary origin and vary in sensitivity from 10 around the Göthenburg area to 400 in some areas along the Göta River [Flodin & Broms (1981)]. Various organic, silty soft clays are found in Northern Germany. This soil is characterized by its secondary compression exhibiting settlements for decades after the application of overburden loads. Canadian Champlain clays are of Pleistocene origin and are similar to Norwegian clays.

They cover most of the banks of the rivers St. Laurent, Ottawa, and Saguenay as well as the Lac St. Jean area (Leda Clay) [Kenney (1964)].

Finally, one must also consider Mexico City Clay although this is not a clay in the mineralogical sense since it is of volcanic origin. The behavior of this material warrants its name since it characteristically shows a high voids ratio, high in-situ water content and high compressibility.

1.4.3. Japan

In Japan, the advent of vast land reclamation projects necessitated the construction of large earthworks on soft marine clays (alluvial clays). Man made islands have been built in Tokyo Bay, Osaka Bay, Kobe port, Hiroshima and most other population centers. The fact that most of these islands support important installations (airports, ports, power plants etc.) has necessitated the research programmes undertaken by the Japanese academic and industrial circles.

Most of coastal Japan is covered with normally consolidated and lightly over consolidated soft clays. The following examples from some urban centers are important in showing the economic and social impact of land reclamation projects in Japan.

The filling of the Tokyo Bay has been underway since early 18th century and most of the city's numerous down-town areas are built on what once was the sea bottom. In addition to the land designated for residential and industrial purposes, most of the port facilities are also built on man made islands. The city of Kawasaki (also in Tokyo Bay) also has had its share of reclamations. Ohgishima Island, facing Kawasaki has been built in the early 70's by a sandy fill (from Futtsu across the Bay) on the marine alluvial clays.

Osaka, Japan's second most densely populated metropolitan center has a parallel history. The city itself has been marching towards the sea over the last 200 years and Osaka Bay is literally dotted with near shore man made islands such as the ports of Hannan, Sempoku, Sakai, Osaka, Amagasaki, Nishinomiya and Kobe. The Osaka South Port Island is zoned for wharves, residential, commercial and recreational purposes. The island has been filled with dredged clay. Kobe Port

island, started in 1966 has been filled with weathered granite called Masa soil. Among other urban uses, it houses a 12 storey hospital. Other notable reclamations include Rokko Island, the Koshien reclamation, and Osaka-Nanko Islands.

Another important land development project has been undertaken in Hiroshima. In addition to residential and commercial areas, the Port of Hiroshima and Hiroshima Airport are built on reclaimed land, not without extensive ecological damage to valuable coral reefs in the Hiroshima Bay. A similar situation exists in the island of Okinawa where Nakasugu Bay harbor reclamation project has been going on since about the mid fifties.

Perhaps the most important current project in Japan is the construction of the ambitious Kansai International Airport. Built in Osaka Bay, the Airport consists of a rectangular island (1.25 km. by 4.35 km.) built over soft marine clays extending to depths up to 20 m. The project exemplifies the state of the art in the analysis and construction methods in Japan since the soil conditions under Osaka Bay are typical of the majority of soft marine clays in the country. It has therefore had the effect of refocusing the attention of researchers and developers on the importance of understanding the mechanical behavior of soft clays.

From a construction perspective, the project has shown a very bold soil improvement program which consists of the installation of vertical sand drains (1.5 m. in diameter) with a spacing of 2.0 m. along the short direction and 3.0 m. along the longer direction. Due to the sheer weight of the structure, the effect of the deformation of deep diluvial clays was necessarily considered and included in the predictions of final settlements.

This thesis has been inspired by a land reclamation project in Japan. The example which has been used as a starting block is a reclamation site in Yorishima (Kasaoka City, Okayama Prefecture). The construction was started in 1984 and completed in 1987. The area reclaimed is roughly 500 m^2 and the land is scheduled to house a power plant after sufficient self weight consolidation has taken place.

The landfill area is subdivided into five zones, separated by steel sheet piles. The drainage of the landfill was regulated by a system of channels among these five sections, the water being discharged to the sea. Due to human error in controlling water levels at the two sides of each sheet pile, a section of the sheet pile collapsed early in 1987. During the repair works, the sheet pile was driven deeper and the soil in the immediate vicinity was replaced by quality granular mountain soil. It was also deemed useful to install inclinometers along the sheet piles to monitor lateral flow of the fill. It was observed that lateral deformations continued to increase well after the end of construction. The short term stability of the fill was thus threatened quite unexpectedly since no surcharge load was applied on the fill. Upon further consideration however, the contractor deduced that the pore pressure increase could be related to the number of dump trucks used in the reconstruction process. Indeed, the horizontal displacements at the face of the sheet pile follow closely the cumulative number of trucks travelling in the vicinity of the measurement devices. It was also apparent that the weight of the trucks alone (25.4 t.) could not account for the observed lateral flow. It was then deemed necessary to evaluate the vibratory nature of the loading imposed on the fill. Extensive in situ tests have been carried out by monitoring pore pressures and displacements while running a fully loaded truck in the vicinity of the sheet piles. The data shows a marked correlation between pore pressures and horizontal displacements and the number of truck passages. The dominant frequency of the induced vibration is 3 Hz. and the accelerations are between 0.1 to 0.4 g. More detailed information on the site is given in Chapter 10.

1.5. Conclusion

In view of the relative importance of soft clay behavior understanding, the thesis will present the argument that the susceptibility of soft clays to major horizontal displacements is inherently connected with the strain rate (i.e., time) dependence of their mechanical behavior, and as such can be properly described by an elasto-viscoplastic constitutive model. The following chapters will further provide anlytical and numerical evidence to support this argument.

CHAPTER 2 : CHARACTERISTICS OF SOFT CLAYS

2.1. Preliminaries

Soft clays have relatively low permeability and an undrained shear strength (c_u) of less than 50.0 kPa. Within the context of this thesis, the term soft clay describes those clays having an undrained shear strength of less than 25 kPa. These clays are relatively recent (within the last 10 000 years or between 10 000 and 12 000 years ago) alluvial deposits. Where they are found, the ground surface will be more or less featureless and rather flat. Although they are usually classified as normally consolidated with overburden stresses in the order of 100-150 kPa. they nevertheless exhibit the behavioral characteristics of light overconsolidation, with an overconsolidation ratio up to 1.2 . This is partly due to the susceptibility of soft clays to ageing [Bjerrum (1972) & (1967)] in the form of weathering (due to environmental agents), desiccation (due to natural or imposed fluctuations of the ground water level), cementation, and leaching (both due to chemical processes). The sedimentation as well as the sum total of the post depositional processes determine the micro-structure of the clay and therefore govern its mechanical behavior. For example, aged clays will usually show increased preconsolidation pressures and undrained shear strengths [Brenner et al. (1981)]. Not withstanding this fact, the focus of this thesis is on the rate dependent behavior of normally consolidated soft clays and the sedimentation and ageing effects will not be further considered. In addition, the aforementioned light overconsolidation is usually confined to the surface of the soil where the Engineer's interest is limited.

2.2. Mineral and Structural Composition of Soft Clays

The mathematical modeling of soils involves the description of physical phenomena by means of a number of variables that can be realistically measured in order to verify the validity of such models. As far as the material itself is concerned however, the model is purely an abstraction. It is therefore essential that the actual physical structure and composition of the soil in question be thoroughly understood.

Clays are made up of crystalline minerals consisting of hydrous aluminum silicates. The aluminum positions are sometimes occupied by iron or magnesium. The sizes of the crystals vary between 0.05μ (Kaolinite) to 10μ (Illite). The crystals are bonded together in sheets (tetrahedral or octahedral) with repeating atomic structure. The various arrangements of these sheets and the metallic ions present result in various clay minerals [Christoulas et al. (1987)]. The chemical make up of clays govern the observable mechanical response [Mitchell (1976)].

The clay sheets or flakes are usually found to be in clusters formed by a number of smaller groups of particles [Yong et al. (1973), Pusch (1973), Collins et al. (1974)]. This is referred to as structure and conceivably reflects the most elementary properties of the clay mass and governs its mechanical response. If this argument is accepted, the description of conventional stress-strain behavior can then be founded on a physical basis whereby the full effect of the structure of the material with its related implications (elasticity, plasticity, hardening, softening, creep, and others) will be possible.

2.3. Overall Behavior of Soft Clays

The deformation behavior of soft clay is non-linear, anisotropic, rate dependent, and vary with stress or strain level. The most relevant soil parameters for soft clay are compressibility, permeability, strength, and stiffness. The long term response of a soft clay of a given structure and chemical composition will depend on the strain (or stress) state, the strain (or stress) history, time (or strain rate) history, and the direction and magnitude of the imposed stress (or strain) increment. The strength of a soft clay on the other hand, is mainly a function of the drainage conditions. The undrained strength of a soft clay foundation is likely to be lower than the drained strength. Thus, for stability analyses, clear distinctions must be made between undrained (i.e., during and immediately after construction), drained (i.e., at the end of consolidation) and especially partially drained conditions (i.e., during consolidation). Soft clays are also particularly susceptible to creep strains which may pose long term stability and settlement problems.

2.4. *Essentials in Soft Clay Behavior Description*

The mechanical behavior of soft clays may be studied from different view points, including shear strength, deformation, rheological properties, consolidation, microscopic structure of soil skeleton, etc. In the most general instance, the mechanical state of a soil element might be represented by a constitutive equation, giving a surface in the space defined by stress, strain, time, and temperature. The points obtained by means of the constitutive equation are called state points and the space defined by the variables of this equation is called the state space. A transition in the mechanical state is described by a locus of state space and this locus is called the state path.

2.5. *Characterization Parameters*

The parameters defining the compressibility and swelling of clays can be grouped as follows: strain measures are the rate of change of voids ratio e (it should be noted that this is an incomplete measure of strain), vertical strain (ε_{11}), and specific volume ($v = 1+e$) as well as stress measures are the vertical effective stress (σ'_{11}) and the mean effective stress (σ'_m) which requires the definition of the horizontal effective stress. The list of compressibility and swelling parameters is given in Table 2.1.

Among the parameters generally used to describe the clay soils, perhaps the most elementary are the Atterberg Limits. Although the effects of soil structure and composition on the mechanical properties of softer clays (i.e., higher plasticity clays) are not necessarily reflected in the changes in Atterberg Limits there is a considerable wealth of correlation studies between the Limits and other strength parameters. For example, in the case of relatively homogeneous clays the plasticity index (PI) is usually sufficient for a useful description, namely through C_c, the compression index [Mayne & Kulhawy (1982), Wroth (1979)] or through the effects of the PI on the shape of (e-log σ'_{11}) plots. It is seen that with increasing plasticity the non-linearity of the (e-log σ'_{11}) relationship becomes more pronounced. The compressibility and the equilibrium voids ratio also increase with increasing plasticity index [Lambe & Whitman (1969)]. Another generally observed relationship is the reduction of the effective shearing

resistance and the related reduction in the value of K_o with higher values of PI [Christoulas et al. (1987)].

Table 2.1: Clay Compressibility and Swelling Parameters

Parameter	Name	Description
a_v	Coefficient of compressibility	$-de/d\sigma'_{11}$ from a plot of vertical effective stress vs. voids ratio
m_v	Coefficient of volume reduction	$d\sigma'_{11}/d\varepsilon_{11}$ from a plot of vertical effective stress vs. vertical strain
C_c	Compression index	$-de/d(\log \sigma'_{11})$ from the loading portion of a plot of $\log \sigma'_{11}$ vs. e
C_s	Swelling index	$de/d(\log \sigma'_{11})$ from the unloading portion of a plot of $\log \sigma'_{11}$ vs. e
λ	Slope of the virgin compression line	$-dv/d(\log \sigma'_m)$ from the loading portion of a plot of $\log \sigma'_m$ vs. v
κ	Slope of the swelling line	$dv/d(\log \sigma'_m)$ from the unloading portion of a plot of $\log \sigma'_m$ vs. v
C_R	Virgin compression ratio	$d\varepsilon_{11}/d(\log \sigma'_{11})$ from the loading portion of a plot of $\log \sigma'_{11}$ vs. ε_{11}
S_R	Swelling ratio	$d\varepsilon_{11}/d(\log \sigma'_{11})$ from the unloading portion of a plot of $\log \sigma'_{11}$ vs. ε_{11}

There is also evidence that the liquidity index (LI) correlates with c_u [Skempton & Northey (1952), Mitchell (1976), Wroth & Wood (1978)] and the liquidity index versus overburden pressure plots give an impression of post depositional effects: once the curves for young clays are established, deviations from these can be

interpreted as ageing effects. Most young marine clays in situ and at moderate depths can be expected to have LI between 1 and 1.75 and decreasing with depth [Skempton (1970), Locat & Lefebvre (1985)]. The LI is also a fairly effective normalizing factor in plots of (e-log σ'_v): when the voids ratio is replaced by LI, a considerable portion of scatter can be eliminated.

2.6. Consolidation Behavior of Soft Clays

Soft clays exhibit rather unique consolidation patterns which must be specifically addressed in a comprehensive analysis. First, the classical assumption of initial magnitude and distribution of excess pore pressures must be revised to take into account the lag of pressure transfer due to the time dependent nature of soft clays. Such a revision is also essential in understanding the continuing pore pressure generation after the completion of loading, differences between field consolidation rates and laboratory consolidation rates and the changes in the rate of pore pressure dissipation during and following loading.

Even under K_o loading (typical K_o values vary between 0.5 to 1.2 [Tavenas et al. (1975), Massarsch et al. (1975)]), the dissipation of excess pressures does not occur over the full height of the clay deposit until a considerable time after the start of consolidation and although consolidation is fairly rapid in the vicinity of the drainage boundaries. The overall consolidation slows down with time as well as increasing excess overburden pressures. The evolution of the consolidation phenomena is such that the dissipation times are much shorter (faster consolidation) when the overburden pressure is lower than the preconsolidation pressure. It is important to note that the considerably slower consolidation rates under stresses exceeding the preconsolidation stress are not equivalent to the classical secondary consolidation process. The changes, however small, in the void ratio during consolidation still depend on the magnitude of the excess overburden stress increment and the duration of the process is a function of the drainage conditions. In this sense, even for very slow consolidation rates, it is assumed that primary consolidation continues as opposed to secondary compression which is characterized by similar rates but is the result of an entirely different process associated with creep deformations. The striking similarities between the later stages of the primary consolidation (mainly a plastic

deformation process for stresses exceeding the preconsolidation pressure) and the conventional idea of secondary compression (mainly a viscoplastic process under constant effective stress) is perhaps the most convincing argument for the necessity to consider these two types of behavior simultaneously.

2.7. Undrained Compression Behavior of Normally Consolidated Soft Clays

Plots of axial strain vs. axial effective stress will help demonstrate the following salient compressibility features of soft clays : first, the preconsolidation pressure is well defined with a relatively stiff response (generally non linear elastic) prior to it and a progressively increasing compressibility (strain hardening plastic) afterwards. Second, higher plasticity clays will have higher strains when they reach their preconsolidation pressures and will show a more subtle change in compressibility at this stage [Leroueil et al. (1985), Lacasse et al. (1985)].

In undrained triaxial compression, the peak undrained compressive strength is observed at a relatively low axial strain. This strength may be much higher than the ultimate undrained compressive strength mobilized at large strains: this fact is described as undrained brittleness.

It has been already stated that most soft clays actually show the behavioral characteristics (due to post depositional effects) of slightly overconsolidated clays. In this respect, the overall compressibility patterns of clays with low overconsolidation ratios (OCRs) is of interest. In undrained triaxial compression, low OCR clays are brittle and hence the similarities with normally consolidated soft clays. The brittleness decreases with higher OCR and peak strengths are mobilized at lower effective stresses than ultimate strengths.

2.8. Time and Path Dependence of Soft Clay

The rate dependency of clay is due to the time required for the rearrangement of clay particles to attain an equilibrium state following changes in external agents. One can intuitively deduce that faster shearing rates will produce stiffer responses just as a pool of water becomes a stiffer medium for a diver jumping

from increasing heights. The tendency of the stiffening of the undrained response with increasing rate of shear may in fact be due to the generation of pore pressures during the pre-yield portion of the stress-strain curve [Casagrande (1949), Casagrande & Wilson (1951), Bishop & Henkel (1962), Richardson & Whitman (1963), Eide (1967)].

There is a marked increase of peak strength with increasing rate of shear although the ultimate strength is not much affected by it. Strains to mobilize the peak strength do not appear to be affected by the rate of shear at low OCR however these strains decrease with increasing rates of shear at higher values of OCR [Hight et al. (1985)].

Another observed rate effect is due to the fact that the in situ behavior of soils depends on stress rates while most laboratory tests are conducted by controlling the strain rates. Strain rates continuously increase during constant stress rate loading and close to the failure, a small increase in the loading rate will cause a smaller increase in the strain rate, this is in direct contrast to the failure of a strain rate controlled specimen: stress controlled tests lead to higher peak strengths and lower ultimate strengths compared to strain controlled tests.

The effective stress paths in ordinary undrained shear tests on normally consolidated clays are also affected by strain rates. The equi-maximum principal strain lines obtained on effective stress paths corresponding to two different constant strain rate tests are found to be parallel to the maximum principal stress axis. It is also found that the deviatoric stress increases proportionally with the logarithm of strain rate. No obvious strain rate effect on the excess pore pressure is observed. This may mean that the pore water pressure is a function of strain state and not of the strain rate. Evidence for this argument can be found in undrained relaxation tests where excess pore pressure remains constant [Adachi & Okano (1974)].

In the discussion of strain rate dependence, one must include the creep behavior of soft clays. The nature of creep is such that strain rates change rapidly with time after the start of creep, leading to changes in the effective stress and the structure of the soil. Effective stresses themselves play a major role in the development of creep. While at any given stress the creep strain rate decreases

regularly with time, it is not uncommon that high plasticity clays return to undrained conditions well after the consolidation process has stopped [Leonards (1979)]. It is not difficult to visiualize that the increased compressibility accompanying the onset of pronounced creep deformations could result in pore pressure buildup in the clay mass. The corresponding reduction in the effective stresses are now due to the progressive softening of the soil; the end result is still a danger of undrained failure, this time long after the end of primary consolidation. The proper evaluation of the yield states by considering strain rate effects is obviously crucial if one is to keep the stress state within the yield surface to prevent undrained softening behavior [Tavenas & Leroueil (1977)].

The mechanical behavior of clay is governed by the rearrangement of particles due to external agencies, therefore it is not only dependent on the present state but also on state history (i.e. state path). The mechanical behavior therefore depends on the stress and/or strain history. As a result, the behavior of clay under shear with smoothly and monotonically increasing shear strain is different from its behavior under shear with cyclic shear strain. Dependency on state history and dependency on strain history are equivalent terms in the case of stable (normally consolidated) clays but not in the case of unstable (overconsolidated) clays where strain softening is observed.

2.9. Permeability of Soft Clays

Darcy's law and permeability are important aspects of the mechanical behavior of soft clays however the validity of Darcy's law is not to be taken for granted in the case of soft and very soft clays. It is conceivable that there be a specific hydraulic gradient below which the flow of the pore water cannot occur [Blümel & Tamminga (1987)]. It is then concluded that the permeability should be a function of the pressure gradient in which case Darcy's law is no longer valid. For naturally occurring soft clays, Darcy's law has been found to be valid for all non zero hydraulic gradients [Tavenas et al. (1983)].

There is considerably more agreement on the dependence of the coefficient of permeability k on the voids ratio. The relationship of (e-log k) is more or less linear even in the case of very soft clays with high voids ratios [Been & Sills

(1981)] or soils with high organic content [Lefebvre et al. (1984)]. During virgin consolidation the voids ratio (e), the coefficient of permeability (k), and the coefficient of volume compressibility (m_v) all decrease. Consequently, during this stage, the coefficient of consolidation c_v is basically constant. Upon reaching the preconsolidation pressure, there is a marked reduction in c_v [Christoulas et al. (1987)].

2.10. Conclusion

• Soft clays have relatively low permeability and an undrained shear strength (c_u) of less than 50.0 kPa. Within the context of this thesis, the term soft clay describes those clays having an undrained shear strength of less than 25 kPa.

• The behavior of soft clay is non-linear, anisotropic, rate dependent, and vary with stress or strain level. The most relevant soil parameters for soft clay are compressibility, permeability, strength, and stiffness. Soft clays are also particularly suceptible to creep strains which may pose long term stability and settlement problems.

• The consolidation of soft clays is characterized by continuing pore pressure generation after the completion of loading, differences between field consolidation rates and laboratory consolidation rates and the changes in the rate of pore pressure dissipation during and following loading.

• There is a marked increase of peak strength with increasing rate of shear although the ultimate strength is not much affected by it.

• Time and rate dependency of clay is due to the time required for the rearrangement of clay particles to attain an equilibrium state following changes in external agents.

• The coefficient of permeability is a function of the voids ratio, hence the stress or strain state.

CHAPTER 3 : THE CLASSICAL THEORY OF PLASTICITY

3.1. Basic Definitions

The origin of the word plastic appears to be the Greek word for clay, *pelos*. Ancient Greeks called the ability of clays to retain their deformed shapes *plasticotis*. The current use of the term plasticity was probably coined in the late 19th century however the rational theoretical description of permanent deformations was not accomplished until the middle of 20th century.

The normal and shearing components of the stress vector T_i on a plane n_i are given by Cauchy's formulas:

$T_i = \sigma_{ij} n_j$	stress vector
$\sigma_n = \sigma_{ij} n_j n_i$	normal stress
$s^2_n = T_i T_i - \sigma^2_n$	shear stress

In the above, σ_{ij} represents the stress tensor and the vector n_i is the unit normal to the plane under consideration. The vector obtained through the multiplication of the stress tensor and the unit normal is co-directional with the unit vector. The three solutions to the characteristic equation of a tensor of second order are called *invariants;* the stress and strain invariants are almost always used in the formulation of plasticity theory in particular and continuum mechanics in general. The stress deviation tensor is obtained by subtracting the 1st invariant of the stress tensor from the stress tensor. This operation does not affect the principal directions and consequently the stress deviation and the stress tensors are co-axial. The invariants of the stress deviation tensor are the solutions to its characteristic equation (see Table 3.1 for definitions).

The three dimensional space formed by the three principal stresses is called the *Haigh-Westergaard space*. In this space, the plane which is normal to the space diagonal ($\sigma_1 + \sigma_2 + \sigma_3$ = constant) is called the *octahedral plane.*

The Cauchy formulas for strain define the sum of all changes in elemental lengths in all directions. For any line element in any direction n_i having the normal strain ε_n (along n_i) and shear strain ε_{nt} (along t_i perpendicular to n_i) these equations are:

$$\varepsilon_n = \varepsilon_{ij} n_i n_j$$

$$\varepsilon_{nt} = \varepsilon_{ij} n_j t_i$$

Perhaps the most important theoretical concept in classical plasticity is the coincidence of axes of strain rate and of stress (in elasticity theory, the axes of strain rate and stress rate are coincident).

Table 3.1. Invariants of stress and stress deviation

Invariants of the stress tensor	Invariants of the stress deviation tensor
$I_1 = \sigma_{ii}$	$J_1 = 0$
$I_2 = (\sigma_{ij}\sigma_{ij} - \sigma_{ii}\sigma_{jj})/2$	$J_2 = s_{ij}s_{ij}$ (*)
$I_3 = (\varepsilon_{ijk}\varepsilon_{pqr}\sigma_{ip}\sigma_{jq}\sigma_{kr})/6$	$J_3 = s_{ij}s_{jk}s_{ki}$

(*) the deviatoric stress $s_{ij} = \sigma_{ij} - (\sigma_{kk}\delta_{ij})/3$

A law defining the limit of elasticity under general stress states is defined as a *yield condition.* If various combinations of stress components are plotted together, all stress states lie on a yield curve and all stress states at failure lie on a failure envelope. The failure envelope may or may not be geometrically similar to the yield curve. A yield surface separates states of stress which cause only elastic strains from states of stress which cause both elastic and plastic strains. The yield criterion is expressed as a function of stresses or stress invariants (see Table 3.2. for examples of yield criteria).

Only functions symmetrical in the three principal stresses are permissible as yield functions. A material can obviously have different yield stresses in compression and extension: this is called the *Bauschinger effect.* If the yield criterion is a function of the third stress invariant, the sign will change between compression and tension. Therefore the yield function must be an even function of the third stress invariant. If yielding is independent of the hydrostatic

pressure, as in the case of most metals, the yield surface must be perpendicular to the space diagonal. For soils, since the hydrostatic pressure results in plastic strains (volumetric) the yield surface is shaped like a cap [Drucker et al. (1957)]. If the Bauschinger effect is not considered, the yield stress will be the same in compression and extension. In this case, the yield locus described by the yield surface must be symmetric about the origin (the space diagonal), i.e., about the principal stress axes. In soils, the yield strength is found to be a function of spherical pressure and specific volume. Therefore a major change of yield strength is to be expected on reversal of stress.

A *loading function* f is defined as a function $f(\sigma_{ij})=k$ such that further plastic deformation takes place only for $f(\sigma_{ij}) > k$. Both f and k may depend on the existing state of stress and on strain history. In the theory of classical plasticity, the material behavior is fully elastic until an initial yield surface is reached. A *loading* process is said to have taken place if the stress point moves outside the current yield surface, thus creating a new yield surface. A *neutral loading* process is one in which any movement of the stress state point does not result in plastic deformations; this is possible when the stress point travels along the yield curve. An *unloading* process occurs when the stress point moves inside the current yield surface. Deformations associated with this process are wholly elastic and the theory of plasticity no longer applies.

For elastic-perfectly plastic bodies (i.e., $f(\sigma_{ij})=0$), the elastic constants are assumed to be retained after plastic deformations. These constants must be defined with respect to the current shape of the element. An element recovers its initial shape when reloaded along the same load path to the initial state of stress.

Table 3.2. Examples of Yield Criteria

Theory	Criteria
Rankine	Yielding will occur when one of the principal stresses reaches the yield stress in tension or compression
Saint Venant	Yielding will occur when the maximum principal strain reaches the yield strain in simple tension or compression

Tresca[1] - Coulomb	Yielding will occur when the maximum shear stress reaches the value of the yield shear stress occurring under pure shear.
Beltrami	Yielding will occur when the total strain energy per unit volume equals the total strain energy per unit volume at yielding in uniaxial tension or compression.
von Mises[2]	Yielding begins when the distortion energy equals the distortion energy at yield in simple tension.
Mohr - Coulomb[3]	Yielding will occur for those states of stress for which the largest of the Mohr's circles is tangent to the failure envelope.

(1) The effect of the mean stress on the failure surface is not considered in this model. In soil mechanics, the Tresca condition is suitable for total stress analysis of undrained saturated soils.

(2) In soil mechanics, the von Mises model suffers from the same limitations as the Tresca criterion. While the Tresca theory assumes that the intermediate stress has no effect on yielding the von Mises theory gives all three principal stresses equal importance.

(3) The assumption in the Mohr-Coulomb theory [Bishop (1966)] is that the critical shear stress is not necessarily equal to the maximum shear stress but depends also on the normal stress acting on the shearing plane. In general the greater the normal stress, the lower is the critical shear stress. The limitations of the model include (i) a constant angle of internal friction, (ii) a disregard for the intermediate principal stress, (iii) the existence of corners on the yield surface in three dimensions. In a special case of Mohr theory (Internal friction theory), the critical shear stress is assumed to be a linear function of the normal stress acting on the plane of maximum shear.

3.2. A Historical Perspective on Plastic Analyses

Since Hooke's Law was put to practical use in the analysis and design of cast iron structures, notably by great engineers such as Eiffel, the theory of elasticity had been the dominating tool in engineering. As plasticity concepts became more widely known, solutions for the ultimate failure of systems were obtained. The two (i.e., equilibrium and stability solutions) did not come to be united in progressive failure solutions until relatively recently. Furthermore, in the case of applications to soil mechanics this seems to have taken even longer [Drucker & Prager (1952)]. This seems rather ironic considering the fact that on of the earliest works on plasticity was conducted by Coulomb (1773) in the context of soil mechanics. The Coulomb criterion was interpreted as an extended Tresca condition [Drucker (1953)] as well as an extended von Mises condition [Drucker & Prager (1952)]. The introduction of work hardening plasticity models to soil

mechanics occurred in 1957 [Drucker et al. (1957)]. The work hardening cap and the use of the volumetric plastic strain of the soil as a state variable describing the hardening state were introduced in this paper. It is not difficult to see that these ideas have found their analogies in the works of the late Prof. Roscoe and the entire series of Cambridge constitutive models.

3.3. Incremental Equations of Classical Plasticity

The term incremental is used here to differentiate the approach from the deformation theories of plasticity. While the former describes a relationship between plastic strain rate and stress state or stress rate, the latter assumes a one-to-one relationship between states of stress and states of strain. It should be noted that the deformation theory of plasticity is seldom used because it is only applicable to a restricted number of stress paths.

The rigorous derivation of the incremental equations of classical plasticity is possible through the following basic assumptions: (i) there exists a yield surface which is associated with the yield limit at any state of stress reached from any stress path. In the stress space, plastic strains occur for all outward probing stress increments. Inside the yield surface, the behavior is elastic; (ii) there is a linear relationship between incremental stresses and incremental plastic strain. The equations must also satisfy the following conditions: (i) *continuity* which requires that neutral loading does not cause plastic deformations; (ii) *uniqueness* which requires that at any state of stress, the increments of stress produce a unique increment of strain; (iii) *irreversibility* which requires that the work done on the plastic displacements are non negative; (iv) *consistency* which requires that the yield criterion is satisfied as long as the state is plastic.

The co-axiality of principle axes of stress and strain are expressed by either the Lévy-Mises or Prandtl-Reuss equations. While the former describes large plastic flows, outside the elastoplastic domain, the latter describes the relationship between the ratios of plastic strain increments in different directions. The increments of plastic strain depend on the current values of the deviatoric stress state, not on the stress increment required to reach this state; to determine the actual magnitudes of the increments, a yield criterion is necessary.

$d\varepsilon_{ij} = d\lambda\, s_{ij}$ Lévy - Mises

$d\varepsilon^{p}_{ij} = d\lambda s_{ij}$ Prandtl - Reuss

s_{ij} is the stress deviator tensor

$d\lambda$ is a non-negative scalar of proportionality varying throughout the loading history.

3.4. General Stress-Strain Equations in Classical Plasticity

Three assumptions are sufficient for the derivation of the general incremental plasticity equations [Yang et al. (1987)]: (i) the total strain increment can be decomposed into its elastic and plastic parts; (ii) a scalar yield function exists complying with the requirements stated earlier; (iii) the dissipated of the mechanical energy is non negative (irreversibility).

The total strain increment is given as

$$d\varepsilon_{ij} = d\varepsilon^{e}_{ij} + d\varepsilon^{p}_{ij} \tag{1}$$

The elastic response of the material is governed by the generalized Hooke's law such that

$$d\varepsilon^{e}_{ij} = C^{e}_{ijkl}\, d\sigma'_{kl} \tag{2}$$

for isotropic materials this relationship becomes

$$d\varepsilon^{e}_{ij} = \frac{dI_1}{9K}\delta_{ij} + \frac{ds_{ij}}{2G} \tag{3}$$

Where $I_1 = \sigma'_{kk}$; $s_{ij} = \sigma'_{ij} - (I_1\, \delta_{ij})/3$; K is the elastic bulk modulus and G is the elastic shear modulus. C^{e}_{ijkl} is the elastic compliance tensor.

Next, a yield (loading) function f must be assumed in the form $f = f(\sigma'_{ij}) = k$. If k is a constant then the material cannot harden. Depending on the nature of

hardening, k is made to be a function of strain history (strain hardening) or total plastic work (work hardening). It is further assumed that the shape of the yield locus does not change during deformation and therefore f is a function of stress components and independent of strain history. The sign of the yield function f is chosen so that $df > 0$ represents loading.

$$df = \frac{\partial f}{\partial \sigma'_{ij}} d\sigma'_{ij} > 0 \tag{4}$$

A neutral change in stress state cannot produce plastic deformations (consistency condition), therefore a general neutral change $d\sigma_{ij}$ is such that

$$df = \frac{\partial f}{\partial \sigma'_{ij}} d\sigma'_{ij} = 0 \tag{5}$$

Therefore for this change $d\sigma'_{ij}$ there is no change in the yield locus. Now if the plastic strain is related to the changes in the yield locus through a function G_{ij}:

$$d\varepsilon^{p}_{ij} = G_{ij}\, df \tag{6}$$

It is seen that if $df = 0$, then $d\varepsilon^{p}_{ij} = 0$. Consequently the condition of continuity is satisfied. G is by definition a symmetric tensor. The functions G_{ij} are assumed to be functions of the stress components, possibly the strain history, but not the stress increment $d\sigma_{ij}$. This means that the components of the plastic strain increments are not functions of stress increments that cause them, but the current state reached by these stress increments. The principal axes of the plastic strain increment tensor and the axes of functions G_{ij} must coincide for isotropic materials. To satisfy all these requirements, G_{ij} can be expressed as

$$G_{ij} = h \frac{\partial g}{\partial \sigma'_{ij}} \tag{7}$$

The functions h and g may depend on stress invariants and on strain history. Upon substitution of equation (7) into equation (6), the plastic strain can be expressed as

$$d\varepsilon^{p}_{ij} = \left\{ h \frac{\partial g}{\partial \sigma'_{ij}} \right\} df \tag{8}$$

Since the subsequent loading surface must contain the new stress point, the functions h and g cannot be arbitrarily chosen. The function g can be taken to be a homogeneous function of stress components and independent of strain history. In this case, the surface g = 0 is a cylinder. The intersection of this cylinder with a plane perpendicular to the space diagonal (Π plane) will describe a curve Γ. The plastic strain vector lies in the same plane as the curve Γ. The plastic strain increment vector $d\varepsilon^{p}_{ij}$ is parallel to the normal to Γ at the point of intersection with the stress vector. The stress vector is also in this plane since it is independent of the first invariant of stress I_1. It is seen that the function g defines the ratios of components of strain increment (hence its direction with respect to the principal axes) and will be called the *plastic potential function*. The simple relation f = g will be an expression of the associated flow rule or the normality condition. On the other hand, the function h will be called the hardening rule. The only restriction on this function is that it must be positive.

$$f(\sigma'_{ij}) = k\left(d\varepsilon^{p}_{ij}\right) \tag{9}$$

The hardening function k is a monotonically increasing function by definition. It is determined from the stress-strain curve once the yield function f has been determined. The general expression of the plastic strain increment in classical plasticity is given in equation (10).

$$d\varepsilon^{p}_{ij} = h \frac{\partial g}{\partial \sigma'_{ij}} \frac{\partial f}{\partial \sigma'_{kl}} d\sigma'_{kl} \tag{10}$$

Invoking the normality condition, we have g=f.

$$d\lambda = h \frac{\partial f}{\partial \sigma'_{kl}} d\sigma'_{kl} \tag{11}$$

$$d\varepsilon^{p}_{ij} = d\lambda \frac{\partial g}{\partial \sigma'_{ij}} = d\lambda \frac{\partial f}{\partial \sigma'_{ij}} \tag{12}$$

The complete elasto-plastic constitutive law is given in equation (13).

$$d\varepsilon_{ij} = C^{e}_{ijkl} d\sigma'_{kl} + C^{p}_{ijkl} d\sigma'_{kl} = C^{ep}_{ijkl} d\sigma'_{kl} \tag{13}$$

The elasto-plastic constitutive compliance tensor is given in equation (15).

$$C^{ep}_{ijkl} = C^{e}_{ijkl} + h \frac{\partial g}{\partial \sigma'_{ij}} \frac{\partial f}{\partial \sigma'_{kl}} \tag{14}$$

3.5. Collateral Concepts Included in Plasticity Theories

3.5.1. Hardening Rule

One of the main problems in plasticity is the determination of the subsequent yield or loading surfaces. This post yielding response is described by the hardening rule which specifies the rule for the expansion of the loading surfaces during the course of plastic deformations. The relationship between the change of yield stress (yield locii) and the plastic strain is known as the strain hardening law.

Strain hardening laws relate the magnitude of the plastic strain increment to the magnitude of an increment of stress as the stress state exceeds the current yield surface. The major assumption in this case is that no matter by what strain path a particular stress state is reached, the yield locus is always the same. This leads to a contradiction in that the yield locus depends on internal stresses which in turn depend on strain history. However, this fact is usually disregarded by the same reason the Bauschinger effect is disregarded. The consequence of strain hardening rules is that the yield locus of an ideal plastic body is uniquely determined by the final plastic state of stress.

Work hardening suggests that the degree of hardening is a function of the total plastic work only. Since the strain energy produced by deformation does not necessarily equal the external plastic work, the yield criterion is used to measure the amount of plastic work. This functional relationship between the yield function and plastic work can be obtained experimentally. For a material in a

given state of stress that is further loaded by an external agency and subsequently unloaded, work hardening implies that for all such added sets of stresses the material will remain in equilibrium and there is positive work done by the external agency during the application of stresses and the net work done by the external agency over the cycle of stressing and unloading is zero or positive. Therefore, work hardening implies that useful energy over and above the elastic energy cannot be extracted from a material and the system of forces acting on it [Drucker (1951)].

Cap models are based on the fact that the volumetric hysteresis exhibited by many geologic materials can also be described by a plasticity model if this model includes a hardening yield surface as a function of the hydrostatic pressure. The soil is represented as an elasto-plastic work or strain hardening material. The successive yield surfaces resemble Von Mises cones representing plastic behavior and convex spherical end caps representing hardening effects. The cap is not fixed in the stress space as it changes with plastic deformations. The movement of the cap is controlled by the measure of hardening used and allows the simulation of a variety of material behaviors. The Cambridge models are more advanced examples of cap models [Roscoe et al. (1963), Schofield & Wroth (1968)]. A more generalized cap model has also been proposed [DiMaggio & Sandler (1971)]. This model is a combination of a perfectly plastic yield condition with an elliptical cap fitted to its open end. The versatility of the cap models is perhaps best illustrated by the model proposed by Lade (1977,1979). This model consists of a conical yield surface closed up by a hemispherical cap. The interesting feature here is that although a non-associated flow rule was used for the conical portion, the cap itself was left to evolve according to an associated flow rule.

The *kinematic hardening* rules assume that during deformations, the loading surface translates without rotations as a rigid body in the stress space, maintaining the size and shape of the initial yield surface. This type of model is particularly well suited for the description of materials with pronounced Bauschinger effects such as soils under cyclic loads. Instead of a single yield surface in stress space, a family of yield surfaces are used [Iwan (1967), Mroz (1967), Prevost (1977)]. Each surface translates in a purely kinematic manner, or

individually obeying a linear work hardening rule. An isotropic hardening rule can also be introduced in addition to kinematic hardening [Prevost et al. (1981)].

3.5.2. *The Flow Rule*

The flow rule relates the ratio of the components of plastic strains (volumetric and shear) in an increment of plastic deformation to the state of stress causing these plastic deformations. It thus relates the direction of the vector of plastic strain increment to the yield surface. The gradient of the vector of plastic strain increment is related to the vector of stress and is independent of the change of stress causing the plastic strain. This is in full contrast with the elastic behavior where elastic strains are wholly dependent on the change of stress.

An assumption that the plastic strain increment vector is normal to the current yield surface is called an associated flow rule or the normality condition and is a direct result of Drucker's stability postulate for stable plastic material [Drucker (1959, 1964a)]. An assumption to the contrary will lead to a non associated flow rule. The direction of the plastic strain increment vector in the case of a non associated flow rule can be calculated from some energy equation relating stresses to strain rates.

3.5.3. *Drucker's Siability Postulate*

The term stable system means that under virtually no external agents acting on the system, virtually nothing will happen to it. The term stable material is an extension of this stable system concept. Geometric stability is taken for granted in this context by assuming that deformations are small and the equations of equilibrium are satisfied in the undeformed state.

The stability postulate states that for all stress increment probes directed outward from the tangent to the yield locus, the vector product of the stress increment vector $d\sigma'_{ij}$ with the associated plastic strain increment vector $d\varepsilon^P_{ij}$ will be non negative ($d\sigma'_{ij}\, d\varepsilon^P_{ij} \geq 0$). For elastic and isotropic materials this condition implies the convexity of the constant strain energy surfaces. In the case of isothermal, plastic, isotropic materials, the postulate implies the convexity of the yield

surface as well as subsequent loading surfaces and the normality of the plastic strain increment to these surfaces [Drucker (1964b)].

3.6. Conclusion

It was shown in Chapter 2 that soft clays are highly plastic materials and consequently their constitutive description requires the use of the theory of plasticity. Although the initial development of this theory was concerned with the plastic deformations of metals, the last three decades have seen a progressive proliferation of plasticity models for soils.

Regardless of the material, the theory requires a yield function defining the limit of elastic behavior, a hardening rule defining the size of the subsequent loading surface, and a plastic flow rule determining the relationship of the strain increment with stress. The proper choice of these fundamental functions will ensure the correct representation of inelastic behavior under most stress paths.

CHAPTER 4 : CRITICAL STATE SOIL MECHANICS

4.1. Preliminaries

Critical State soil mechanics is one of the better known applications of the plasticity theory in geotechnical engineering although the derivation and use of the Critical State equations seldom refer to the fundamental plasticity concepts. The equations are nevertheless classical plasticity equations attempting the prediction of the change in the material state when the distortion process is not carried too far.

The state of stress is assumed to be completely defined by the three principal stresses, their directions and the pore pressure. The instantaneous state of effective stress in an element may be plotted as a point (representing the magnitude) and the line joining all such points is called the *effective stress path* (ESP). From the theory of plasticity, it is concluded that the effective stress path for a soil eventually reaches the yield surface and moves on this surface for each subsequent loading increment. On the yield surface, the existence of a "final" destination state for the ESP is postulated and called the *critical state.*

4.2. Origins

The fact that the shear stress at failure is a function of the effective normal stress and the voids ratio (both associated with the plane of failure) [Hvorslev (1937)] is the basis of the critical state concept. The main impact of the concept has been the gradual but detailed understanding of how exactly the effective stress path reaches its ultimate state and where it goes once it gets there.

By plotting triaxial test results in the ($\sigma'_1 - \sqrt{2}\,\sigma'_3$) space, Rendulic showed in 1937 that the effective stress paths obtained from undrained tests corresponded very closely to the constant voids ratio interpolated from drained test results. Rendulic's Postulate states, "There exists a unique relationship between the voids ratio and the effective stress for a clay in a given initial state of stress and stress history." This work provides the foundation for relating changes of stress

to volumetric strain and to changes in pore pressure under axisymmetric conditions. The existence of some critical voids ratio was postulated by Casagrande (1938) and defined as the voids ratio at which continuing shear distortions in drained tests cease to cause any changes in the voids ratio. An alternative approach was adopted by Taylor (1948) where the effective stresses during undrained tests will come to reach a state at which they will remain and the corresponding voids ratio is defined as being critical. Combining the results of drained and undrained tests in the light of Rendulic's postulate, it is concluded that there is in fact a unique state (the critical state) towards which drained and undrained stress paths converge and that the critical voids ratios of both are one and the same. If the yield conditions for drained and undrained loading paths coincide, then for a given clay the critical state and the yield surface can be defined under all drainage conditions. The formulation of the reasoning just presented has been one of the objectives of Roscoe's landmark paper of 1958.

The Critical State Model came to maturation in the sixties with: (i) the definition of the dissipated energy and the development of a two-dimensional method to plot the stress boundary surface [Poorooshasb & Roscoe (1961)]; (ii) the derivation of the complete stress-strain equations without the use of the theory of plasticity and the ability to predict shear strains along with volumetric strains [Roscoe & Poorooshasb (1963)]; (iii) the derivation of complete stress-strain equations based on the normality rule of plasticity theory and the differentiation of the state boundary surface from the yield surface [Roscoe et al. (1963)]; the development of a new work equation which somewhat eliminates the over prediction of shear strains at low stress ratios [Burland (1965), Roscoe & Burland (1968)].

4.3. The Critical State Line

The single and unique line of failure points of both drained and undrained tests is defined as the Critical State Line. Its crucial property is that failure of initially isotropically compressed samples will occur once the stress states of the sample reach the line, irrespective of the effective stress path followed. Failure is defined as the state where large shear strains occur with no change in stress or in specific volume v.

The projection of the critical state line on the q-p' plane is a straight line and is be expressed by the equation

$$q = M\,p' \tag{1}$$

where $q=\sigma_1-\sigma_2$, M is a soil parameter, and $p'=(\sigma'_1+2\sigma'_2)/3$.

The projection of the critical state line on the v-ln p' plane is close to a straight line approximately parallel to the virgin compression line and its equation is given as

$$v = \Gamma - \lambda \ln p' \tag{2}$$

where λ is a soil parameter and Γ is the value of the specific volume corresponding to p'=1.0. One look at this equation reveals its approximate nature: for very large pressures, the specific volume becomes less than 1, which is an impossibility. Therefore equation (2) is only valid in the range of stresses commonly encountered in civil engineering.

Whenever yielding occurs, the sample will suffer permanent deformations so that after the removal of the external agency the sample will have marginally changed its specific volume and in effect will have distorted into a different rigid sample with a different specific volume and therefore can be classified as an entirely different material. On the plot of v-ln p', there should be a clear break between an area of the plot where samples are weak at failure and another area where the samples are strong at failure. These areas lie on either side of the critical state line and clearly the critical state line should be one of the loading lines (λ lines). Thus, the critical state line divides all possible states of the material into two categories: weak at yield and strong at yield.

4.3.1. Samples weak at yield

The application of an outward load increment from an initial stress state p'_i indicates stable yielding. This phenomenon is called hardening and will be the consequence of any outward load increment that applies to the sample with stress state $0 < q' < Mp'$. The volumetric strain increment is positive and the change in specific volume is negative so that the specimen will compact to a smaller specific volume at which it will have a new and larger yield curve.

4.3.2. *Samples strong at yield*

An inward load increment indicates unstable yielding. Upon yield, such an increment will cause a negative volumetric strain increment and a positive specific volume increment. The sample must therefore expand to a larger volume and this looser specimen will be governed by a new and smaller yield curve. It will be impossible to restore the material to its initial state since the sample can no longer sustain that stress state. The effect of the inward load increment has been to transform the sample into a weaker one.

4.4. Triaxial Tests on Clays

4.4.1. *Drained Tests*

The specific volume of a normally consolidated sample decreases during such a test. The axial strain is over 20% at failure and there is a relatively large compression of the sample. Therefore such a sample must always compress during shear. This compression can be associated with positive pore pressures that are generated during undrained tests. Before the stress path reaches the current yield locus B (Fig. 4.1) the behavior is elastic. Plastic strains occur from B to F as the material is undergoing continuous yielding. When the stress path reaches the critical state line at F the soil has failed.

An overconsolidated sample must expand during shear and failure occurs before the test path reaches the critical state line (Fig. 4.2). The most important feature of this test is that the maximum value of q reached is much higher than the one reached by the normally consolidated sample under the same conditions. The volumetric strain curve is also different from the normally consolidated clay sample (Fig. 4.3). It is seen from this curve that the overconsolidated sample initially contracts but subsequently dilates strongly. The expansion of samples during shearing can be associated with the generation of negative pore pressures generated in undrained tests.

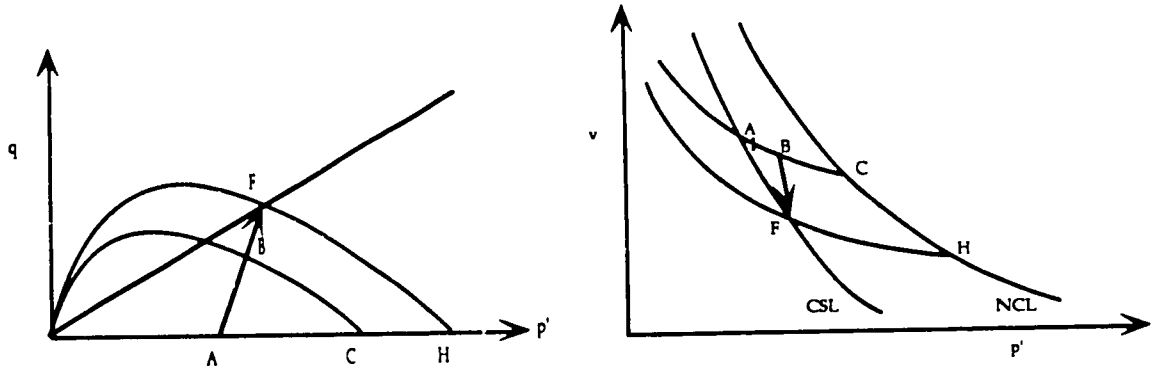

Figure 4.1 Drained stress paths for normally consolidated clay

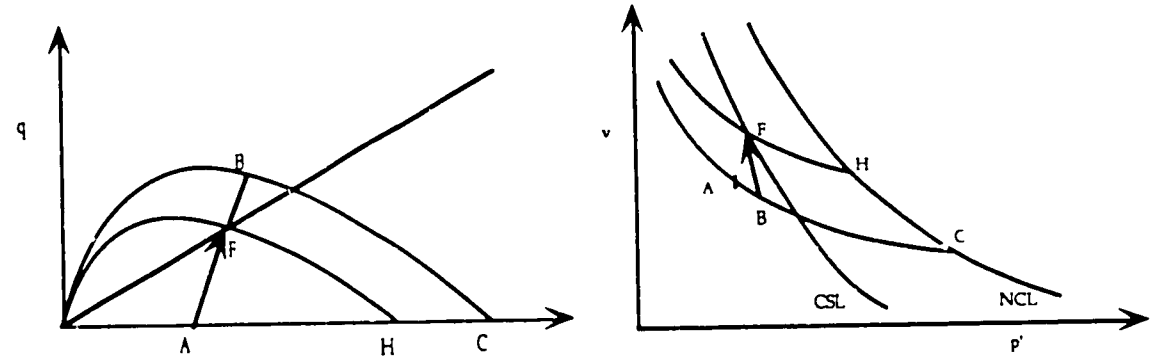

Figure 4.2 Drained stress paths for overconsolidated clay

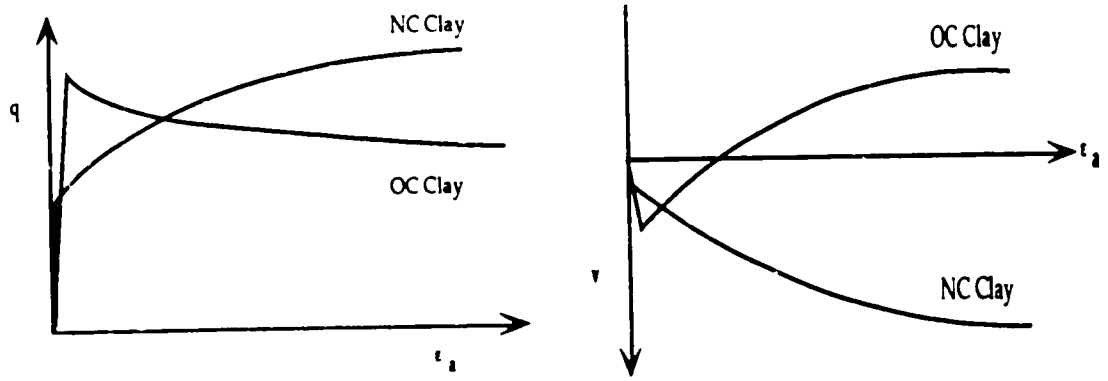

Figure 4.3 Stress-strain-volume relations for drained tests on clays

4.3.2. Undrained Tests

The failure must be without specific volume change (Fig. 4.4) and for normally consolidated samples, it is accompanied by positive pore pressure generation. Again there is a large amount of strain at failure, however, since no reduction in volume is allowed, a relatively large positive pore pressure is generated. This pore pressure reduces the effective stress in the sample and in a way, compensates for the reduction in volume that would have occurred in drained test conditions.

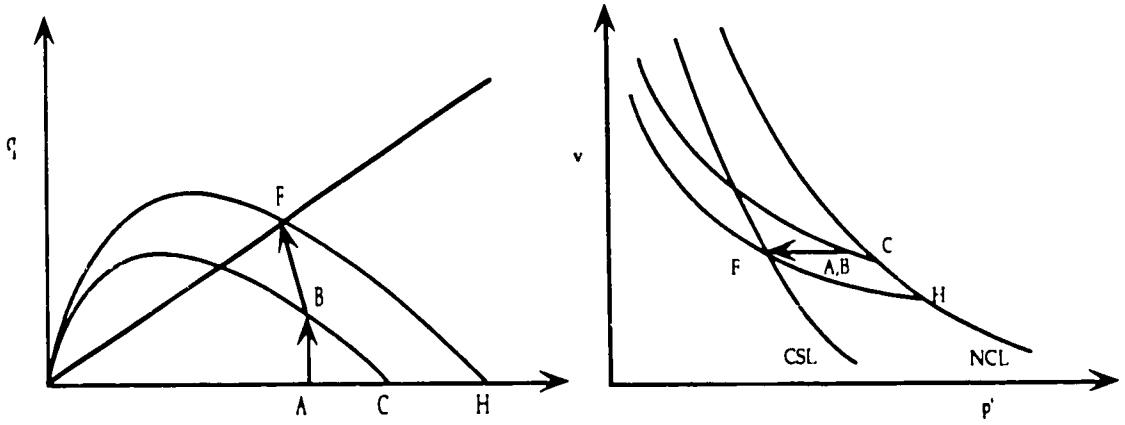

Figure 4.4 Undrained stress paths for normally consolidated clay

In the case of overconsolidated samples (Fig. 4.5), failure is accompanied by negative pore pressure generation. The shape of the q vs. ε_a curve is similar to the normally consolidated sample's curve. Large strains are developed prior to failure and the maximum value q is comparable to the one attained by the normally consolidated sample at failure. From a comparison of the Δu vs. ε_a curve of the undrained overconsolidated sample and the ε_v vs. ε_a curve (Fig. 4.6) of the drained overconsolidated sample, it can be concluded that the change in pore water pressure in an undrained test is a different manifestation of the same physical phenomenon which gives raise to volume changes in drained tests.

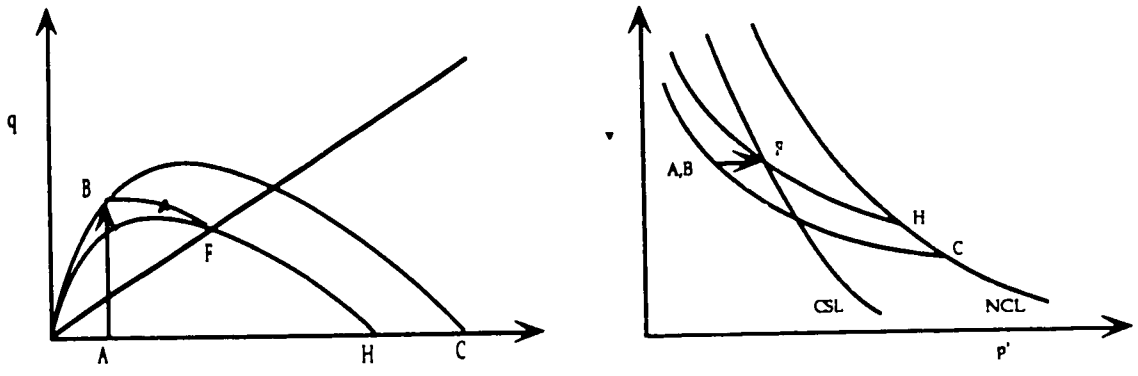

Figure 4.5 Undrained stress paths for overconsolidated clay

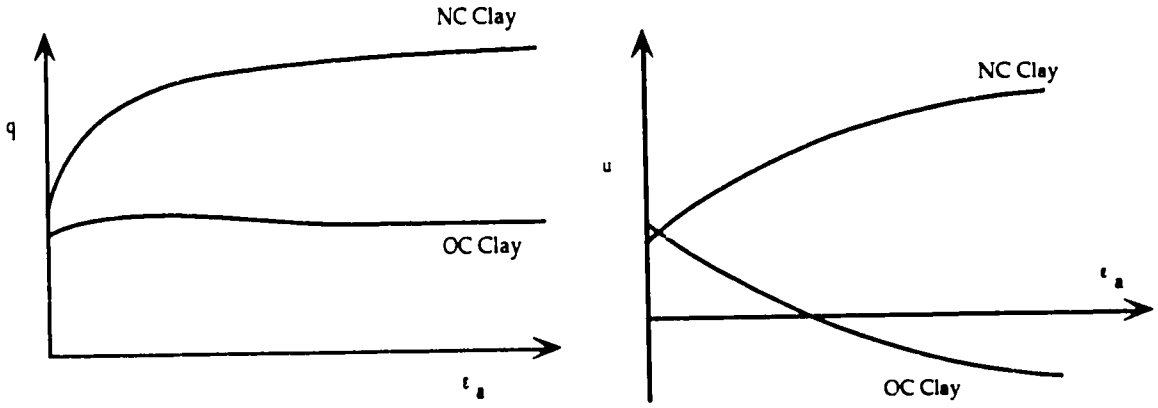

Figure 4.6 Stress-strain-pore pressure relations for undrained tests on clays

4.5. Normally Consolidated Clay and the Roscoe Surface

The surface traced out in q-p'-v space by families of drained and undrained tests is unique and is called the Roscoe surface. This surface is followed by all isotropically normally consolidated samples loaded in compression in the triaxial apparatus.

The Roscoe surface separates those states which the samples can achieve from those that the states samples can never achieve. At a given stress level, samples can neither exist at a higher specific volume than that on the normal consolidation line at that stress level nor above and to the right of the normal consolidation line which is the part of the Roscoe surface on the p'-v plane. The Roscoe surface is therefore defined as a *state boundary surface.*

The uniqueness of the Roscoe surface involves the comparison of drained and undrained test paths. The specific volume changes in drained tests so the stress path moves through a succession of constant specific volume sections. Even though the size of these successive sections is different, it is seen that their shapes are similar in the q-p' plane. As a consequence, each v=const. section can be normalized by the mean effective stress (p'_e) and could be collapsed into a single curve in the q'/p'_e - p'/p'_e plane. The value of (p'_e) is obtained from the equation of the normal consolidation line given a specific volume at any stress level. The q-ε_a curves are also all of the same shape and samples which have been compressed to higher stresses exhibit higher values of q at failure. These curves may be normalized and a single curve in the q/p'_e - ε_a plane.

If the same argument and methodology are applied to a series of undrained test results, it is seen that stress paths can similarly be collapsed into a single curve and that this curve is the same as the one obtained from the drained test results. Therefore, the critical state line for a given normally consolidated clay sample is the final destination for all stress paths under any drainage condition.

4.6. Overconsolidated Clay and the Hvorslev Surface

The Hvorslev surface is the state boundary surface for heavily overconsolidated samples. Consider an isotropically consolidated sample which is subsequently allowed to swell isotropically. A typical drained test on such a sample shows on a q-ε_a curve that the sample has a peak strength after which the value of q falls as ε_a increases. The substantial expansion of the sample is preceded by an initial decrease in volume. The test path in the q-p' space moves above the projection of the critical state line to the failure point before moving back along the same path towards the projection of the critical state line. The state boundary surface for

overconsolidated samples must therefore have a projection that lies above the projection of the critical state line in the q-p' space.

In undrained tests, it will be assumed that different constant v sections are similar in shape but different in size. The comparison of the drained test paths and the undrained test paths is done by normalizing the stress components by the mean effective stress (p'_e) at that specific volume. Just as in the case of the Roscoe surface, it is concluded that these stress paths collapse into a single line upon normalization. The state boundary surface thus obtained is called the Hvorslev surface. The significant feature of this surface is that the shear strength of the specimen at failure is a function of both the mean normal stress p' and the specific volume v of the specimen at failure. The Hvorslev surface and the Roscoe surface intersect at the critical state line.

4.7. Yield Criteria for Normally Consolidated Clay

The assumptions of the original Cam Clay model are: (i) in the q-p'-v space, the region below the current yield surface is elastic and is made up of a succession of vertical elastic walls directly above the corresponding swelling lines; (ii) there is never any elastic shear strain and consequently, in the elastic range only volumetric strain are allowed; (iii) between two successive elastic walls, the change in specific volume is the same; (iv) when plastic deformations occur, the internal work is given by $W_i = Mp'\delta\varepsilon^p$; (v) intersection of the yield locus and the p' axis corresponds to the isotropic normal consolidation line and this point specifies the size of the yield locus; (vi) the theory is based on triaxial isotropy, the volumetric strain is given by $\delta v=\delta\varepsilon_1+2\delta\varepsilon_2$ and the shear strain is given by $\delta\varepsilon=2(\delta\varepsilon_1-\delta\varepsilon_2)/3$. These quantities correspond to the stresses p' and q respectively and together satisfy the fundamental work equation.

From this point on, general states of stress (as opposed to triaxial states) will be considered. The definitions of the Cam Clay variables will be modified accordingly (see Table 4.1) and all equations will be written in tensorial form. It will also be noticed that the Cam Clay model is a genuine plasticity model and the concept of critical state is not needed for its derivation: only the assumptions

(iv) and (v), the yield condition and the hardening law respectively, are in fact used. As a corollary, the Cam Clay yield condition can be considered to be an extended von Mises condition, yielding when the internal energy reaches a critical value.

Table 4.1 Stress and strain variables used in generalized Cam Clay equations

Variable	Expression	Description
s_{ij}	$\sigma_{ij} - \sigma_{kk}\frac{\delta_{ij}}{3}$	deviator stress
σ'_m	$\frac{\sigma'_{kk}}{3}$	mean effective stress
J_2	$\frac{1}{2}(s_{ij}\, s_{ij})$	second invariant of the deviatoric stress tensor
e_{ij}	$\varepsilon_{ij} - \varepsilon_{kk}\frac{\delta_{ij}}{3}$	deviator strain
I_2	$\frac{1}{2}(\dot{e}_{ij}\, \dot{e}_{ij})$	second invariant of the increment of deviatoric strain tensor
η^*	$\frac{\sqrt{2J_2}}{\sigma'_m}$	stress ratio in terms of general stresses
ψ^*	$\frac{\dot{\varepsilon}^P_{kk}}{\sqrt{2I_2^P}}$	ratio of plastic volumetric strain to plastic deviatoric strain (i.e., flow rule)
M^*	$\frac{\sqrt{2J_2}}{\sigma'_m}$	stress ratio at critical state in terms of general stresses

Based on assumption (iv), the incremental energy balance equation is

$$\dot{W}_{ex} = \dot{W}_{in} \tag{3}$$

or

$$\sigma'_m\, \dot{\varepsilon}^P_{kk} + s_{ij}\, \dot{e}^P_{ij} = M^*\, \sigma'_m \sqrt{2I_2^P} \tag{4}$$

Since the co-axiality of the deviatoric stress and deviatoric strain has been established, we may write

$$s_{ij}\, \dot{e}_{ij} = \sqrt{2J_2}\, \sqrt{2I_2^P} \tag{5}$$

The stress-strain relationship is hence derived using equation (5) in equation (4)

$$\frac{\dot{\varepsilon}^{p}_{kk}}{\sqrt{2I_2^{p}}} = M^{*} - \frac{\sqrt{2J_2}}{\sigma'_m} \tag{6}$$

Conventional consolidation test results are used for the expression of total and elastic volumetric strains.

$$\dot{\varepsilon}_{kk} = \frac{\lambda}{1+e}\frac{\dot{\sigma}'_m}{\sigma'_m} \tag{7}$$

$$\dot{\varepsilon}^{e}_{kk} = \frac{\kappa}{1+e}\frac{\dot{\sigma}'_m}{\sigma'_m} \tag{8}$$

In equations (7) and (8), e is the voids ratio, λ is the slope of the consolidation line and κ is the slope of the swelling line in the e-ln p′ plots.

Assuming that the normality condition is satisfied (see Chapter 3) we may then write

$$\dot{\sigma}'_{ij}\,\dot{\varepsilon}^{p}_{ij} = \dot{\sigma}'_m\,\dot{\varepsilon}^{p}_{kk} + \sqrt{2\dot{J}_2}\sqrt{2I_2^{p}} = 0 \tag{9}$$

or

$$\frac{\dot{\sigma}'_m}{\sigma'_m} + \frac{\dot{\eta}^{*}}{\psi^{*}+\eta^{*}} = 0 \tag{10}$$

Upon integration, equation (10) determines the yield surface. Obviously, the parameter ψ^{*} must be given to accomplish this integration. It was stated earlier that the state boundary surface can be collapsed into a single line. This in turn suggests that the successive yield surfaces are similar in shape but only differing in their size. Following this observation, it is concluded that ψ^{*} is a function of stresses only and can be expressed as $\psi^{*}=\psi^{*}(\sigma'_{ij})$. In this case, the differential equation (10) has the general solution

$$\sigma'_m = Cf(\eta^{*}) \tag{11}$$

The constant of integration C is the value of σ'_m at $\eta^{*}=0$ and will be called σ'_{my}, representing isotropic hardening effects [Calladine (1963)].

$$\ln\left(\frac{\sigma'_m}{\sigma'_{my}}\right) + \int_0^{\eta^*} \frac{d\eta^*}{\psi^* + \eta^*} = 0 \qquad (12)$$

The equation of the state boundary surface is similarly obtained by making use of equation (2), namely

$$\sigma'_{me} = \exp\left(\frac{e_a - e}{\lambda}\right) \qquad (2 \text{ bis})$$

where e_a is the voids ratio at $\sigma'_{me} = 1$. Therefore the state boundary surface is

$$\ln\left(\frac{\sigma'_m}{\sigma'_{me}}\right) + \left(\frac{\lambda - \kappa}{\lambda}\right) \int_0^{\eta^*} \frac{d\eta^*}{\psi^* + \eta^*} = 0 \qquad (13)$$

The equations (12) and (13) provide the basis for the derivation of the yield and state boundary expressions for the Cam Clay. The final form of the constitutive equations will depend on the choice of the expression of the dissipated energy which comes into the equations in the from of the function ψ^*, thereby affecting the shape of the yield locus in the stress space. Since the yield surface is also the plastic potential, the function ψ^* also governs the ratio of the plastic volumetric strains to the plastic shear strains.

4.7.1. Original Cam Clay Yield Condition

The equation (4) is the incremental energy equation adopted in the Original Cam Clay theory.

$$\sigma'_m \dot{\varepsilon}^p_{kk} + s_{ij} \dot{e}^p_{ij} = M^* \sigma'_m \sqrt{2I_2^p} \qquad (4 \text{ bis})$$

The function ψ^* (as defined in Table 4.1) therefore is

$$\psi^* = M^* - \eta^* \qquad (14)$$

Upon substitution into equations (12) and (13), the yield condition and the equation of the state boundary are respectively given in equations (15) and (16).

$$\ln \sigma'_m + \frac{\eta^*}{M^*} = \ln \sigma'_{my} \tag{15 a}$$

$$\sigma'_m \exp\left(\frac{\eta^*}{M^*}\right) = \sigma'_{my} \tag{15 b}$$

$$\ln \frac{\sigma'_{me}}{\sigma'_m} = \left(\frac{\lambda - \kappa}{\lambda}\right)\frac{\eta^*}{M^*} \tag{16 a}$$

$$\sigma'_m \exp\left(\frac{\lambda - \kappa}{\lambda}\frac{\eta^*}{M^*}\right) = \sigma'_{me} \tag{16 b}$$

4.7.2. Modified Cam Clay Yield Condition

The Modified theory differs from the original theory in its definition of the dissipated energy associated with plastic deformations [Burland (1965)]. The incremental energy balance equation is defined as

$$\sigma'_m \dot{\varepsilon}^p_{kk} + s_{ij}\dot{e}^p_{ij} = \sigma'_m \sqrt{\left[\dot{\varepsilon}^p_{kk}\right]^2 + M^{*2} I_2^p} \tag{17}$$

The plastic flow function is obtained the same manner as before and it gives

$$\psi^* = \frac{M^{*2} - \eta^{*2}}{2\eta} \tag{18}$$

Substitution of equation (18) in equations (12) and (13) gives the yield function and the equation (equations 19 and 20) of the state boundary surface for the Modified Cam Clay theory.

$$\ln\left(\frac{\sigma'_m}{\sigma'_{my}}\right) + \ln\left(\frac{M^{*2} + \eta^{*2}}{M^{*2}}\right) = 0 \tag{19 a}$$

$$\sigma'_m \left(\frac{M^{*2} + \eta^{*2}}{M^{*2}} \right) = \sigma'_{my} \qquad (19\,b)$$

$$\ln \left(\frac{\sigma'_m}{\sigma'_{me}} \right) + \left(\frac{\lambda - \kappa}{\lambda} \right) \ln \left(\frac{M^{*2} + \eta^{*2}}{M^{*2}} \right) = 0 \qquad (20\,a)$$

$$\sigma'_m \left(\frac{M^{*2} + \eta^{*2}}{M^{*2}} \right)^{\frac{\lambda-\kappa}{\lambda}} = \sigma'_{me} \qquad (20\,b)$$

4.8. Conclusion

The Cambridge Cam Clay theory is a hardening plasticity model much along the lines of the first such model proposed for soils [Drucker et al. (1957)]. There are similarities as well as differences with the earlier model however. For example, while the normality of the plastic strain increment to the yield surface was adopted in Cam Clay it was not applied to the failure surface but to the yield surfaces. This happens to be one of the innovations of the model: up until Cam Clay, there was not a distinction between the failure condition and the yield condition. The yield conditions that have been used in the context of Cambridge theories are extended von Mises conditions since yielding starts when the internal dissipated energy (plastic work) reaches a critical value. Different estimations of the plastic work result in various forms of the model but the overall structure remains the same. The hardening rule is a function of the isotropic mean effective stress and as a consequence the yield locus is circular in the deviatoric (Π) plane. The yield surface being akin to Mohr-Coulomb or extended von Mises cone and the open end is closed by successive yield surfaces, shaped like caps. The isotropic hardening results in the expansion of these caps due to successive yielding.

Although the Critical State Line (and the concept of a critical state) is viewed as an integral part of the theory, it is obvious that the Cam Clay yield criterion is derived without resorting to the line itself. In this regard, the Cam Clay model is a pure hardening plasticity model. The use of the critical state line in the p'-e

plane was however an entirely new approach and allows for the consistent representation of stress paths under any drainage condition. Another feature that distinguished the Cam Clay theory apart from all others was the fact that, for the first time up until the early sixties, it offered the description of the volume response under shear.

Despite its innovative features and relative simplicity, the Original Cam Clay theory has its draw-backs. For one, the yield surface contains a corner; this in itself is not a theoretical impossibility [Köiter (1953)]. However the experimental data suggests that the shear strains calculated at low stress ratios (in the vicinity of the corner) are over predicted and the predicted value of K_o is much higher than the measured values. In the stress space, the yield surface is a little too rounded and the stress paths move too rapidly towards the critical state line. These deficiencies formed the rationale behind the development of the Modified Cam Clay yield surface which intersects the p'-e plane at right angles thus eliminating the discontinuity in the slope of the yield surface.

There is sufficient reason to believe that the Cam Clay equations work remarkably well when applied to lightly over-consolidated clays. It has been already established that the soft clays, although generally normally consolidated, behave as lightly over-consolidated clays. Therefore it is concluded that the Cam Clay yield criterion is adequate for the analysis of soft clay behavior.

CHAPTER 5 : ELASTO-VISCOPLASTIC CONSTITUTIVE THEORIES

5.1. Preliminaries

The basic premise of elastoplastic constitutive models is the ability of materials to undergo small permanent changes as well as recoverable changes during a given load increment. Similarly, a viscoplastic constitutive law is based on a further assumption that the plastic deformations depend on the duration of the application of the load increment. An essential feature of viscoplasticity is the simultaneous description of rheological and plastic behavior of materials since the viscous nature of materials accounts for the time dependence of the stress and strain states while the plastic nature of materials accounts for the dependence of these states on the stress path and history.

All materials possess viscous properties in different levels of importance and for many materials these properties are more pronounced after the onset of plastic deformations. Hence, in these instances, it can be assumed that viscosity appears in the plastic range only. Such materials are generally termed rate sensitive (time dependent) plastic materials or elastic-viscoplastic materials of rate type.

Since the rate effects are only accounted for after the onset of plasticity, the yield condition for the material may be one of the types used in inviscid plastic theories. In fact, this criterion must satisfy all known requirements of inviscid plastic theories. It is therefore the "excess" stress above the one causing yield that is responsible for the onset of rate dependent behavior (i.e., creep). The yield condition for this material will be the same as the static yield condition in the inviscid theory of plasticity.

As is the case for most soils (e.g., soft clays), increasing deformation rates cause an increase in strength [Chadwick et al. (1964), Skempton & Bishop (1954)]. Therefore, associated with each strain rate, there exists a unique yield surface, called the *dynamic yield surface* (the term dynamic is used to indicate non-constant strain rate during deformation). Consequently, the overall shape of the stress-strain curves for dynamic loading will often be different from static loading curves. This aspect of rate dependence of materials has quite an interesting

consequence. Consider a material which shows hardening behavior under a given increasing strain rate regime. If a strain hardening yield condition is used, the effects of the hardening rule and rate effects are additive and result in a stiffer response. Assume now that the strain rate regime is made to be decreasing at a given time during the deformation. Although the hardening law would still predict a stiffer response the rate effects will now cause the material to behave in a "softer" manner. It is thus that while hardening occurs in the classical sense, a softening behavior can conceivably be observed.

5.2. The Theoretical Structure of Viscoplastic Models

The domain $\mathcal{D}$ is defined as a plane in (σ, ε) containing the origin and is called the state domain. The functions φ and ψ will be called material functions and together with the domain $\mathcal{D}$ define the behavior of the material.

The material behavior is said to be of quasi-linear rate type if, for any state of the domain $\mathcal{D}$ and the strain rate at this state, the stress rate at this state is given by

$$\dot{\sigma}_{ij} = \varphi(\sigma_{ij},\varepsilon_{ij})\,\dot{\varepsilon}_{ij} + \psi(\sigma_{ij},\varepsilon_{ij}) \tag{1}$$

Although not initially obvious, equation (1) was first proposed by Maxwell in 1867 with $\varphi(\sigma,\varepsilon) = E$ and $\psi(\sigma,\varepsilon) = -\sigma$. The condition $\varphi(\sigma,\varepsilon) > 0$ ensures that the solution of the set of partial differential equations formed by the constitutive equation, the equation of momentum and the equation of compatibility will be a hyperbolic system (i.e., wave equation) and thus have real acceleration waves in domain $\mathcal{D}$. In this case, the role of $d\varepsilon$ and $d\sigma$ can be interchanged.

Let (σ_o,ε_o) in $\mathcal{D}$ define a state where $\psi(\sigma_o,\varepsilon_o) \neq 0$. If a strain increment $\Delta\varepsilon$ is applied at (σ_o,ε_o), then the corresponding stress increment $\Delta\sigma$ will only be known if and only if the time interval Δt during which $\Delta\varepsilon$ is applied is known.

$$\text{if } \varepsilon_{ij}(t) = \varepsilon_{ij\,(0)} \Rightarrow \dot{\sigma}_{ij} = \psi(\sigma_{ij},\varepsilon_{ij\,(0)}) \text{ with } \sigma_{ij}(0) = \sigma_{ij\,(0)} \tag{2}$$

$$\text{if } \sigma_{ij}(t) = \sigma_{ij\,(0)} \Rightarrow \dot{\varepsilon}_{ij} = -\frac{\psi(\sigma_{ij\,(0)},\varepsilon_{ij})}{\varphi(\sigma_{ij\,(0)},\varepsilon_{ij})} \text{ with } \varepsilon_{ij}(0) = \varepsilon_{ij\,(0)} \tag{3}$$

Equation (2) describes relaxation under constant strain (null strain rate) while equation (3) is the expression for creep under constant stress (null stress rate). It is apparent from the equations (2) and (3) that the function ψ describes the viscoplastic properties of the material and in equation (1), it provides the essential departure from the classical plasticity theory. Alternatively, points in $\mathcal{D}$ such that $\psi(\sigma_o,\varepsilon_o)=0$ define the equilibrium states where the behavior is elastic.

5.3. A Historical Perspective on the Viscoplastic Constitutive Laws

The development of material models which include time effects has been concentrated on two main avenues. The first is known as the endochronic theory [Valanis (1975), (1971), Bazant (1978)] and it is a model with an intrinsic time variable in addition to the internal state variables based on thermodynamics. The second is the theory of elasto-viscoplasticity based on structures similar to the plasticity theory. Viscoplastic models use separate functions for the magnitude (hardening law) and the direction (plastic potential) of the viscoplastic strain rate. There seems to have been three separate approaches to elasto-viscoplasticity: (i) in the "flow surface theory," a yield condition and a corresponding loading-unloading criterion are used and the viscoplastic strain potential function includes time as an explicit variable (in contrast to the endochronic theory); (ii) in "overstress theory," the yield condition for dynamic loading is specified however no loading-unloading criterion is used, the dynamic yield condition is also the viscoplastic potential surface and the magnitude of the viscoplastic strain rate is defined with respect to a reference state (the static, or constant strain rate condition) and it is the stress in excess of this reference stress that cause rate dependent deformations; (iii) in "creep potential theory" it is assumed that elastic and viscoplastic strains occur simultaneously and only a viscoplastic potential is required for their prediction, the strain rate is governed by internal state variables and their respective evolution equations and consequently there is neither a yield condition nor a loading-unloading criterion.

The remainder of this Chapter will be devoted to the evolution of the overstress type models since the early thirties. Clearly, many combinations of the strain increment components (elastic, plastic, viscous, viscoelastic, viscoplastic) can be used to describe material behavior like the "elastic-viscous-plastic" models

[Freudenthal (1958)], the "viscoelastic-plastic" models [Naghdi & Murch (1963)], the "elastic-viscoplastic-plastic" models [Cristescu (1967)]. Therefore, it is necessary to narrow further the area of interest in this work to those combinations involving elastic and viscoplastic strain increments (i.e., the elastic-viscoplastic models).

5.3.1. *The Bingham Model*

The main feature of the Bingham model [Bingham (1922)] is that the material starts to flow only after the applied force exceeds a certain limit, called the yield limit. This model is an extension of the rigid-plastic model in classical plasticity with the difference that while stresses in excess of the yield limit are not permissible in classical plasticity, they are the only ones that cause deformations in the Bingham model. Of course, as in the case of plasticity, the yield stress can be made a function of strain and thus include hardening effects. The material functions per equation (1) are $\varphi(\sigma,\varepsilon) = 2\eta$ and $\psi(\sigma,\varepsilon) = -s_{ij} = -f(\varepsilon_{ij})$.

$$\dot{e}_{ij} = \begin{cases} \dfrac{s_{ij} - f(\varepsilon_{ij})}{2\eta} & \text{if } s_{ij} > f(\varepsilon_{ij}) \\ 0 & \text{if } 0 < s_{ij} \leq f(\varepsilon_{ij}) \end{cases} \tag{4}$$

The volumetric behavior is rigid under any circumstances and the yield stress $f(\varepsilon_{ij})$ is the yield at pure shear. The viscosity coefficient η expresses the rate effects on the material and is only constant for a limited range of strain rates.

5.3.2. *Hohenemser-Prager Model*

The Hohenemser-Prager [Hohenemser & Prager (1932), Prager (1937), (1954)] model includes elastic strains in addition to the features described for the Bingham Model. The principle of the additivity of elastic and inelastic strain increment components is invoked and the elastic deformation of the volume is included.

$$\dot{\varepsilon}_{ij} = \begin{cases} \dfrac{\dot{s}_{ij}}{2G} + \dfrac{\dot{\sigma}'_m}{3K}\delta_{ij} + \dfrac{s_{ij} - f(\varepsilon_{ij})}{2\eta} & \text{if } s_{ij} > f(\varepsilon_{ij}) \\ \dfrac{\dot{s}_{ij}}{2G} + \dfrac{\dot{\sigma}'_m}{3K}\delta_{ij} & \text{if } 0 < s_{ij} \le f(\varepsilon_{ij}) \end{cases} \tag{5}$$

The yield stress and the viscosity coefficient have the same meanings as in the Bingham model, G and K are the elastic shear and bulk modulii respectively. This model is a generalized Maxwell model (see equation (1)) with a variable viscosity coefficient.

5.3.3. Sokolovski Model

Sokolovski [Sokolovski (1948)] introduced the following material functions in domain $\mathcal{D}$

$$\varphi(\sigma_{ij},\varepsilon_{ij}) = E$$

$$\psi(\sigma_{ij},\varepsilon_{ij}) = \begin{cases} 0 & \text{if } |\sigma_{ij}| < \sigma_{ij\,y} \\ -(\text{sign } \sigma_{ij})F(|\sigma_{ij} - \sigma_{ij\,y}|) & \text{if } |\sigma_{ij}| \ge \sigma_{ij\,y} \end{cases} \tag{6}$$

In equation (6), $\sigma_{ij\,y} > 0$ is the yield limit and F is a smooth function with $F(r) > 0$, $F'(r) > 0$, $F(0) > 0$ and $r > 0$ where r is the heat supply. The simplest form of F in the literature is $F(r) = kEr$ with k as the viscosity coefficient.

This model predicts that from any state (σ, ε) with $|\sigma_{ij}| > \sigma_{ij\,y}$, the material always relaxes to state $(\sigma_{ij\,y}, \varepsilon)$. Creep from any state (σ, ε) with $|\sigma_{ij}| > \sigma_{ij\,y}$ always takes place with constant strain rate.

5.3.4. Malvern Model

Malvern [Malvern (1951a), (1951b)] generalized the material functions proposed by Sokolovski by assuming that ψ is dependent on both state variables. The material functions are given in domain $\mathcal{D}$, ($\varepsilon \ge 0$, $\sigma \ge 0$) or ($\varepsilon \le 0$, $\sigma \le 0$).

$$\varphi(\sigma_{ij},\varepsilon_{ij}) = E$$

$$\psi(\sigma_{ij},\varepsilon_{ij}) = \begin{cases} 0 & \text{if } 0 \le \sigma_{ij} \le f(\varepsilon_{ij}) \;;\; \varepsilon_{ij} \ge 0 \\ -k\,F(\sigma_{ij} - f(\varepsilon_{ij})) & \text{if } \sigma_{ij} > f(\varepsilon_{ij}) \;;\; \varepsilon_{ij} \ge 0 \end{cases} \tag{7}$$

The function F has the same meaning as in the Sokolovski model and $k > 0$ is a viscosity constant. The continuous curve $\sigma=f(\varepsilon)$ is called the quasi-static loading curve from an initial state (0,0). The material behaves elastically for $\sigma < f(\varepsilon)$. Malvern's theory predicts that creep from state (σ,ε) with $\sigma > f(\varepsilon)$ can take place up to a fixed state on the curve $\sigma=f(\varepsilon)$.

The constitutive models described above are based on hypotheses which result in linear acceleration waves. However since all use non-linear evolution equations for the internal state variables, the set of differential equations governing the material behavior is a semi-linear one. As a corollary to the existence of linear acceleration waves, the speed of acceleration (or shock) waves at a given equilibrium state is path independent. Therefore under constant strain and temperature conditions, an acceleration wave will travel with elastic wave speed.

5.3.5. Perzyna Model

Along the lines of the equations (6) and (7), Perzyna [Perzyna (1963), (1964), (1966)] offered a more generalized version of the Hohenemser-Prager model with an increased number of parameters. Starting from the Hohenemser-Prager model, it is assumed that the total deviatoric strain rate de_{ij} is made up from elastic and viscoplastic components.

$$\dot{e}_{ij} = \dot{e}^{e}_{ij} + \dot{e}^{vp}_{ij} \tag{8}$$

The elastic response is governed by Hooke's law such that

$$\dot{e}^{e}_{ij} = \frac{\dot{s}_{ij}}{2G} \tag{9}$$

The viscoplastic stress rate deviator is given by a Bingham type law :

$$s_{ij} = k_{ij} + 2\eta \dot{e}_{ij}^{vp} \tag{10}$$

$$\dot{e}_{ij}^{vp} = \begin{cases} \dfrac{1}{2\eta}\left(\dfrac{\sqrt{J_2} - k}{\sqrt{J_2}}\right) & \text{if } J_2 > k^2 \\ 0 & \text{if } J_2 \le k^2 \end{cases} \tag{11}$$

where

s_{ij}	$= s_{ij} + \sigma_{kk}\,\delta_{ij}/3$	stress rate deviator
de_{ij}	$= d\varepsilon_{ij} + \varepsilon_{kk}\,\delta_{ij}/3$	strain rate deviator
k_{ij}	part of s_{ij} corresponding to plastic properties	
η	viscosity coefficient	
k	yield limit in shear	
J_2	second invariant of the stress deviator tensor and $J_2 > k^2$	

Therefore the total deviatoric strain rate tensor can be expressed as follows :

$$\dot{e}_{ij} = \frac{\dot{s}_{ij}}{2G} + \frac{s_{ij}}{2\eta}\left(\frac{\sqrt{J_2} - k}{\sqrt{J_2}}\right) \tag{12}$$

The behavior of the volume is elastic and is given by

$$\dot{\varepsilon}_{kk} = \frac{\dot{\sigma}_{ij}}{3K} \tag{13}$$

So far, equation (12) is in the form proposed by Hohenemser-Prager (1932) as well as Freudenthal (1958). It is apparent that the coupling of the viscous and plastic strain increments have not been considered although the yield criterion can be made to depend on strains. However, since the strain rates influence strain states which in turn govern the hardening of the material, effective description of material behavior must include the effects of strain hardening on the yield criterion. This is not only necessary for states on the yield surface but also for states within the elastic range.

Perzyna's model is based on this premise (see also Cristescu & Siliciu (1976)) and defines the viscoplastic strain rates by the combination of two functions: (i) the overstress function expresses the fact that viscoplastic strains only occur when the stress state is in excess of a yield condition and only the excess over yield stress is responsible for viscoplastic deformations; (ii) the dynamic property function expresses the non-linearity of the viscoplastic strain rates with respect to the overstress function due to strain rate effects on the yield condition.

Thus, Perzyna formulated the equations (12) and (13) as

$$\dot{\varepsilon}_{ij} = \frac{\dot{s}_{ij}}{2G} + \frac{\dot{\sigma}_m}{3K}\delta_{ij} + \gamma\langle\Phi(F)\rangle\frac{\partial F}{\partial \sigma_{kl}} \tag{14}$$

where γ is a coefficient of viscosity, F is the overstress function and $\Phi(F)$ is the dynamic property function which has the following property

$$\Phi(F) = 0 \qquad \text{for } F \leq 0$$
$$\Phi(F) = \Phi(F) \qquad \text{for } F > 0$$

The general form of the overstress function is expressed with respect to a reference state (eq. 15), namely the yield condition under static (constant strain rate) loading conditions. The yield criterion can be chosen from the various forms presented in Chapters 3 and 4, the structure of the overstress model will remain the same.

$$F = \frac{f_d\left(\sigma_{ij}, \varepsilon_{ij}^{vp}\right)}{f_s\left(\sigma_{ij}, \varepsilon_{ij}^{vp}\right)} - 1 \tag{15}$$

$f_d(\sigma_{ij}, \varepsilon^{vp}{}_{ij}) = k_d$ dynamic yield criterion

$f_s(\sigma_{ij}, \varepsilon^{vp}{}_{ij}) = k_s$ static yield criterion

The hardening parameters k_s and k_d can be chosen to represent work or strain hardening effects [Hill (1950), Naghdi (1960)].

The rheological model for Perzyna's theory consists of a spring in series with a slider and a dashpot connected in parallel. In this sense in can be thought of as an improvement over Bingham's model where no deformations are predicted unless the yield stress is exceeded. The viscoplastic deformation is described by the slider - dashpot system and is governed by the excess stress over yield and the slider resistance k incorporates the effects of work hardening.

5.3.6. Classical Inviscid Plasticity as a Special Case of Perzyna's Theory

Inviscid plasticity is obtained as a limiting case of the elasto-viscoplastic constitutive equation. The existence of a subsequent dynamic loading surface is postulated and its convexity is obtained by applying Drucker's stability criterion. The normality condition is also satisfied by the inelastic strain rate tensor as a result of this criterion. A static yield function containing work hardening effects is assumed. A dynamic property function is assumed and a relationship between the inelastic strain tensor and the excess stress above the static yield condition is established as a Maxwell type viscosity law as discussed before. The elastic strains are assumed to be independent of strain rates. It is then apparent that the general assumptions listed above are the same as those proposed by Malvern in his equations for the one dimensional elastic-viscoplastic stress-strain relations. Therefore, as in Malvern's model, it is possible to reach an equilibrium state on the curve $\sigma=f(\varepsilon)$.

If the coefficient of viscosity is assumed to be infinite, the inviscid plastic constitutive theory can be obtained. In this case, F = 0 and consequently the yield condition reduces to

$$f(\sigma_{ij}, \varepsilon^{vp}_{ij}) = k$$

Since the assumption of $\gamma \rightarrow \infty$ implies that $\Phi(F) \rightarrow 0$ by definition, the product of these two terms in the equation (14) is an indeterminate quantity that is expressed by a scalar Λ

$$\dot{\varepsilon}^{p}_{ij} = \Lambda \frac{\partial F}{\partial \sigma_{ij}} \qquad (16)$$

Equation (16) is recognized as the definition of classical plasticity theory. The quantity Λ can be obtained from the condition of consistency F=0 . During a loading process, the static yield criterion must always be satisfied since the material is in the elasto-viscoplastic range at all times. Therefore for loading, the time derivative of the yield function must vanish. The time derivative of the yield function is

$$\dot{F} = \dot{\sigma}_{ij} \frac{\partial F}{\partial \sigma_{ij}} + \dot{\varepsilon}^{P}_{kl} \frac{\partial F}{\partial \varepsilon^{P}_{kl}} = 0 \tag{17}$$

or

$$\dot{\varepsilon}^{P}_{kl} = - \frac{\dot{\sigma}_{ij} \dfrac{\partial F}{\partial \sigma_{ij}}}{\dfrac{\partial F}{\partial \varepsilon^{P}_{kl}}} \tag{18}$$

hence substituting equation (18) into equation (16)

$$\Lambda = - \frac{\dot{\sigma}_{ij} \dfrac{\partial F}{\partial \sigma_{ij}}}{\dfrac{\partial F}{\partial \varepsilon^{P}_{kl}} \dfrac{\partial F}{\partial \sigma_{kl}}} \tag{19}$$

Equation (19) is the definition of the flow rule in classical plasticity and therefore the overstress viscoplasticity is a generalized plasticity model.

5.4. Conclusion

Chapters 1 to 5 lead to the following sequence of arguments:

• Normally consolidated scft clays are highly plastic and susceptible to creep deformations and they behave like lightly overconsolidated clays.

• The Cam Clay equations are classical plasticity models and they describe the plastic behavior of normally and lightly over consolidated clays quite adequately.

• The overstress type viscoplastic constitutive equations are used to describe the rate dependent nature of deformations. The use of the yield conditions from the theory of classical plasticity theory is also permitted.

• As a consequence, the rate dependent plastic deformation of normally consolidated soft clays can be predicted using the Cam Clay yield condition within the structure of an overstress viscoplasticity model.

CHAPTER 6 : ELASTO-VISCOPLASTIC MODELS FOR SOFT CLAY

6.1. Preliminaries

The term viscoplastic has been demonstrated to apply to those materials which behave differently under dynamic and static conditions and the difference is due to the strain rate sensitivity of the material. For the purposes of this study, normally consolidated soft clay will be assumed to be an elasto-viscoplastic continuum made up of the soil skeleton and the pore water. This assumption is well suited to the generally accepted behavior characteristics of normally consolidated clays, namely, work hardening, rate sensitivity, and dilatancy. The findings which justify the use of the above assumption will now be outlined.

• The effective stress paths are affected by strain rates in undrained shear tests [Akai et al. (1962)]. Furthermore, it is seen that the plots of the equi-maximum strain lines corresponding to two different strain rates are parallel to the maximum stress axis (σ'_1) under the same testing conditions as above [Richardson & Whitman (1963)]. It is also seen that the deviatoric stress increases as the strain rate increases, but the pore pressure generation does not seem to be affected by the strain rates used (with strain rates from 0.005 to 10 %/min. and strains from 0.05 to 8 %) [Akai et al. (1962)].

• In stress relaxation tests with constant axial strain ε_{11}, the effective stress paths are again seen to be parallel to the maximum principal stress axis. This should come as no surprise since the pore water pressure does not change during a stress relaxation process. This further confirms that the pore pressure is dependent on the strain state but not on the strain rate [Akai et al. (1962)].

• The conclusion of these findings can be interpreted as follows: assume two different effective stress paths each with its own constant strain rate. Consider also two states on these paths where the principal inelastic maximum strains are equal. From the above tests we have established that the line joining these two states is parallel to the σ'_1 axis. At this point, it is natural to assume that the work hardening effects on these two states have been the same (assuming also that work hardening depends only on the inelastic strain state) since the same

principal inelastic strain has been reached. It can then be argued that the differences in the effective stress paths are entirely due to rate effects. A similar conclusion was attained by Tavenas et al. (1978) who stated that the time dependent behavior of clay can be represented entirely by the time dependent changes of its limit state surface in the stress space.

6.2. Static Loading

It has been stressed in Chapter 5 that the viscoplastic deformation is governed by the excess stress over a reference state, namely the yield condition in static loading. By definition, static loading corresponds to an equilibrium state where the strain rates are zero and the material has reached an elasto-viscoplastic configuration under the given load increments. Furthermore, the material is expected to remain in that configuration indefinitely if nothing else is done to it. This assumption is common to all inviscid theories of deformation.

This equilibrium state has been quite elusive in laboratory tests. Although stress states are found to be decreasing linearly with the logarithm of time [Murayama & Shibata (1961)], equilibrium conditions are not achieved for tests up to 400 minutes [Vialov & Skibitsky (1961)] or even 24 hours [Wu et al. (1962)]. Creep tests on fully saturated normally consolidated clay specimens suggest that these samples may never reach their equilibrium states even at the end of primary consolidation [Oka (1981), Arai (1985)]. This is deduced from the fact that during creep tests lasting up to 10 000 minutes, the creep velocity was found to be non zero at the end of the loading stage. There is also evidence that a limiting equilibrium state exists although the stress paths predicted by the Cam Clay model lie slightly above this state but are similar in shape [Oda et al. (1988)].

The original Cam Clay model has been found to underestimate the strain by about 50% compared to the experimental results for undrained constant strain rate tests. On the other hand, the stress paths traced by the model obviously define a "destination" state for the creep stress paths in the sense that the slower the strain rate, the closer the stress path is to the Cam Clay prediction [Akai et al. (1975)]. Therefore, in the stress space, the original Roscoe model provides a reasonable static loading condition.

6.3. A Historical Perspective on Viscoplastic Modeling of Clay Behavior

Naghdi and Murch (1963) proposed a unified theory of linear viscoelasticity and inviscid plasticity for viscoplastic solids. It was then concluded that the plastic strain rate is dependent not only on path history but time history of stress as well. The application of this idea to the rate dependency of clays has been carried out by Singh and Mitchell (1968), Barden (1969), Walker (1969), Nova (1982), Faruque (1986). These studies on the viscoplasticity of normally consolidated clays suggested that the creep rate of clays is dependent on the stress ratio.

The viscoplasticity of normally consolidated clays has also been studied by Sekiguchi (1977,1984). The proposed model is a generalization of the Shibata model [Murayama & Shibata (1964)] and is based on the viscoplastic potential surface theory. The Matsui-Abe (1982) model is in turn based on the Sekiguchi (1977) model with a non associated flow rule and a viscoplastic potential which follows the plastic potential surface. The viscoplastic strain increment was obtained by the addition of plastic and creep strain increments. Another theory based on the Sekiguchi-Ohta (1977) model has been proposed by Matsui (1988) for monotonic as well as cyclic loading under general stress conditions. This model is based on the viscoplastic potential theory of and does not define an elastic domain and therefore does not use a yield condition. Finally, one of the most recent variations of the Sekiguchi model has been proposed by Mimura and Sekiguchi (1986). A finite element analysis of soft clay marine foundations based on this model was conducted by Mimura et al. (1990).

Adachi and Okano (1974) developed a constitutive law for the time dependent behavior of normally consolidated clays by extending the Original Cam Clay theory within the framework provided by Perzyna's formulation of overstress viscoplasticity. This model was further extended and generalized to describe secondary consolidation [Adachi & Oka (1982)] and overconsolidated clay behavior [Oka (1982)]. A consolidation analysis using this elasto-viscoplastic law and the finite element method was provided [Adachi et al. (1982), Oka et al. (1986)]. The description of the acceleration creep process was later included in the model [Adachi et al. (1987)]. Another model capable of describing rate dependency as well as acceleration creep is based on the internal state variables with memory of the continuum thermodynamics theory [Oka (1985)]. The Cam

Clay yield condition also appears in more recent models. Kamei and Hirai (1990) proposed an elasto-viscoplastic model incorporating a generalized form of the Cam Clay model, kinematic and isotropic hardening rules and a non-associated flow rule.

Naturally, there are constitutive relations which approach the rate dependent behavior of clays from entirely different angles. The Arai model [Arai et al. (1988)] is based on the assumption that the stresses behave in a way to minimize the total dissipated energy. The conditions to be satisfied are the equations of equilibrium, continuity, stress-volume change relations, and the time-dilatancy relations. The model consists of simultaneous evaluation of the state variables with respect to spatial and time coordinates. A model based on the concept of bounding surface in stress space was also proposed [Kaliakin & Dafalias (1990)] within the framework of coupled elastoplasticity/elasto-viscoplasticity and Critical State soil mechanics and is not restricted to normally consolidated soils.

6.4. Elasto-Viscoplastic Constitutive Law with Cam Clay Yield Condition

The general form of the constitutive equation developed by Perzyna was given in Chapter 5 as

$$\dot{\varepsilon}_{ij} = \frac{\dot{s}_{ij}}{2G} + \frac{\dot{\sigma}_m}{3K}\delta_{ij} + \gamma \langle \Phi(F) \rangle \frac{\partial F}{\partial \sigma_{kl}} \tag{1}$$

$$\Phi(F) = 0 \qquad \text{for } F \le 0$$
$$\Phi(F) = \Phi(F) \quad \text{for } F > 0$$

$$F = \frac{f_d\left(\sigma_{ij}, \varepsilon_{ij}^{vp}\right)}{f_s\left(\sigma_{ij}, \varepsilon_{ij}^{vp}\right)} - 1 \tag{2}$$

where

G, K	elastic shear and bulk modulii
$d\sigma_m = \sigma_{ii}/3$	first invariant of the total stress tensor
γ	a viscosity constant of the material
$f_d(\sigma_{ij}, \varepsilon^{vp}{}_{ij}) = k_d$	dynamic yield criterion
$f_s(\sigma_{ij}, \varepsilon^{vp}{}_{ij}) = k_s$	static yield criterion

The use of this equation has been popular due to its versatility and relative simplicity. The incorporation of various yield functions is easily accomplished and the number of rate dependent parameters is well suited to the description of different time related phenomena. What is more, the numerical application of equation (1) has been presented using an explicit forward marching scheme, complete with stability requirements [Zienkiewicz & Cormeau (1974)].

Some yield criteria associated with soil mechanics problems will be placed within the formulation presented in equation (1) and (2). Following the soil mechanics sign convention, the compression will be taken as positive and all stresses are effective stresses unless indicated otherwise.

6.4.1. Extended Von Mises Yield Criterion

Assume that the behavior of a given soil can be described by the extended von Mises criterion for static and dynamic loading respectively.

$$\begin{aligned} f_s\left(\sigma_{ij}, \varepsilon_{ij}^{vp}\right) &= \left[\sqrt{J_2} - \alpha\sigma'_m\right]_s = k_s \\ f_d\left(\sigma_{ij}, \varepsilon_{ij}^{vp}\right) &= \left[\sqrt{J_2} - \alpha\sigma'_m\right]_d = k_d \end{aligned} \tag{3}$$

where α is a constant describing the dilatation rate of the soil.

The overstress function F is given as

$$F = \frac{\left[\sqrt{J_2} - \alpha\sigma'_m\right]_d}{k_s} - 1 \tag{4}$$

The substitution of this equation (4) into equation (1) will give the rate dependent stress-strain relations of a soil described by the extended von Mises yield criterion.

$$\dot{\varepsilon}_{ij} = \frac{\dot{s}_{ij}}{2G} + \frac{\dot{\sigma}_m}{3K}\delta_{ij} + \gamma\left\langle\Phi\left(\frac{\left[\sqrt{J_2} - \alpha\sigma'_m\right]}{k_s} - 1\right)\right\rangle\left(\frac{s_{ij}}{2\sqrt{J_2}} - \alpha\,\delta_{ij}\right) \tag{5}$$

The meaning of the constant α is made clear when the rate of volumetric strain is considered. It is seen that the inelastic deformation is accompanied by a decrease

of volume for all $\alpha \neq 0$. This result is characteristic of stable yielding and describes the behavior of wet soils, i.e., normally consolidated clay or loose sand.

6.4.2. Original Critical State Theory Yield Criterion

The constitutive equations which will be presented here were initially developed by Adachi and Okano (1974) at Kyoto University. Numerous improvements have been performed under the leadership of Prof. Adachi to bring the model to its current state [Adachi et al. (1987)]. The underlying feature of the model is the combination of Perzyna's viscoplastic constitutive laws with the Cambridge Critical State Theory yield criteria. The static yield condition is given by

$$f_s = \frac{\sqrt{2J_{2\,(s)}}}{M^*\,\sigma'_{m\,(s)}} + \ln \sigma'_{m\,(s)} = \ln \sigma'_{my\,(s)} = k_s \tag{6}$$

The stress invariants are as defined previously, $\sigma'_{my\,(s)}$ is the static pre-consolidation pressure and k_s is the hardening parameter which can be related to the plastic volumetric strain by the following expressions

$$\dot{\varepsilon}^p_{kk} = \frac{\lambda - \kappa}{1 + e}\,\frac{\dot{\sigma}'_{my}}{\sigma'_{my}} \tag{7a}$$

$$\varepsilon^p_{kk} - \varepsilon^p_{kk\,(i)} = \frac{\lambda - \kappa}{1 + e}\,\ln\frac{\sigma'_{my}}{\sigma'_{my\,(i)}} \tag{7b}$$

The equation (7b) is the integral of (7a) under the initial conditions $\varepsilon^p_{kk} = \varepsilon^p_{kk\,(i)}$ and $\sigma'_{my} = \sigma'_{my\,(i)}$.

The dynamic yield criterion is assumed to be similar in shape to equation (6) so that as a limiting case, the two can be merged. The stress states in the dynamic case will be denoted with the subscript "d".

$$f_d = \frac{\sqrt{2J_{2\,(d)}}}{M^*\,\sigma'_{m\,(d)}} + \ln \sigma'_{m\,(d)} = \ln \sigma'_{my\,(d)} = k_d \tag{8}$$

The hardening parameter k_d expresses the change of the dynamic yield function f_d due to inelastic strain rate $d\varepsilon^p_{ij}$ and the inelastic volumetric strain rate dv^p. The strain rate effects on the hardening rule are accounted for by virtue of the overstress function F.

$$F = \frac{\ln \sigma'_{my\,(d)} - \ln \sigma'_{my\,(s)}}{\ln \sigma'_{my\,(s)}} \tag{9}$$

The overstress function given in equation (9), is based on equation (2). The dynamic hardening will differ from the static hardening by an amount (k_s F), and this difference is a function of strain rate.

$$f_d(\sigma_{ij}, \varepsilon^p_{ij}) = k_s\,(F+1) = k_d \tag{10}$$

For static deformations where F=0 (i.e. $d\varepsilon_{ij}=dv=0$), the dynamic yield function loses its rate sensitivity and the constitutive equation becomes an inviscid model of the Cambridge type.

The rate dependence of the overstress function is expressed by the dynamic property function $\Phi(F)$. This follows from the definition of the viscoplastic strain rate as in equation (11) and equations (12) and (13) are then obtained as a corollary.

$$\dot{\varepsilon}^{vp}_{ij} = \Phi(F)\,\frac{\partial f_d}{\partial \sigma'_{ij}} \tag{11}$$

$$\Phi(F) = \sqrt{\frac{\dot{\varepsilon}^{vp}_{ij}\,\dot{\varepsilon}^{vp}_{ij}}{\frac{\partial f_d}{\partial \sigma'_{ij}}\,\frac{\partial f_d}{\partial \sigma'_{ij}}}} \tag{12}$$

$$F = \Phi^{-1}\left\{\sqrt{\frac{\dot{\varepsilon}^{vp}_{ij}\,\dot{\varepsilon}^{vp}_{ij}}{\frac{\partial f_d}{\partial \sigma'_{ij}}\,\frac{\partial f_d}{\partial \sigma'_{ij}}}}\right\} \tag{13}$$

The actual form of the dynamic property function requires the separation of viscoplastic strains from elastic strains. Results of undrained creep tests provide the necessary information since the rate of change of deviatoric stress is zero and hence the elastic strains vanish. The plots of strain rate against stress ratio will determine the shape of $\Phi(F)$ in accordance with equation (12). The general form of this function has been given by Adachi and Okano (1974) and Oka (1979).

$$\Phi(F) = c_o \exp\left[m' \ln \frac{\sigma'_{my\,(d)}}{\sigma'_{my\,(s)}}\right] \tag{14}$$

The constants c_o and m' in equation (14) are time dependent material properties. From the dynamic yield condition in equation (8), the overstress function in equation (9), and the dynamic property function (equation 14) the viscoplastic strain rate (equation 11) becomes

$$\dot{\varepsilon}^{vp}_{ij} = c_o \exp\left[m' \ln \frac{\sigma'_{my\,(d)}}{\sigma'_{my\,(s)}}\right] \frac{1}{M^* \sigma'_m} \left\{ \frac{s_{ij}}{\sqrt{2J_2}} + \left(M^* - \frac{\sqrt{2J_2}}{\sigma'_m}\right) \frac{\delta_{ij}}{3} \right\} \tag{15}$$

With the addition of elastic strain rates and the substitution of the static and dynamic hardening parameters from equations (6) and (8), the total strain rate equation is derived.

$$\begin{aligned} \dot{\varepsilon}_{ij} = {} & \frac{\dot{s}_{ij}}{2G} + \frac{\kappa}{1+e} \frac{\dot{\sigma}'_m}{\sigma'_m} \frac{\delta_{ij}}{3} + \\ & + c_o \exp\left[m' \left(\frac{\sqrt{2J_{2\,(d)}}}{M^* \sigma'_{m\,(d)}} + \ln \sigma'_{m(d)} - \ln \sigma'_{my\,(s)}\right)\right] \times \\ & \times \frac{1}{M^* \sigma'_m} \left\{ \frac{s_{ij}}{\sqrt{2J_2}} + \left(M^* - \frac{\sqrt{2J_2}}{\sigma'_m}\right) \frac{\delta_{ij}}{3} \right\} \end{aligned} \tag{16}$$

Substituting equation (7b) in (16) the constitutive equation is completed (equation 17). There are eight parameters in total: λ, κ, e, G, M^*, m', c_o, $\sigma'_{myi\,(s)}$. Note that c_o, m', and $\sigma'_{myi\,(s)}$ are time dependent variables expressing the dependence of strain rates on overstress as well as the non-linearity of this dependence.

$$\dot{\varepsilon}_{ij} = \frac{\dot{s}_{ij}}{2G} + \frac{\kappa}{1+e}\frac{\dot{\sigma}'_m}{\sigma'_m}\frac{\delta_{ij}}{3} +$$

$$+ c_o \exp\left[m' \left(\frac{\sqrt{2J_{2(d)}}}{M^* \sigma'_{m(d)}} + \ln \sigma'_{m(d)} - \ln \sigma'_{my(i)} - \frac{1+e}{\lambda-\kappa} \varepsilon^p_{kk} \right) \right] \times \qquad (17)$$

$$\times \frac{1}{M^* \sigma'_m} \left\{ \frac{s_{ij}}{\sqrt{2J_2}} + \left(M^* - \frac{\sqrt{2J_2}}{\sigma'_m} \right) \frac{\delta_{ij}}{3} \right\}$$

6.4.3. Determination of parameters

•The parameters λ, κ, e can be obtained from conventional consolidation and swelling test results.

•The elastic shear modulus G and the critical state index M* are obtained through conventional triaxial compression tests.

•The parameter m' is the slope of the equi-inelastic volumetric strain line for a given M = M*√(3/2) in a plot of (q/σ'_m) vs. $(\ln d\varepsilon_{11})$ obtained from undrained triaxial compression tests (Fig. 6.1). Its definition reflects mathematically (equation 18) the argument presented in section 6.1 and expresses the rate dependence of the stress path.

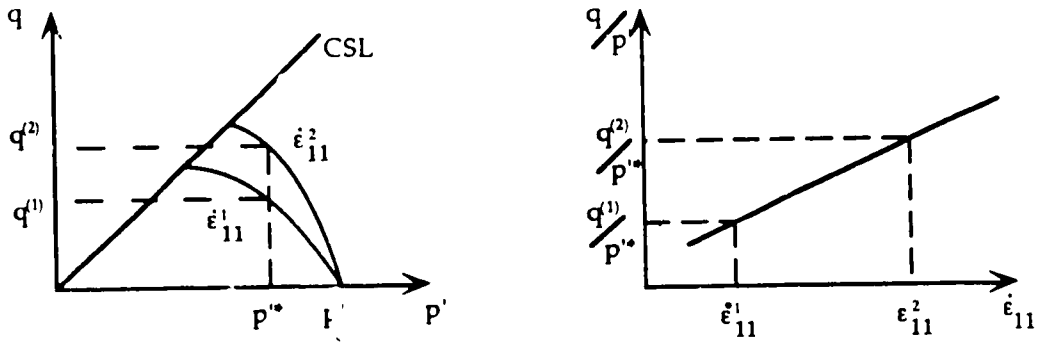

Figure 6.1. Determination of the time dependent parameter m'

$$\ln \left(\frac{\dot{\varepsilon}_{11}^{(1)}}{\dot{\varepsilon}_{11}^{(2)}} \right) = \frac{m'}{M^*} \left(\frac{q^{(1)}}{p'^*} - \frac{q^{(2)}}{p'^*} \right) \tag{18}$$

The slope m' has been found to be a function of strain for strains lower than roughly 1% and remains constant for strains exceeding this value [Akai et al. (1975)].

• The other two time dependent parameters have been combined by introducing the equivalent mean effective stress σ'_{me} in equation (17). The reason for this is that the initial static hardening parameter $\sigma'_{myi\,(s)}$ refers to a static equilibrium state which cannot be attained in testing.

$$\dot{\varepsilon}_{ij} = \frac{\dot{s}_{ij}}{2G} + \frac{\kappa}{1+e} \frac{\dot{\sigma}'_m}{\sigma'_m} \frac{\delta_{ij}}{3} + \frac{c_o}{M^* \sigma'_m} \exp\left[- m' \ln \left(\frac{\sigma'_{my\,(i)}}{\sigma'_{me}} \right) \right] \times$$

$$\times \exp\left[m' \left(\frac{\sqrt{2J_{2\,(d)}}}{M^* \sigma'_{m\,(d)}} + \ln \frac{\sigma'_{m(d)}}{\sigma'_{me}} - \frac{1+e}{\lambda - \kappa} \varepsilon_{kk}^p \right) \right] \times \tag{19}$$

$$\times \left\{ \frac{s_{ij}}{\sqrt{2J_2}} + \left(M^* - \frac{\sqrt{2J_2}}{\sigma'_m} \right) \frac{\delta_{ij}}{3} \right\}$$

The parameters c_o and $\sigma'_{myi\,(s)}$ have been replaced by a viscoplastic parameter C as

$$C = \frac{c_o}{M^* \sigma'_m} \exp\left[- m' \ln \left(\frac{\sigma'_{my\,(i)}}{\sigma'_{me}} \right) \right] \tag{20}$$

The value of C is determined from the constitutive equation once the strain rate, the stress ratio, the plastic volumetric strain and m' have been obtained.

With these modifications, the complete stress-strain relationship is

$$\dot{\varepsilon}_{ij} = \frac{\dot{s}_{ij}}{2G} + \frac{\kappa}{1+e} \frac{\dot{\sigma}'_m}{\sigma'_m} \frac{\delta_{ij}}{3} +$$

$$+ C \exp\left[m' \left(\frac{\sqrt{2J_{2\,(d)}}}{M^* \sigma'_{m\,(d)}} + \ln \frac{\sigma'_{m(d)}}{\sigma'_{me}} - \frac{1+e}{\lambda - \kappa} \varepsilon_{kk}^p \right) \right] \left\{ \frac{s_{ij}}{\sqrt{2J_2}} + \left(M^* - \frac{\sqrt{2J_2}}{\sigma'_m} \right) \frac{\delta_{ij}}{3} \right\} \tag{21}$$

The overstress viscoplasticity predicts that for $t \to \infty$ the strain rate converges to a finite value. This has been shown in section 5.3.6. and as such the overstress model cannot describe the acceleration creep (creep rupture) where the strain rates diverge to infinity immediately after reaching their minimum value. To overcome this deficiency, the parameter C is made a function of the stress ratio by using undrained triaxial creep test results [Adachi et al. (1987)].

$$C = \exp\left(\frac{\delta}{\left(M^* - \frac{\sqrt{2J_2}}{\sigma'_m} \right)} - \xi \right) \tag{22}$$

The additional constants δ and ξ are material parameters obtained from the experimental curve for C vs. $(M^*-\eta)$ with η as the stress ratio.

6.5. Conclusion

The Adachi model presented in section 6.4. is a combination of tried and proved theories: the Perzyna overstress viscoplastic law is a practical and reliable rate dependent theory while the Cam Clay has been successfully used in the analysis of soft clays. The parameters are easily defined through consolidation and undrained triaxial compression and creep tests. It is possible to describe acceleration creep through the use of a stress dependent viscoplastic parameter. It was also verified that the model can be used in the prediction of deformations and pore pressures under an embankment [Adachi et al. (1987)].

The Adachi model is a purely phenomenological model and as such offers no explanation to the physical processes that are at the root of rate dependent behavior. This discussion will be the subject of the next chapter.

CHAPTER 7: DISCUSSION CONCERNING THE ADACHI MODEL

7.1. Introduction

There is strong evidence that the Adachi model described in Chapter 6 is a viable tool for the analysis of the progressive failure of soft clays, including advanced descriptive capabilities such as rate dependence, acceleration creep, and secondary consolidation. The comparative performance of the model has already been established [Adachi et al. (1984), (1985)] however the exact nature and mechanism by which rate effects change the mechanical behavior of the material is still not clear.

7.2. Rate Dependent Variables in the Adachi Model

The effects of strain or stress rate are included by means of two material variables, namely c and m'. The determination of these parameters yield little insight on their nature (see section 6.4.3.) and furthermore a physical description of these variables has not been made so far.

7.2.1. Viscoplastic Parameter c

At first glance, the location of the parameter c within the model suggests that it is somewhat akin to the coefficient of viscosity also found as γ in Perzyna's original formulation. Although it basically is a variable describing the integrity of the material structure, it is not a viscosity constant as defined by Mitchell (1976). Since viscosity is the resistance offered to external stresses, high creep rates imply low viscosity constants. It will be made clear in the following that the parameter c does not agree with this definition.

The evolution of the viscoplastic parameter c can be studied by back analyzing undrained triaxial creep test data. During undrained creep, effective stresses and strain rates decrease continuously until creep rupture where the effective stress is equal to its critical value and the strain rates diverge to infinity. By calculating the theoretical values for c for each pair of effective stress-strain rate

measurements, Adachi et al. (1987) concluded that the parameter C must in fact increase gently up to failure and then must diverge to infinity and that this behavior is independent of the creep stress.

Assuming that the effective stress monitors the structural integrity of the clay mass, the variations of the viscoplastic parameter C with respect to the effective stress can be thought to represent the deterioration of this integrity during undrained creep (Fig. 7.1). On the other hand, the relationship between C and the strain rate is unique during primary and steady creep. The relationship is a function of the creep stress during acceleration creep (Fig. 7.2). Consequently, the Adachi model requires that C remain constant during constant strain rates in order to comply with the relationship obtained in (Fig. 7.2). This obviously refutes that C is a measure of the "deterioration" itself (since effective stresses also decrease during constant strain rate tests), if anything it must be a measure of the cumulative contribution of the strain rate on material degradation.

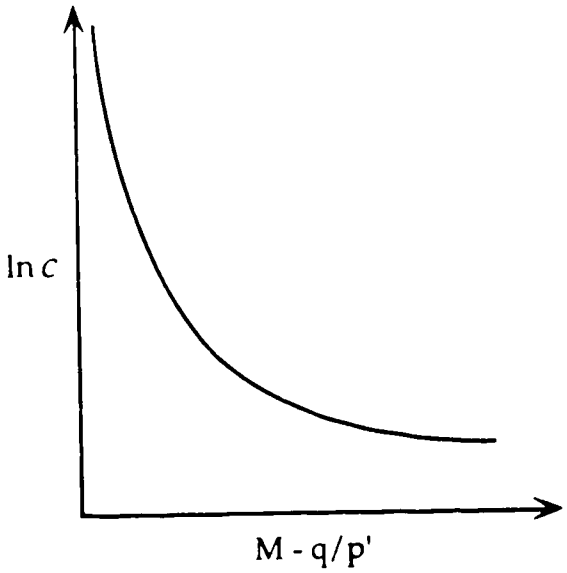

Figure 7.1 Stress ratio-C behavior for undrained creep

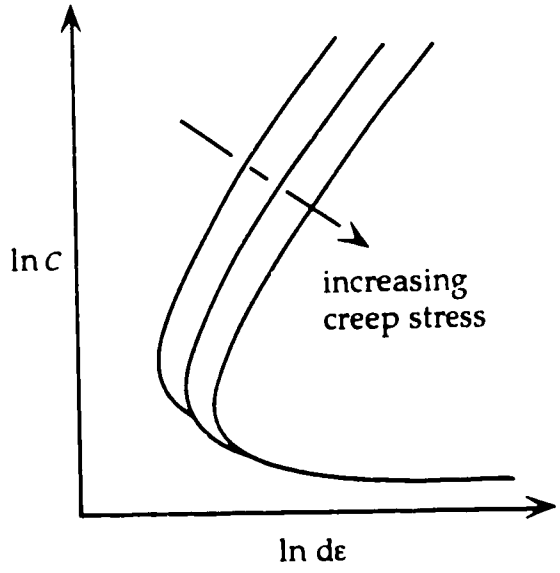

Figure 7.2 Strain rate-C behavior for undrained creep

It has also been seen that when the Adachi model is used in consolidation analysis, the ageing effects so often observed in soft clays can be simulated by

using a lower C value than one obtained from a similar "young" clay [Oka et al. (1986)]. Although the variation of C with strain rates was not considered in this study, the aged clays, showing stiffer responses, must have held consistently lower values than their younger counterparts.

7.2.2. Viscoplastic Parameter m'

It is evident that this value describes the expansion of the stress path due to strain rate effects. Consequently, the parameter m' is a measure of the apparent hardening that can be induced in the material due to faster strain rates. In this respect, m' is a coefficient that works in parallel with the strain hardening parameter k_d. Since the stress path increases linearly with the natural logarithm of the strain rate, the slope m' describes the relative ability of the material to show stiffer responses according to the current strain rates. The parameter m' will be called the strain rate hardening parameter: it compensates the strain hardening parameter for strain rate effects.

In support of this argument, consider the following: although m' has been found to be constant for strains exceeding 1%, prior to this strain state, it has been shown to increase linearly with increasing strains [Akai et al. (1975)]. What is interesting is that the range 0 to 1% happens to correspond to the hardening portions of the stress strain curves used in the derivation of this relationship.

7.3. Physical Analogies for the Viscoplastic Parameters

The plastic and creep deformation of a given body must involve changes to the micro-structure of the material which is generally defined by physical variables such as activation energy, flow unit, and entropy The movement of clusters of molecules (flow units) requires the input of additional energy to the system and the resulting deformation changes the configuration of the material micro-structure (entropy). This premise can be formulated mathematically by an Arrhenius type equation [Mitchell et al. (1968), Erol et al. (1977)].

$$\dot{e}_{ij} = A \exp\left(-\frac{\Delta F}{k T}\right) \exp\left(-\frac{\beta s_{ij}}{k T}\right) \qquad (1)$$

where de_{ij} is the shear strain rate, A is a proportionality constant, ΔF is the activation free enthalpy or bond energy, β/kT is a stress factor, β is the flow volume, k is Boltzmann's constant (1.38×10^{-16} erg/^{o}K), and T is the absolute temperature in ^{o}K, s_{ij} is the deviatoric stress.

The parameter A in equation (1) represents the activation entropy and hence should be a function of time, number of flow units effected by the deformation, and the actual displacement component in the direction of flow unit movement. In the absence of external agents, the flow units vibrate with a frequency of kT/h and cross energy barriers randomly in all directions as a consequence of their thermal energy where h (6.624×10^{-27} erg/sec.) is Planck's constant. When stress is applied to the material, the crossing of the energy barriers will be encouraged in the direction of deformation.

The first exponential in equation (1) describes the response to the applied stresses. The higher the activation energy ΔF (harder states), the more resistance will be offered by the energy barriers and the lower the strain rates will become. This means that in addition to the energy dissipated by plastic deformation, some energy is stored by the flow units thereby providing increased resistance to displacement upon further loading. Therefore, ΔF is a measure of inter-particle bond strength between flow units.

The second exponential term of equation (1) is an expression of the external agents that will cause the deformations to occur in the first place. The stress is multiplied by a stress factor (β/kT) to obtain the average force acting on the flow units.

7.4. Observed Evolution of the Physical Parameters

During an undrained creep process of normally consolidated clay, three distinct phases are apparent and it can be concluded from a plot of strain-time that the strain rate decreases with time up to an inflection point after which the reverse process takes place. Therefore, at constant shear stress, either the activation enthalpy, or the activation entropy, or the flow unit, or any combination of the

three may be varying. For example, the reorientation of the clay particles during deformation would result in a variation of the parameter A and since the bond strengths between the original structural particles would change during deformation, variations in the values of β and ΔF should also be expected. The time dependence of A and ΔF is supported by the fact that creep strain rates which depend on these variables decrease with time.

Shear box tests conducted on clay specimens also confirm [Erol et al. (1977)] the validity of the above argument. Up to the creep rupture, the flow volume and the activation enthalpy increase while the activation entropy decreases. During acceleration creep, the trends are reversed. This can be physically interpreted as follows : in the strain hardening process the particles may be welding to form larger (higher flow unit) and stronger (higher activation enthalpy) clusters while the material is progressively increasing in orderliness (decreasing entropy).

Erol et al. (1977) found that the relationship between the strain rate and shear stress is maintained throughout the entire creep process. This in turn suggests that the entire creep behavior is governed by one flow mechanism. The fact that rate of change of the flow volume is dependent on the creep stress leads to the conclusion that at equivalent time of shear, the log of strain rate vs. shear stress plots would not be linear. This argument is not in agreement with the idea that equivalent structures are found at states of equal strain hardening as assumed by Adachi and Okano (1974) or similarly at equivalent time of shear as adopted by Mitchell et al. (1968).

7.5 Observed Evolution of the Viscoplastic Parameters

7.5.1. Viscoplastic Parameter m'

In the Adachi model, the definition and determination of m' is equivalent to the stress factor β/kT in equation (1). Differences between these two quantities are the result of the the methods of testing as well as the stress variables used in their representation. While Erol et al. based their data on simple shear tests, the data of Adachi et al. come from undrained triaxial compression tests. Consequently, the normal stress σ and the shear stress τ are used in the former case, the triaxial

parameters σ'_m , q, and M are used in the latter. Despite the fact that even the clays tested were different, there are unmistakable similarities between the two graphs: each of the lines presented in (Fig. 7.3) are representative of a series of parallel lines and the effect of the slope of these lines is the same in their respective theories, namely it accounts for rate dependent increase in flow unit or hardening.

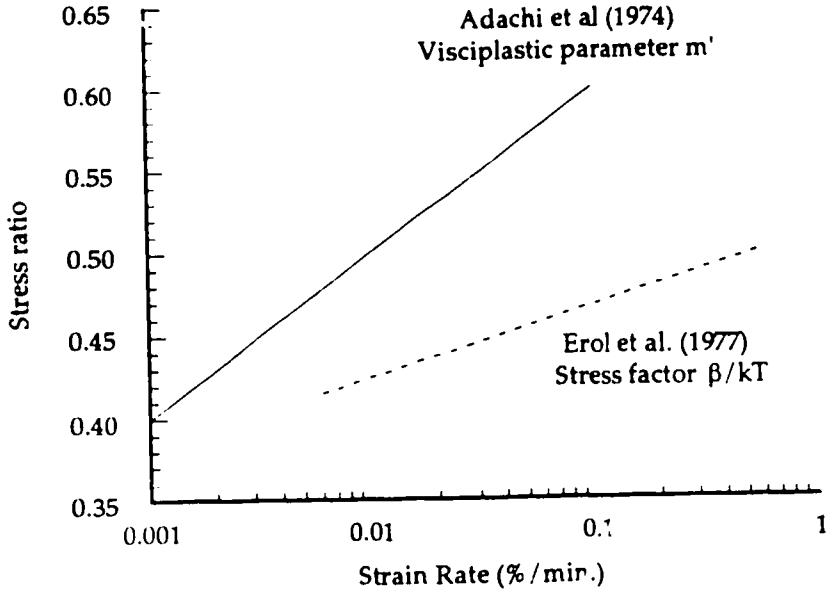

Figure 7.3 Comparison between the stress factor and the parameter m'

7.5.2. Viscoplastic Parameter C

From the undrained creep test results reported by Sekiguchi (1984), Adachi et al. (1987) deduced the behavior of the material parameter *C*. The conclusions have been summarized in (Figs. 7.1 & 7.2) as follows: *C* remains *constant* during constant strain rates, increases with *decreasing* strain rates before creep rupture, increases with *increasing* strain rates after creep rupture. It therefore reverses its relationship to strain rate upon failure. The point of reversal corresponds to the end of steady creep which is accompanied by hardening of the material. The information presented by Adachi et al. will be re-examined by considering the

change of the parameter C with respect to strain rate. It has been already stated that the parameter C measures the cumulative effect of the strain rate on the material deterioration and this is deduced from (Fig. 7.4). The actual effect of the strain rate on the parameter can therefore be described by the derivative of C (defined as a in the relationship $\ln C = a \ln d\varepsilon$) with respect to the strain rate.

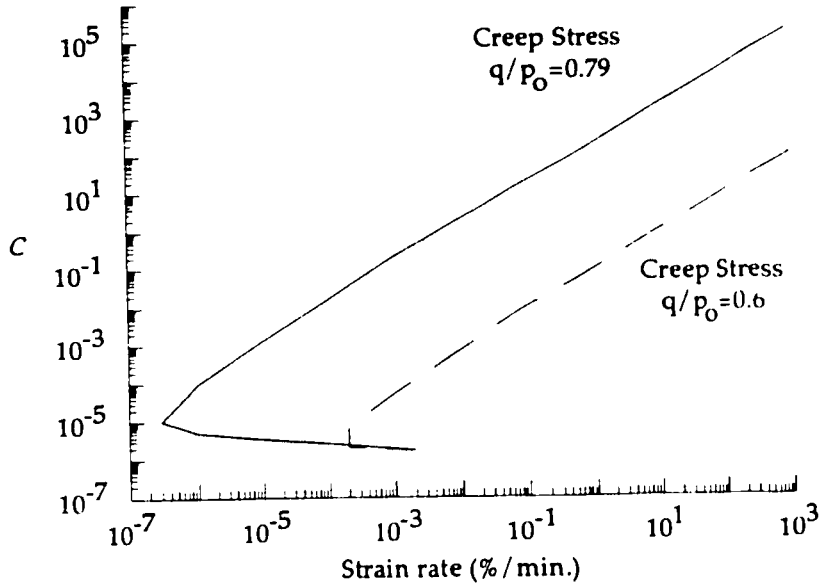

Figure 7.4 Evolution of C with respect to strain rate

The (Fig. 7.4) shows that the variation of C with strain rate has a negative slope up to the start of the acceleration creep after which point the variation has a positive slope. This relationship is seen to be unique during steady creep but a function of the creep stress after the onset of acceleration creep. However, (Fig. 7.4) clearly shows that the curves for creep stresses are similar to each other and that the difference between them is only the duration of creep rupture. The two curves therefore can be collapsed into a single curve (Fig. 7.5) if normalized by their respective creep rupture strains, times or strain rates. The unique curve thus obtained would express the behavior of samples under different creep stresses but at equivalent structures and therefore be a unique relationship between C and the strain rate.

The new parameter a therefore behaves somewhat like entropy during the deformation process, decreasing during steady creep (indicating increased orderliness) and increasing during acceleration creep (indicating increasing chaos).

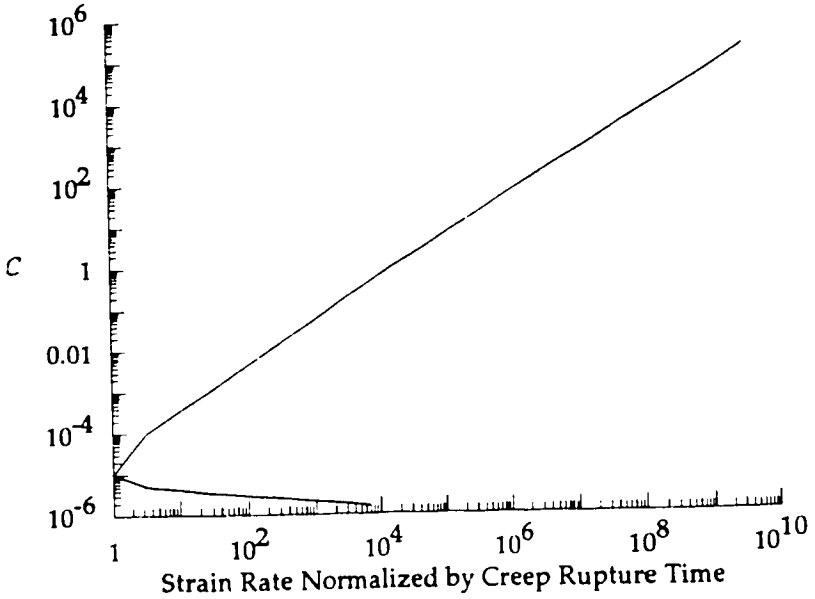

Figure 7.5 Evolution of C with respect to normalized strain rate

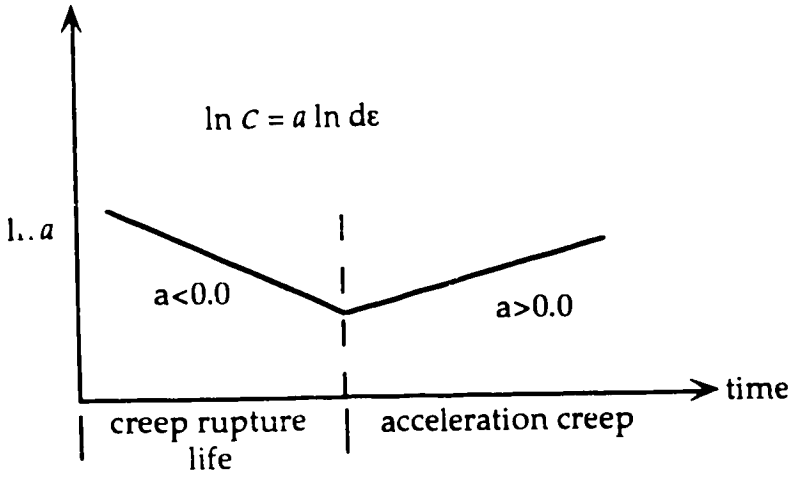

Figure 7.6 Rate of change of C with time

7.6. Synthesis of the Observations

The relationship of C with the stress ratio and the strain rate defines a three dimensional curve in the stress-strain rate-C coordinate system. This space provides the description of the physical processes occurring within the material. As such, the curve defines the structural changes in the material fabric for a given stress-strain relationship. The projections of the curve in the ln C-(M-q/p) plane and the ln C-ln $d\varepsilon$ planes have been given in (Fig. 7.1) and (Fig. 7.4) respectively.

The existence of a unique three dimensional curve describing the stress-strain-structure behavior of the material is in accordance with the conclusions reached by Erol et al. concerning the existence of a single process governing the stress-strain-time response of soft clays. The single curve obtained from the Adachi model obeys the principles of the phenomenological viscoplastic models and at the same time, the physical processes are reflected in the evolution of the time dependent parameters used in the model.

The ability of the Adachi model to describe a wide range of time dependent responses seems to stem from the fact that the time dependent parameters required by this model are in fact internal state variables that are the fundamental indicators of the mechanical behavior of materials. The determination of the time dependent parameters are fairly straightforward and even though they do not reflect their physical meanings immediately, complicated measurements and calculations of stress factors and entropies are avoided.

7.7 Conclusion

The parameter m′ has been identified as the equivalent of the stress factor associated with energy barrier height in physical models. This variable determines the relative movement of particle clusters past each other. The stress factor is a function of the size of the clusters (flow volume or flow unit) acting together as well as the energy required to cause deformation. Consequently increasing stress factors or m′ for that matter, indicate hardening behavior and vice versa for softening behavior.

In fact, the increase in the parameter m' has been observed and reported since the conception of the Adachi model. One aspect of m' that has not been discussed in the definition of acceleration creep is that since the creep rupture is the start of the material disintegration, the clusters must get smaller as failure propagates throughout the sample. Therefore, after the onset of acceleration creep, the parameter m' must theoretically start decreasing towards zero.

The viscoplastic parameter C has been identified as a measure of the fact that the structure of the material is necessarily altered during deformations. This alteration is dependent on the strain rate and time. It is seen that the derivative of C with respect to strain rate gives the actual effect of the alterations: during steady creep (when the material is hardening) it is decreasing and during acceleration creep (when the material is softening or failing) it is increasing. The parameter a therefore gives a physical representation of the state of the structural integrity of the material at any given time during creep and the equivalent physical variable is deduced to be *entropy*.

This finding explains the apparent contradiction in the Adachi model concerning the fact that although C is related to material deterioration, it remains constant during constant strain tests. In fact, during constant strain rate tests, it is the rate of deterioration that remains constant, not the actual amount of alterations inflicted on the sample. The parameter a will still be following the behavior depicted in (Fig. 7.6).

CHAPTER 8 : NEW VIBRATIONAL SLUMP TEST FOR VERY SOFT CLAY

8.1. Background

The time dependent parameters which are required by the constitutive equation presented in Chapter 6 have been based on triaxial test results. Although this technique has often proved reliable for most soils, the effects of self weight become important for very soft clays and the triaxial apparatus is not designed to discern the deformations due to applied stresses from the deformations due to the inability of the specimen to support itself under its own weight.

To overcome this difficulty, a new testing technique which takes advantage of the time dependent deformation of a very soft clay specimen under its own weight. The *slump test* was developed at the Civil Engineering Department of Kyoto University by Prof. T. Adachi with the participation of Prof. F. Oka, Dr. M. Mimura and Mr. S. Takigawa.

The objective of the test is to eliminate the difficulties of preparing and testing very soft clays under triaxial or unconfined conditions. The material parameters which require such tests are the critical state parameter M^*, the elastic shear modulus G, and the viscoplastic parameters m' and c. Since M^* is a unique parameter for a given clay, it can be evaluated from samples under higher preconsolidation pressures, therefore eliminating the difficulties associated with very soft samples. The other constants used in the model (λ & κ) are determined from oedometer tests which are valid for even very soft clays. The remaining three parameters (G, m', c) are stress level dependent and must be evaluated by back analyzing the results from the slump tests.

The slump test has proved to be a useful tool for the determination of material parameters when the clay is so soft that it does not lend itself to handling and proper testing by conventional methods. Starting from this fact, a new test has been developed to determine the same material parameters for soft clay samples subjected to vibration. The objective of the test is twofold: to determine (i) the material parameters relevant for vibrational loading conditions and (ii) the effect of vibration on the mechanical and physical behavior of soft clays.

8.2. Description of The Vibrational Slump Test

8.2.1. Test Set-Up

The apparatus is shown in (Fig. 8.1) and consists of a proximitor measuring the vertical displacement of the top surface of the sample, an accelerometer measuring the acceleration of the sample, and the supporting rigid frame. The samples are contained in sampling tubes of inner diameter of 5.0 cm. and the soil is pushed out of the tube immediately prior to the beginning of the test by means of a piston activated by a platform jack.

The piston is inserted into the sampling tube and fixed in position. The test sample being still in the tube, the proximitor target (a thin steel plate with a total weight of 40 gr.) is placed over the surface. The tube clamp is untightened and the piston is jacked up until the prescribed amount of soil is extruded (5 cm. in this study). The slump measurements are taken for a duration of 60 minutes and water content samples are taken immediately after.

The entire frame is mounted on a shaking table which is also fitted with an accelerometer. The characteristics of the table are as follows: maximum amplitude 13 mm. , maximum acceleration 1 G, maximum movable weight 124 kg., frequency range 1-100 Hz.

The readings are collected electronically by the proximitor, the two accelerometers, an LVDT attached to the table, and the frequency output of the shaking table drive unit. The first of these readings provides the vertical slump displacement, the second, accelerations for the sample and the table, the third, horizontal displacement of the table, and the fourth the frequency of vibration. All reading instruments are connected to an X-Y plotter except the table driver unit which is connected to an oscilloscope.

During the initial "empty runs" it was observed that the values of acceleration, frequency and displacement for the table corresponded to the values measured at the top of the frame, therefore establishing that the frame acted as part of the table as far as the vibrations are concerned. All frequency and acceleration setting were determined during these dry runs to ensure precision during tests.

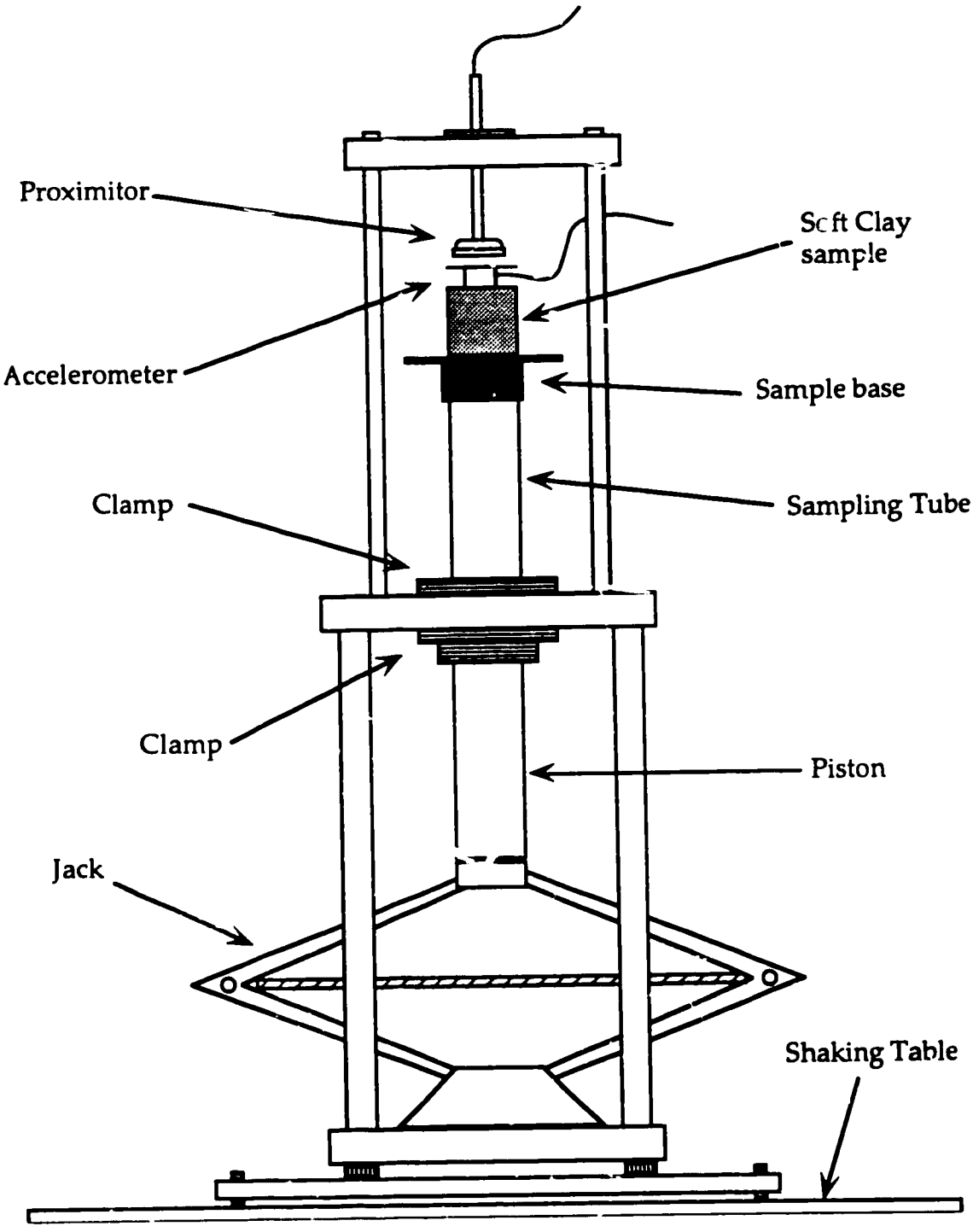

Figure 8.1. The Vibrational Slump Test Apparatus

8.2.2. Sample Description

The soil used for the tests is remoulded Osaka Clay of medium plasticity with the properties as listed in Table 8.1. Two clay mixtures were prepared and placed in rectangular plastic bins where they were left to consolidate for one month under pressures of 0.16 kg/cm^2 (16 kPa.) and 0.08 kg/cm^2 (8 kPa.) respectively. The cohesion intercept from vane tests and the average water content of the bins for both clays are given in Table 8.2.

Table 8.1. Index Properties for Remoulded Osaka Clay

Specific Gravity G_s	2.654
Liquid Limit LL (%)	106.6
Plastic Limit PL (%)	50.2
Plasticity Index PI (%)	56.4

The sampling tubes were subsequently pushed into the clay and typically contained a sample 13 cm. in length. This also meant that the water content of the clay contained in the top half of the tube would be more than the sample at the bottom half. From each soil bin, 11 tubes were filled, enough for 22 slump tests for each clay. One tube was used in the calibration and the first trials of the test apparatus and no record was kept from the test run, leaving a total of 42 tests from which data is reported.

Table 8.2. Mechanical Properties of Remoulded Osaka Clay

Preconsolidation pressure		
16 kPa.	Water content	109.3 %
	Cohesion intercept C	2.96 kPa.
8 kPa.	Water content	126.7 %
	Cohesion intercept C	1.49 kPa.

8.2.3. The Test Program

In addition to static slump tests, both clays were subjected to four frequencies (5, 20, 30, 50 Hz.) with at least two accelerations (0.1 gal, 0.2 gal.) each, except for sample #42 where only one acceleratior (0.05 gal.) was applied. The test program for both clays is presented in Table 8.3 and Table 8.4 .

Table 8.3. Test Conditions for samples preconsolidated to 16 kPa.

Sample No.	Frequency (Hz.)	Acceleration (gal.)	Water Content (%)	Water content / LL
1	0	0	121	1.14
2	0	0	106	1
3	0	0	117	1.1
4	0	0	117.5	1
9	5	0.1	118	1.11
10	5	0.1	107	1
11	5	0.2	114	1.07
12	5	0.2	106	1
13	5	0.3	116.5	1.1
14	5	0.3	107	1
21	20	0.1	116	1.1
22	20	0.1	108	1
23	20	0.2	117	1.1
24	20	0.2	106	1
29	30	0.1	120	1.13
30	30	0.1	107	1
31	30	0.2	117	1.1
32	30	0.2	106	1
37	50	0.1	117.5	1.1
38	50	0.1	106	1
39	50	0.2	120	1.12
40	50	0.2	108	1

Table 8.4. Test Conditions for samples preconsolidated to 8 kPa.

Sample No.	Frequency (Hz.)	Acceleration (gal.)	Water Content (%)	Water content / LL
5	0	0	164	1.55
6	0	0	139	1.3
7	0	0	159	1.5
8	0	0	140	1.3
15	5	0.1	158	1.5
16	5	0.1	138	1.3
17	5	0.2	156	1.5
18	5	0.2	140	1.3
19	5	0.3	163	1.5
20	5	0.3	138	1.3
25	20	0.1	154	1.45
26	20	0.1	140.5	1.3
27	20	0.2	157	1.5
28	20	0.2	133	1.2
33	30	0.1	154	1.45
34	30	0.1	136	1.3
35	30	0.2	164	1.55
36	30	0.2	140	1.3
41	50	0.05	162	1.5
42	50	0.05	136	1.3

All tests were conducted for a duration of 70 minutes out of which the initial 10 minutes were static slump tests. This was done to establish a base line for the comparison of different samples given the fact that samples of the same clay with the same water content may show different slump behavior even under the same vibration. Handling, sample preparation, extrusion from the tube are some of only the more obvious causes of variations in mechanical response.

The frequencies and acceleration used in the test program have been chosen in accordance with field measurements involving accelerometers. The site of the Yorishima landfill has been monitored continuously since construction. The field measurements include measurements of horizontal displacements as well as accelerations with respect to depth due to traffic on the landfill.

The frequency spectrum of the vibrations imposed on the landfill shows a very distinct peak at 3 Hz. and the range of acceleration input from traffic loading is from 0 to 50 gal. It is also observed that the peak accelerations are attenuated to within 10% at a depth of 10 m. and the same contour reaches the surface at about 30 m. from the location of the source. Therefore, the acceleration "bulbs" are rather flat ellipses with their short radii directed towards the depth of the deposit. This is clearly in contrast with the elastic stress distribution in the soil where the pressure bulbs are elongated in the direction of the depth.

The frequency range that has been studied has another, more fundamental significance: the cyclic or repeated loading of clays has historically been studied under very low frequencies. This has been necessary for the accurate measurement of effective stresses. The objective of the vibration test is quite distinct from the objectives of the cyclic tests. Whereas the latter concentrates on the loading-unloading behavior of clays, the former is concerned with the effect of frequency content on the viscoplastic properties of the soil.

8.3. Test Results

The results of the vibration slump test will be presented in the following sequence: the effects of the acceleration on deformation will be presented first, followed by the effects of frequency of vibration on the deformation. The term deformation is taken in its broad mechanical sense, defining displacements, strains and strain rates. Since all tests were conducted under unconfined self-weight loading conditions, all data will be presented as a function of time. Naturally, for each clay only the samples with similar water contents are compared. It is a well known fact that higher water contents imply more deformable clays and therefore this aspect of the findings will be taken for granted.

8.3.1. The Effects of Acceleration on the Deformation

The vibration test results show that the effects of varying accelerations in the range 0.1 gal. to 0.2 gal. do not seem to affect the mechanical behavior of the soil. The strain rate-time plots presented in (Figs. 8.2, 8.3) show that the strain rates vary more with water content than the different accelerations. Although this may be partly due to the small range of accelerations imposed on the samples, the conclusion from the plots is that the behavior of the samples subjected to the same frequencies is independent of the accelerations used in these tests.

This conclusion is a valuable one from the point of view of data analysis in that the values collected with different accelerations of the same frequencies can now be used together as long as the samples are compared to others with similar water contents.

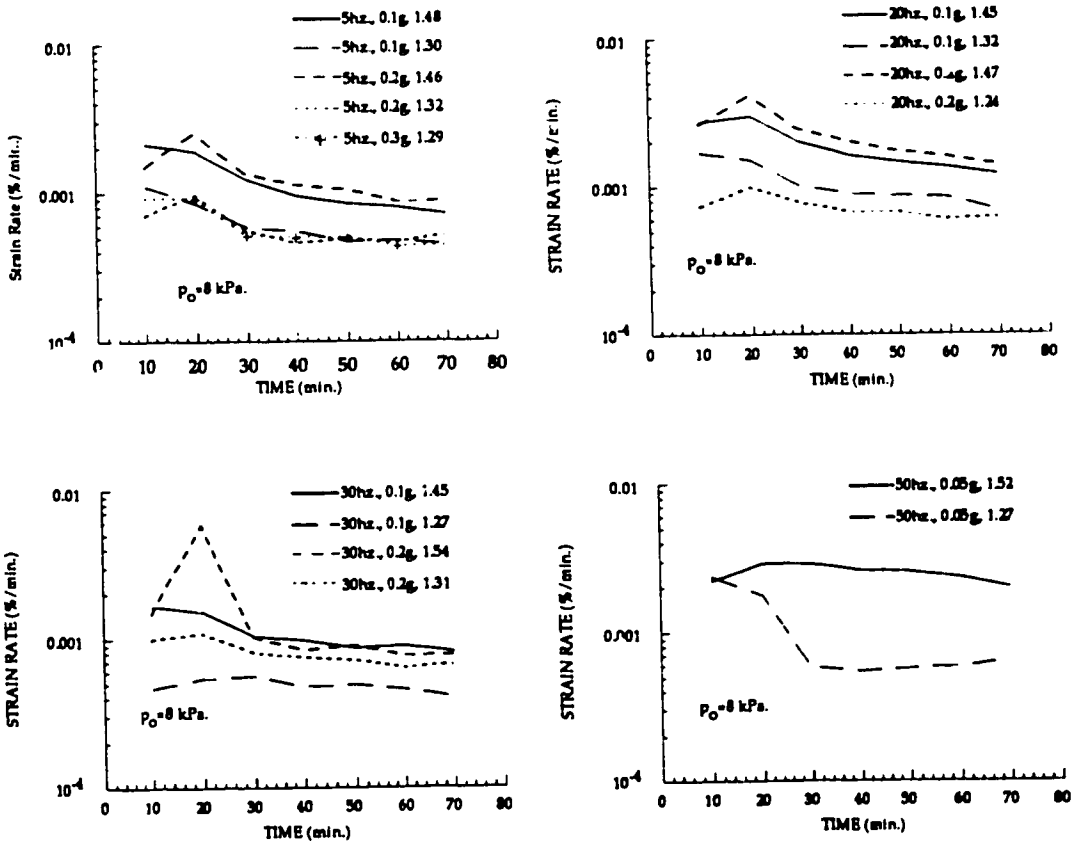

Figure 8.2 Acceleration effects on strain rate for p_o=8 kPa. (legend: frequency, acceleration, normalized water content)

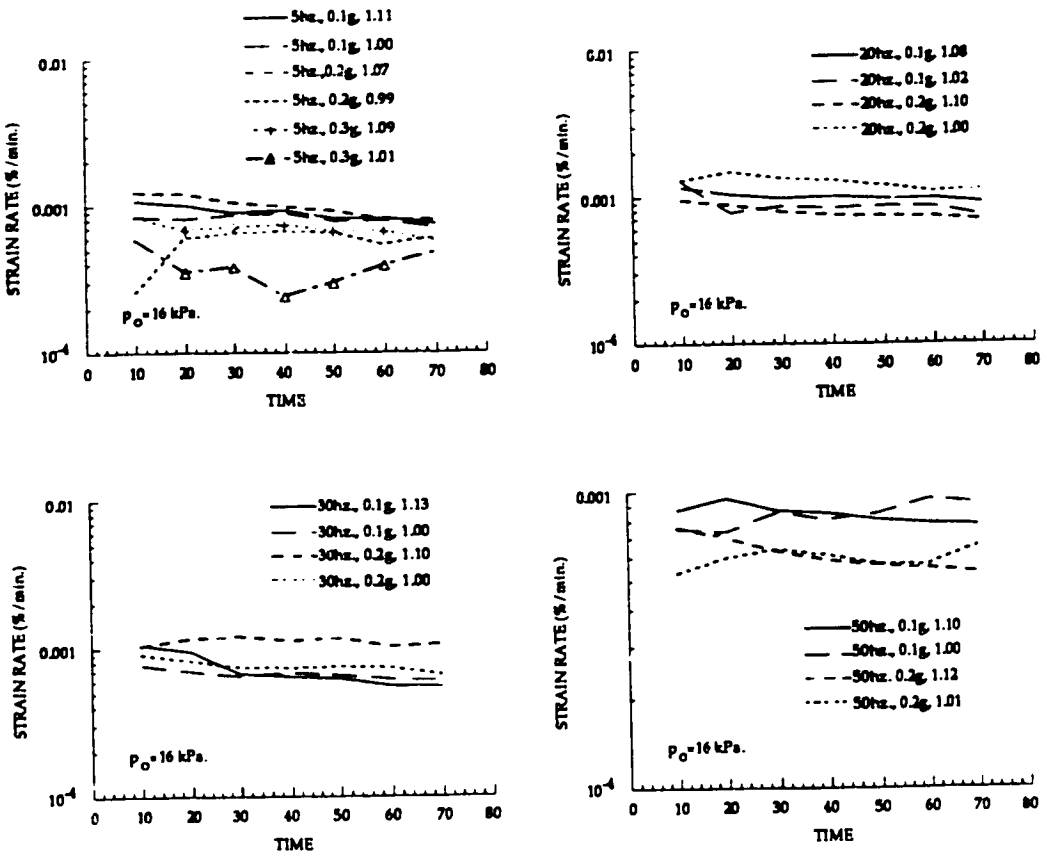

Figure 8.3 Acceleration effects on strain rate for p_o=16 kPa. (legend: frequency, acceleration, normalized water content)

Acceleration effects are visible at the higher frequencies of 30 and 50 Hz. for both soils. For lower frequencies however, the water content, rather than the acceleration dictates the differences between samples subjected to the same vibration. Furthermore, the acceleration does not change the general trends observed in all samples and therefore it will be considered to be inconsequential as far as the response of the sample to frequency is concerned.

8.3.2. The Effects of Water Content on Deformation

The dependency of sample deformation with respect to frequency of excitation will be presented in the form of strain rate-time and strain-time relationships. The strain rate-time relationship is particularly important since it has been already shown that the evolution of the viscoplastic parameters depend on it.

Therefore, a strain rate-time-frequency relationship not only exhibits the dependence of deformation on frequency but also mirrors the physical processes that are associated with vibration effects.

A meaningful comparison between slump deformations under varying excitation frequencies involves the generalization of the deformation history for each frequency, each water content and preconsolidation pressure. Among these categories, the effects of water content for a given soil is shown to be essentially time independent and increasing water contents merely shift the strain or strain rate axes without introducing any additional non-linearities. The assumption made is that once the deformation-frequency-time relationship is given for a soil, it can be adjusted for the proper water content using a linear relationship (Figs. 8.4, 8.5).

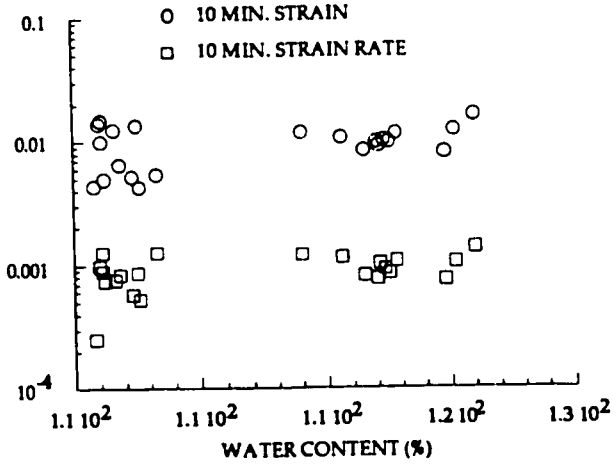

Figure 8.4. Strain and Strain rate dependency on water content (p_o=16 kPa., LL=106)

Based on the conclusions concerning the water content and acceleration, the frequency-deformation relationships are grouped under two categories according to the preconsolidation pressure of the samples.

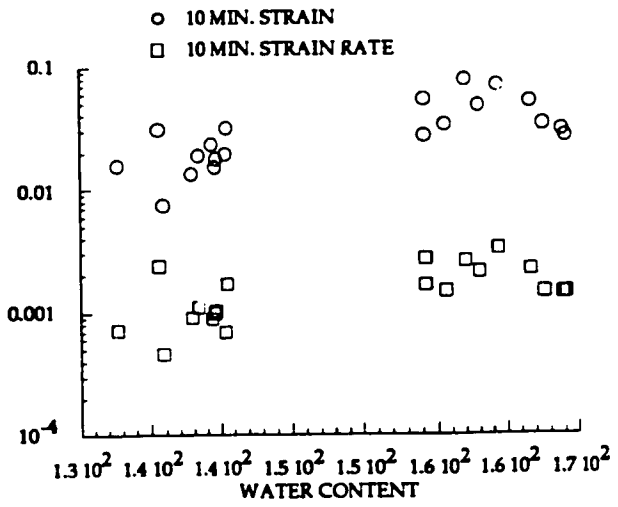

Figure 8.5. Strain and Strain rate dependency on water content (p_o=8 kPa., LL=106)

8.3.3. The Effects of Frequency on Deformation

The effects of vibration frequency on the deformation is presented by means of strain-time and strain rate-time relationships. The final objective in data analysis has been the creation of two plots (strain-time, strain rate-time) for each soil (p_o=8 kPa, p_o=16 kPa.) showing the static, 5, 20, 30, and 50 Hz. curves. To this end, all the strain-time and strain rate-time curves belonging to each frequency for each soil have been approximated as a single curve with a power law equation.

It is noted from the plots of strain-time and strain rate time (Fig. 8.6, 8.7) that most samples were not at equivalent states when the vibrations started at t=10 min. A clearer comparison of the effect of vibration is possible if all the curves are normalized by their respective strain and strain rates at t=10 min. (Fig. 8.8, 8.9). Through these plots, a surface in the frequency-time-deformation domain is obtained. The evolution of strains and strain rate are not directly proportional to the frequency and this point will be considered next.

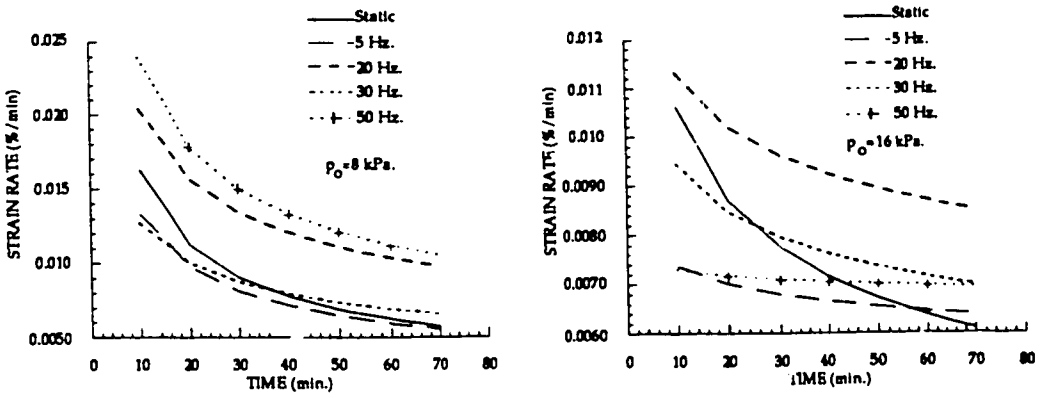

Figure 8.6 Strain rate-Time relationships as condensed from dynamic slump tests

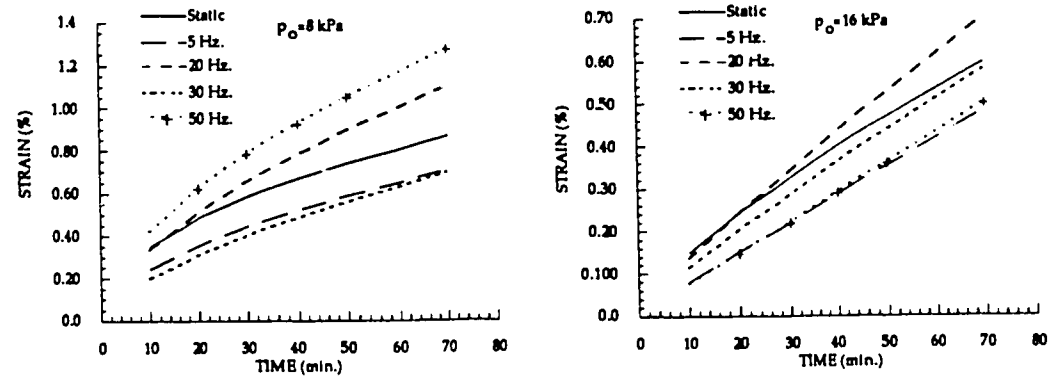

Figure 8.7 Strain-Time relationships as condensed from dynamic slump tests

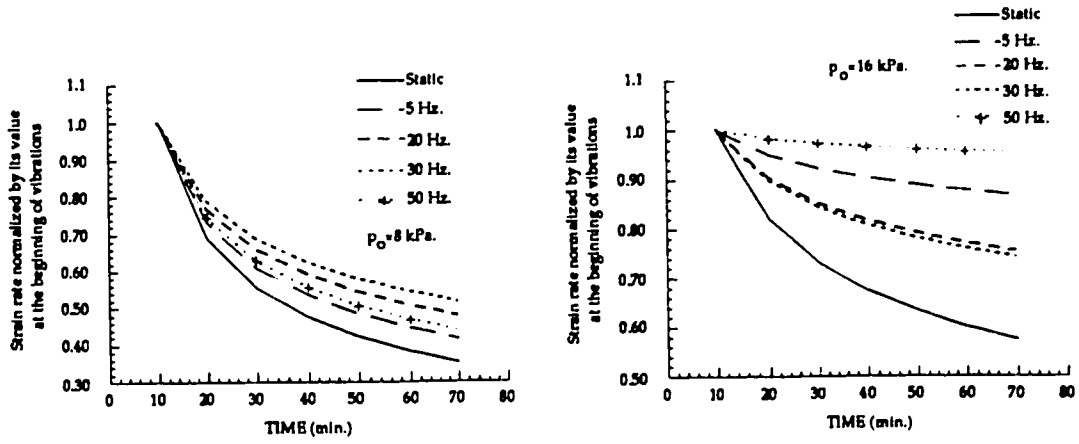

Figure 8.8 Normalized Strain rate-Time relationships as condensed from dynamic slump tests.

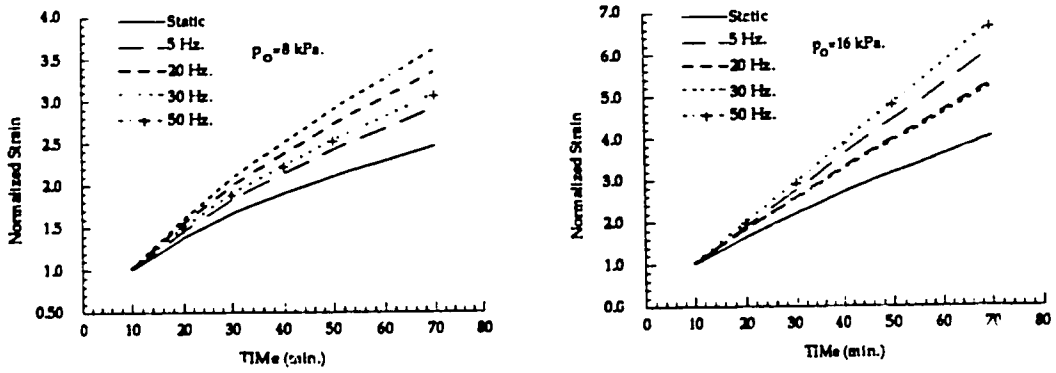

Figure 8.9 Normalized Strain -Time relationships as condensed from dynamic slump tests.

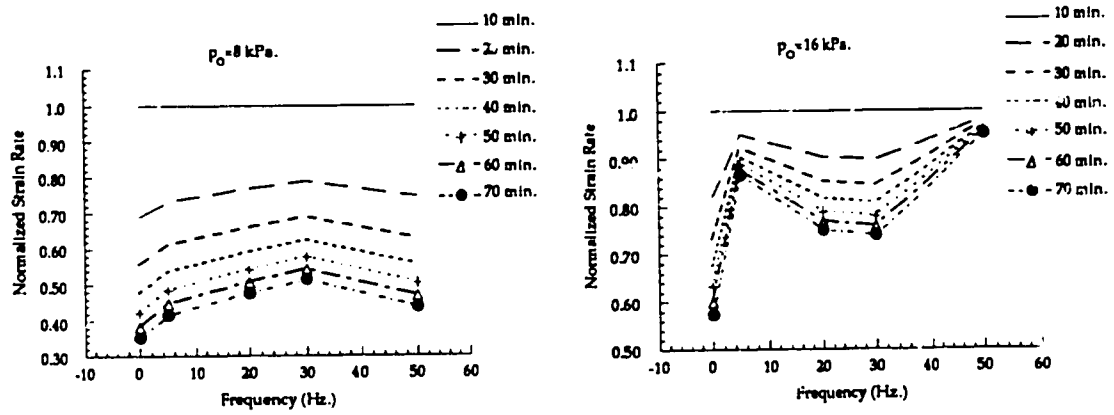

Figure 8.10 Normalized Strain Rate-Time-Frequency surface from dynamic slump tests.

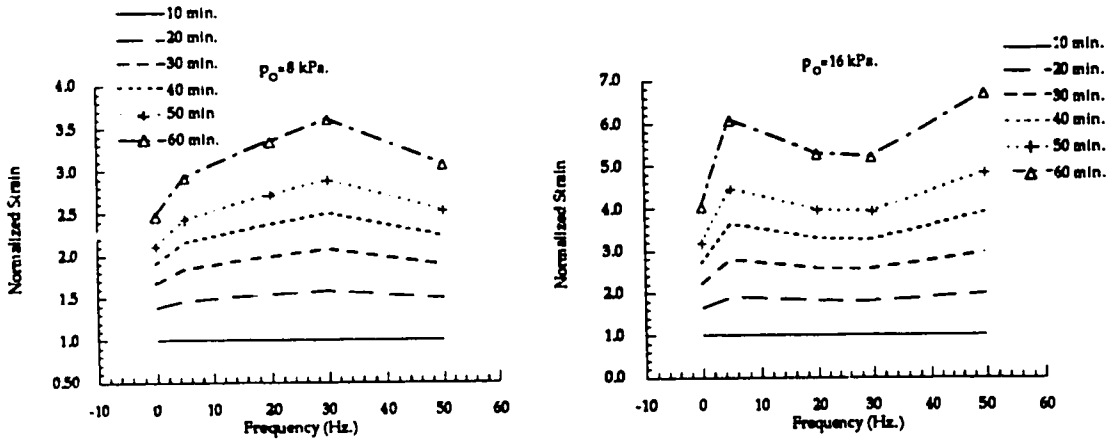

Figure 8.11 Normalized Strain-Time-Frequency surface from dynamic slump tests.

8.4. Discussion on the Vibrational Slump Test Results

It has been stated that the shaking table and the sample vibrations have been measured to correspond, effectively eliminating the possibility of the frequency-time-deformation surface being distorted by the resonance of the test rig or the sample itself.

The normalized frequency-time-strain rate surfaces show that the strain rates at the end of tests become higher with increasing frequencies. The effect is more pronounced for the samples preconsolidated under 16 kPa. This has been observed previously by Ishihara (1967) who concluded that samples with higher water contents are less affected by the frequency content of stress waves than samples with lower water contents, probably due to damping provided by water.

The fact that higher strain rates are maintained for higher frequencies implies that the vibration of the sample prevents the establishment of an equilibrium state where strain rates are zero. Thus within the frequency range studied, the vibrations prolong the steady creep stage for a given soil.

The normalized frequency-time-strain surface also shows that higher frequencies have relatively little effect on strains for both clays. This relationship holds for both clays, however one must keep in mind that the magnitudes of strains attained at the end of the test duration show that the softer clay deforms almost twice as much as the harder one. The published test data on the frequency effects on strain are rather conflicting. While Andersen (1975) reports that cyclic simple shear tests show no frequency effect (in the range 0.01-0.05 Hz.) on strain, Brewer (1972) has reported that in the range 0.01-4 Hz. the strains are inversely related to frequency. On the other, hand Brown et al. (1975) have found that strains are not affected by frequencies in the range 0.01-10 Hz.

It seems that the actual value of the vibration frequency does little as far as the evolution of strains with time is concerned. The flatness of the curves in (Fig. 8.11) implies that the mere existence of vibrations is more important than frequencies. It is also possible that the vibration itself interferes with the soil's tendency to deform under its own weight by not giving it enough time to respond to external agents.

8.5. Implications for the Viscoplastic Theory

The vibration of the unconfined soft clay sample was seen to lead to a softer response and this relationship is more pronounced for the harder sample. This behavior is in accordance with the thixotropic (reduction in strength under constant volume and water content) properties of soft clays where it is found that both the strain level and the water content play a major role in susceptibility to thixotropic effects [Mitchell (1960)]. The remoulding required to initiate thixotropy seems to be provided by the vibration.

The viscoplastic constitutive equation implicitly accounts for time dependency through parameters c and m′. Since the effects of vibrations are also time dependent, it is through the same parameters that they should be accounted for. This idea is further reinforced by the fact that both c and m′ mirror physical processes (stress factor and entropy) that are conceivably influenced by the presence of vibrations. The fact that thixotropic behavior is present indicates some remoulding, albeit in the micro-structural level, is taking place within the sample due to vibrations. Physically speaking, it is not unreasonable that the additional energy provided to the system will help the deformation by counteracting the inter-particle energy barriers, therefore decreasing the stress factor. At the same time, the mechanical effect of vibration would be a general increase in disorder (through remoulding) within the body, therefore increasing entropy.

The viscoplastic law predicts exactly this: keeping all parameters constant, a lower value of m′, or a higher value of c or the two together yield predictions that mimic the trends observed in vibration tests. The said variations cause the prevention of the strain rate decay with time while producing higher strains that show a softer response. For illustration purposes, the calculated effects of the viscoplastic parameters are shown in (Fig. 8.12).

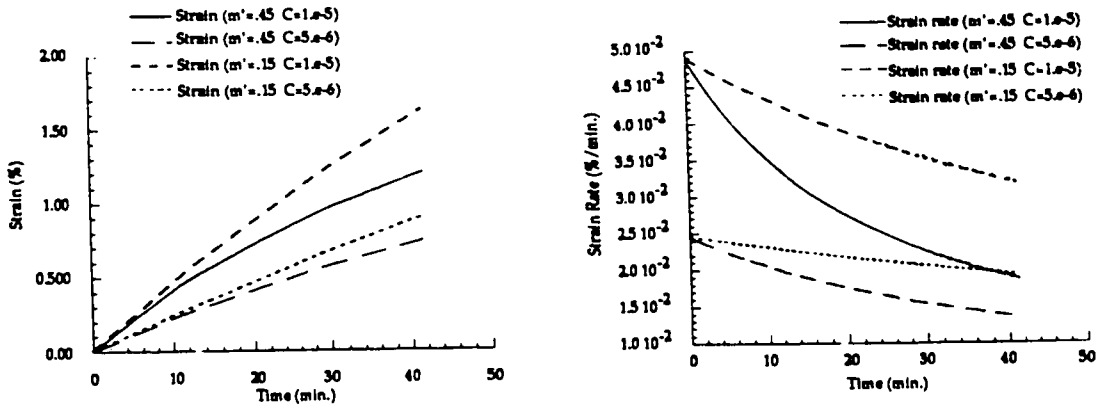

Figure 8.12 Calculated strain-time and strain rate-time curves
e_o=4.25, p_o=8 kPa., G=8 kPa., κ=0.08, λ=0.74, M=1.05 ,*C* and m'as indicated

8.6. Conclusion

The vibrational slump tests have proved to be a valuable tool in confirming the physical nature and significance of the viscoplastic parameters *C* and m'. As discussed earlier, these parameters are not only time dependent but also structure dependent. By establishing the deformation behavior of the material one is able to gain insight into the physical processes leading to the observed evidence.

The behavior of the clay samples show that under their own weight, higher strain rates and strains are sustained (material acting softer) as the frequency of horizontal vibration is increased. This observation is in agreement with the findings of Raymond et al. (1979). According to the viscoplastic constitutive model presented in Chapter 6, this behavior is described by higher values for *C* and lower values for m'. The physical rationale for this has been presented in section 8.5. In fact, it is natural that softer behavior should be characterized by higher *C* values since it was already demonstrated that the ageing effects are described by lower *C* values [Oka et al. (1986)].

CHAPTER 9 : ONE DIMENSIONAL STRESS WAVES IN SOFT CLAY

9.1. Preliminaries

As in the case of most mechanics problems, the propagation of waves through solids was first studied using the elasticity assumption. Lamb (1904) studied the response of an elastic half space vertical vibrations along a line and established solutions for two dimensional wave propagation. He also studied the effect of a single oscillating force in three dimensions which is known as the dynamic Boussinesq loading. The integration of its solution over a finite area of the surface will yield the contact pressure under the surface and so the dynamic response of the solid can be evaluated. This study demonstrated that the horizontal displacements produced by vertically oscillating forces are equal to the vertical displacements produced by horizontally oscillating forces. Reissner (1936,1937) obtained an analytical solution for the periodic vertical displacements at the center of a circular loading area. Sung (1953) described the displacement field under the loaded area with relation to various contact pressure distributions. He also described the response of an oscillating mass based on his calculations of these displacement fields. Quinlan (1956), based on Reissner's solution, accounted for the variation of the contact pressures across the diameter of the loaded area.

9.2. Inelastic Wave Propagation Through Soils

The elastic and the inelastic strains determine the energy losses occurring in the soil mass during the propagation of waves and the small amplitude stress-strain behavior of a soil mass will be assumed define the velocity of wave propagation. Most geotechnical problems (with the exception of earthquake and blast problems) involve harmonic waves (ocean floors subjected to sea waves, foundations under traffic or machinery loads, etc.) therefore the equation of motion is assumed to be valid everywhere in the material. The study of non-harmonic waves such as shock waves would require the use of jump conditions across the shock wave and the solutions would be less rigorous since the equations of motion are not valid at the face of a shock front.

9.2.1. Viscous Waves

Wave propagation in elastic media proceeds without wave form changes while in viscoelastic media, the propagation of waves is frequency dependent. Travelling waves undergo dispersion and the shape of the wave form cannot be preserved under these conditions. This phenomena is called ***wave attenuation*** and is the principal difference between elastic and viscoelastic materials.

The attenuation of the wave form has been studied by Salvadori et al. (1960) using a compacting and locking model. Viscoelastic models describing hysteretic materials have been proposed by Heierli (1962) and Seaman (1966). The latter model was successfully used for the prediction of the peak stress attenuation in clays. The viscoelastic wave propagation in clays was further studied by Vey et al. (1967) who proposed a non-linear Voigt model, and Hampton et al. (1967). These studies showed that the shear modulus and the damping of clays is independent of frequency. On the other hand, Kondner et al. (1965) and Hori (1974) reported that these characteristics do in fact depend on the frequency of the wave. The apparent conflict was explained by Ishihara (1976) and Osaki (1974) who reported that frequency dependence was itself a function of the strain level and water content: low strains or high water contents were found eliminate the dependency of shear modulus and damping on frequency.

9.2.2. Plastic Waves

It is a well known feature of plasticity that the stress-strain curves are different for loading and unloading phenomena. This feature is also the most basic difference between viscous waves and plastic waves. While viscous behavior gives priority to time effects, plastic behavior gives priority to non-linearity effects.

Karman et al. (1950) and Taylor (1958) proposed rate independent plasticity theories for metal bars. The rate dependent models proposed by Rakhmatulin (1945), Sokolovski (1948), Malvern (1951a,b), have laid the foundations of more genralized viscoplastic models by Whitman (1957), Parkin (1962), Perzyna (1963), and Cristescu (1968). The development and the salient features of the rate dependent models have been discussed in Chapter 5.

9.3. Propagation of Waves in Saturated Porous Media

Since natural soils are a mixture of solid and liquid parts, the wave propagation in mixtures must be specifically formulated. The basis of this formulation has been reported by Biot (1941, 1955, 1956, 1962, 1963) and has been the origin of many subsequent dynamic theories for multi-phase materials. The theory was subsequently extended and solidified by Truesdell (1960) who explicitly defined the principles of the theory, and the likes of Eringhen et al. (1967), Bowen (1982), and Prevost (1980) who have used general non-linear equations. The summary and full formulation of the above theories have been documented by Zienkiewicz (1984). In the following pages, the equations of solid-fluid mixture will be presented in the format compatible with soil mechanics problems.

a) State Variables

Total stress	σ_{ij}
Pore pressure	p
Average displacement of solids	u_i
Average relative displacement of fluid with respect to the solid particles	w_i
Pore fluid displacement	w_i/n
Porosity	n
Strain	$(u_{i,j} + u_{j,i})/2$

b) Effective Stress Principle

It is assumed that Terzaghi's effective stress concept is valid and that all strains are due to changes in effective stress σ'_{ij} (first term in eq. 1) and strains due to pore pressure changes are only relevant in materials such as rocks (second term in eq. 1). The strains due to creep, temperature effects are accounted for by the last term in equation (1).

$$\dot{\varepsilon}_{ij} = \dot{\varepsilon}^{\sigma'}_{ij} + \dot{\varepsilon}^{p}_{ij} + \dot{\varepsilon}^{o}_{ij} \qquad (1)$$

c) Constitutive Law

$$\dot{\sigma}'_{ij} = D_{ijkl}\left[\dot{\varepsilon}^{\sigma'}_{kl} + \dot{\varepsilon}^{o}_{kl}\right] \tag{2}$$

The tensor D_{ijkl} is the tangential material constitutive matrix.

d) Overall Equilibrium

$$\dot{\sigma}_{ij,j} + \rho\, g_i = \rho\, \ddot{u}_i + \rho_f\, \dot{w}_i \tag{3}$$

The density of the mixture is ρ, the density of the fluid is ρ_f, and g_i is the acceleration component.

e) Equilibrium of the Fluid Phase

$$-p_{,j} + \rho_f\, g_i = k_{ij}^{-1}\, \dot{w}_j + \rho_f\, \dot{u}_i + \frac{\rho_f}{n}\, \dot{w}_i \tag{4}$$

where k_{ij} is the permeability tensor.

f) Equation of Mass Balance

$$\dot{w}_{i,i} = -\dot{\varepsilon}_{ii} - \frac{(1-n)}{K_s}\dot{p} + \frac{1}{3K_s}\dot{\sigma}'_{ii} - \frac{n}{K_f}\dot{p} \tag{5}$$

where

Rate of pore volume decrease for incompressible soil particles	$-\dot{\varepsilon}_{ii}$
Rate of pore volume increase due to compression of soil grains by hydrostatic pressure	$-\frac{(1-n)}{K_s}\dot{p}$
Rate of pore volume increase due to compression of soil grains by mean effective stress	$\frac{1}{3K_s}\dot{\sigma}'_{ii}$
Rate of fluid expansion	$-\frac{n}{K_f}\dot{p}$
Average bulk modulus of solids	K_s
Average bulk modulus of the fluid	K_f

The terms containing K_s can be omitted for soils since the solid particles are essentially considered to be incompressible. The mass balance is then written as

$$\dot{w}_{i,i} = -\dot{\varepsilon}_{ii} - \frac{n}{K_f}\dot{p} \tag{6}$$

g) Formulation for Slow Speed Phenomena

The acceleration terms are neglected in the formulation of this class of problems.

$$\dot{w}_i \to 0 \quad , \quad \ddot{u}_i \to 0$$

Therefore, equations (4) and (5) will yield the equation of consolidation in the following form:

$$[k_{ij}\, p_{,j}]_{,i} - \dot{\varepsilon}_{ii} - [k_{ij}\, \rho_f\, g_i]_{,i} = \frac{n}{K_f}\dot{p} \tag{7}$$

h) Formulation for Medium Speed Phenomena

The condition for medium speed phenomena is

$$\frac{\dot{w}_i}{\ddot{u}_i} \cong 0$$

and the mass continuity equation (eq. 5) becomes

$$[k_{ij}\, p_{,j}]_{,i} - \dot{\varepsilon}_{ii} - [k_{ij}\, \rho_f\, g_i]_{,i} = \frac{n}{K_f}\dot{p} - [k_{ij}\, \rho\, \ddot{u}_j]_{,i} \tag{8}$$

i) Formulation for High Speed Phenomena

The condition for very rapid phenomena (undrained behavior) is

$$\dot{w}_i \to 0\,,\ \dot{w}_i \to 0\,,\ w_i \to 0$$

or

$$k_{ij} \to 0$$

The equation of mass continuity in this case becomes

$$\dot{\varepsilon}_{ii} = -\frac{n}{K_f}\dot{p} \tag{9}$$

9.4. Solution Semilinear Rate Type Constitutive Equations

The rate type constitutive equation has been presented in Chapter 5 and its solution in the context of viscoplastic propagation of stress waves will be obtained using the method of characteristics [Courant et al. (1962)]. The triaxial undrained conditions will be imposed on the soil and the relative velocity of the solid particles to the fluid is assumed to be zero. Ishihara (1967) has shown that when the relative velocity is non zero and that the frequency of the wave is in the range 0.16-5 Hz. the interaction term in equation (8) becomes predominant and the behavior becomes a consolidation pheomena. The general form of the constitutive equation in domain $\mathcal{D}$ is given by

$$\dot{\sigma} = f(\sigma,\varepsilon)\,\dot{\varepsilon} - g(\sigma,\varepsilon) \tag{10}$$

where ε is the axial strain and σ is the total stress and the dots indicate time derivatives. The functions f and g represent the elastic and time dependent response coefficient matrices. The displacement of any particle is given by where χ is the Lagrangian coordinate and x is the current one.

$$u = \chi - x \tag{11}$$

The strain is therefore defined in equation (12) and is positive in compression.

$$\varepsilon = 1 - \frac{\partial x}{\partial \chi} = \frac{\partial u}{\partial \chi} \tag{12}$$

The compatibility of strains and displacements is

$$-\dot{\varepsilon} = \frac{\partial \dot{u}}{\partial \chi} \tag{13}$$

The balance of momentum will give

$$-\dot{\sigma} = \rho\,\ddot{u} \tag{14}$$

The system of partial differential equations (10), (13), and (14) are to be solved simultaneously for the description of the wave propagation.

$$\begin{aligned} \rho \frac{\partial \dot{u}}{\partial t} - \frac{\partial \sigma}{\partial x} &= 0 \\ \frac{\partial \varepsilon}{\partial t} - \frac{\partial \dot{u}}{\partial x} &= 0 \\ \frac{\partial \sigma}{\partial t} - f(\sigma,\varepsilon)\frac{\partial \dot{u}}{\partial x} + g(\sigma,\varepsilon) &= 0 \end{aligned} \tag{15}$$

The system is written in the normal vectorial form as

$$\frac{\partial U}{\partial t} + A\frac{\partial U}{\partial x} + B = 0 \tag{16}$$

where

$$U = \begin{Bmatrix} \dot{u} \\ \sigma \\ \varepsilon \end{Bmatrix} \quad ; \quad A = \begin{bmatrix} 0 & -\frac{1}{\rho} & 0 \\ -f(\sigma,\varepsilon) & 0 & 0 \\ -1 & 0 & 0 \end{bmatrix} \quad ; \quad B = \begin{Bmatrix} 0 \\ g(\sigma,\varepsilon) \\ 0 \end{Bmatrix}$$

The equation (16) must be hyperbolic for the existence of real acceleration waves and this condition is satisfied if all the Eigenvalues are real and all Eigenvectors are linearly independent [Cristescu (1968)]. Under these conditions, the equation (16) can be represented by its characteristic equation as

$$l_i\left(\frac{\partial U}{\partial t} + \lambda_i \frac{\partial U}{\partial x}\right) + l_i B = 0 \tag{17}$$

with λ_i as Eigenvalues and l_i as the Eigenvectors such that

$$\lambda_i A = \lambda_i l_i \tag{18}$$

The Eigenvalues are determined as the roots of equation (19)

$$\lambda\left(\lambda^2 - \frac{f(\sigma,\varepsilon)}{\rho}\right) = 0 \tag{19}$$

The Eigenvalues are evaluated as

$$\lambda = \frac{\partial x}{\partial t} = 0 \quad ; \quad \lambda = \frac{\partial x}{\partial t} = \sqrt{\frac{f(\sigma,\varepsilon)}{\rho}} \quad ; \quad \lambda = -\frac{\partial x}{\partial t} = -\sqrt{\frac{f(\sigma,\varepsilon)}{\rho}}$$

The corresponding Eigenvectors are

$$l_1 = \begin{Bmatrix} 0 \\ 1 \\ -\rho\lambda \end{Bmatrix} \; ; \; l_2 = \begin{Bmatrix} -\rho\lambda \\ 1 \\ 0 \end{Bmatrix} \; ; \; l_3 = \begin{Bmatrix} \rho\lambda \\ 1 \\ 0 \end{Bmatrix}$$

Along each of these characteristic lines which represent the wave fronts, the relations to be satisfied are respectively (from eq. 15)

$$\begin{aligned} \frac{\partial\sigma}{\partial t} - f(\sigma,\varepsilon)\frac{\partial\varepsilon}{\partial t} + g(\sigma,\varepsilon) = 0 \\ \frac{\partial\sigma}{\partial t} - \rho\lambda\frac{\partial\dot{u}}{\partial t} + g(\sigma,\varepsilon) = 0 \\ \frac{\partial\sigma}{\partial t} + \rho\lambda\frac{\partial\dot{u}}{\partial t} + g(\sigma,\varepsilon) = 0 \end{aligned} \qquad (20)$$

The simultaneous solution of the system will be obtained by the finite difference method with boundary conditions specified at each finite end and the initial conditions along the characteristic $x=\lambda t$. Note that since the strain rate is not present in vector U, it cannot be defined at a finite end. This is physically reasonable since the strain cannot be measured at a free surface of a body.

9.5. Numerical Results and Discussion

The wave propagation through a clay deposit will now be investigated. The constitutive law governing the behavior of the soil is the viscoplastic model described in Chapter 6 and is assumed to be valid everywhere in the deposit. The clay layer is saturated and initially consolidated under K_o conditions. The boundary conditions are specified as horizontal shearing stresses at the bottom of the layer. The shear at the top surface is zero and the velocity is given.

The initial effective stress is $\sigma'_{ij(0)}$ and the initial mean effective stress is given by

$$\sigma'_{m(0)} = \frac{(1 + 2K_o)}{3} \sigma'_{11(0)} \tag{21}$$

The initial deviatoric stress and the second invariant of the deviatoric stress tensor are respectively given as

$$s_{ij(0)} = \begin{bmatrix} \frac{2(K_o - 1)}{3}\sigma'_{11(0)} & 0 & 0 \\ 0 & \frac{(K_o - 1)}{3}\sigma'_{11(0)} & 0 \\ 0 & 0 & \frac{(K_o - 1)}{3}\sigma'_{11(0)} \end{bmatrix} \tag{22}$$

$$\sqrt{2J_2} = \sqrt{\left[(2 - 2K_o)^2 + 2(K_o - 1)^2\right]\frac{\sigma'_{11(0)}}{9}} \tag{23}$$

Neglecting the body forces and the first order terms in the x_2 and x_3 directions and taking compressive strains as positive, the equation of motion and continuity are respectively

$$\rho \frac{\partial \dot{u}_2}{\partial t} = -\frac{\partial \sigma_{21}}{\partial x_1} - \frac{\partial \sigma_{22}}{\partial x_2} - \frac{\partial \sigma_{23}}{\partial x_3} = -\frac{\partial \sigma_{21}}{\partial x_1} \tag{24}$$

$$-\varepsilon_{12} = \frac{1}{2}\left(\frac{\partial u_2}{\partial x_1} + \frac{\partial \sigma_1}{\partial x_2}\right) = \frac{1}{2}\frac{\partial u_2}{\partial x_1} \tag{25}$$

The constitutive equation of the material has been assumed to be

$$\dot{\varepsilon}_{ij} = \frac{\dot{s}_{ij}}{2G} + \frac{\kappa}{1 + e}\frac{\dot{\sigma}'_m}{\sigma'_m}\frac{\delta_{ij}}{3} + \\ + C\exp\left[m'\left(\frac{\sqrt{2J_{2(d)}}}{\sigma'_{m(d)}} + \ln\frac{\sigma'_{m(d)}}{\sigma'_{me}} - \frac{1 + e}{\lambda - \kappa}\varepsilon^p_{kk}\right)\right]\left\langle\frac{s_{ij}}{\sqrt{2J_2}} + \left(M^* - \frac{\sqrt{2J_2}}{\sigma'_m}\right)\frac{\delta_{ij}}{3}\right\rangle \tag{26}$$

More specifically

$$\frac{\partial \varepsilon_{12}}{\partial t} = \frac{1}{2G}\frac{\partial \sigma'_{12}}{\partial t} + \frac{s_{12}}{\sqrt{2J_2}} C \exp\left[m' \left(\frac{\sqrt{2J_{2(d)}}}{\sigma'_{m(d)}} + \ln \frac{\sigma'_{m(d)}}{\sigma'_{me}} - \frac{1+e}{\lambda-\kappa} \varepsilon^p_{kk} \right) \right] \quad (27)$$

and

$$\frac{\partial \varepsilon_{kk}}{\partial t} = \frac{\kappa}{(1+e)\sigma'_m}\frac{\partial \sigma'_m}{\partial t} + C \exp\left[m' \left(\frac{\sqrt{2J_{2(d)}}}{\sigma'_{m(d)}} + \ln \frac{\sigma'_{m(d)}}{\sigma'_{me}} - \frac{1+e}{\lambda-\kappa} \varepsilon^p_{kk} \right) \right] \left(M^* - \frac{\sqrt{2J_2}}{\sigma'_m} \right) \quad (28)$$

The equations (24), (25) and (27) formulate the system of partial differential equations to be solved. Referring to the method of characteristic in the previous section, the differential equations along the characteristic lines are as follows

Along $dx/dt = \pm C$

$$d\sigma'_{12} = \pm C\, d\dot{u}_2 - 2G \frac{\sigma'_{12}}{\sqrt{2J_2}} C \exp\left[m' \left(\frac{\sqrt{2J_{2(d)}}}{\sigma'_{m(d)}} + \ln \frac{\sigma'_{m(d)}}{\sigma'_{me}} - \frac{1+e}{\lambda-\kappa} \varepsilon^p_{kk} \right) \right] dt \quad (29)$$

Along $dx/dt = 0$

$$d\varepsilon_{12} = \frac{d\sigma'_{12}}{2G} - \frac{\sigma'_{12}}{\sqrt{2J_2}} C \exp\left[m' \left(\frac{\sqrt{2J_{2(d)}}}{\sigma'_{m(d)}} + \ln \frac{\sigma'_{m(d)}}{\sigma'_{me}} - \frac{1+e}{\lambda-\kappa} \varepsilon^p_{kk} \right) \right] dt \quad (30)$$

where $C = (G/\rho)^{1/2}$ velocity of wave propagation.

A similar expression can be obtained for the compressive waves travelling through the soil as in the case of traffic loading on the surface of a clay deposit. The stress, strain and velocity components have to be altered accordingly and the following set of differential equations are obtained.

Along $dx/dt = \pm C$

$$d\sigma'_{11} = \pm C\, d\dot{u}_1 - \frac{(1+e)\sigma'_m}{\kappa} C \exp\left[m'\left(\frac{\sqrt{2J_{2(d)}}}{\sigma'_{m(d)}} + \ln\frac{\sigma'_{m(d)}}{\sigma'_{me}} - \frac{1+e}{\lambda-\kappa}\varepsilon^p_{kk}\right)\right]\left(M^* - \frac{\sqrt{2J_2}}{\sigma'_m}\right) dt \tag{31}$$

Along $dx/dt = 0$

$$d\varepsilon_{11} = \frac{\kappa}{(1+e)\sigma'_m} d\sigma_{11} - C \exp\left[m'\left(\frac{\sqrt{2J_{2(d)}}}{\sigma'_{m(d)}} + \ln\frac{\sigma'_{m(d)}}{\sigma'_{me}} - \frac{1+e}{\lambda-\kappa}\varepsilon^p_{kk}\right)\right]\left(M^* - \frac{\sqrt{2J_2}}{\sigma'_m}\right) dt \tag{32}$$

the wave propagation velocity $C = [(1+e)\sigma'_m/\kappa\rho\,]^{1/2}$.

The characteristic net is shown in (Fig. 9.1). The finite difference method is used to evaluate the system of three equations (29) and (30) (or equations 31 and 32). Given the particle velocity at points M_o and M_1 the stress and velocity are determined at point N_o through equations (29) (or eq. 31) while the strain at N_o is obtained by equation (30) (or eq. 32).

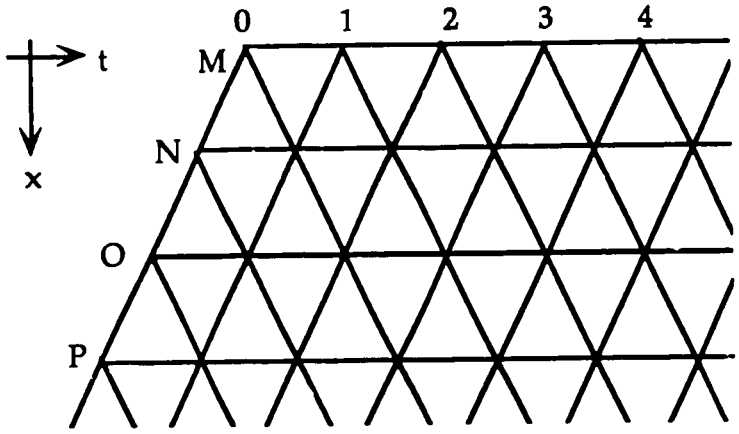

Figure 9.1 Characteristic Net

The analysis is applied to the propagation of one dimensional shear waves in an elasto-viscoplastic half space of 1 m. depth. The time and space increments are numerically the same and vary with the input frequency. The finite difference integration of the equations (31) and (32) has been carried out specifying the stress wave at the surface of the soil deposit at each time increment. Varying cycles were examined and the time increment was accordingly changed to capture the movement of the wave in the desired frequency. The soil was assigned the properties of remoulded Osaka clay with high plasticity and compressibility as described in the previous chapter. The actual parameters are listed below.

e_o	G (kPa.)	λ	κ	M*	c	m'	p_o (kPa.)
4.25	8000.0	0.74	0.08	1.05	$1\,e^{-5}$	0.45	16.0

It is seen (Figs. 9.2, 9.3, 9.4) that the elasto-viscoplastic model describes the wave attenuation phenomena weel. As the wave travels deeper into the clay deposit, its shape collapses due to energy dissipation by plastic deformations. The rate of attenuation of the wave decreases as well.

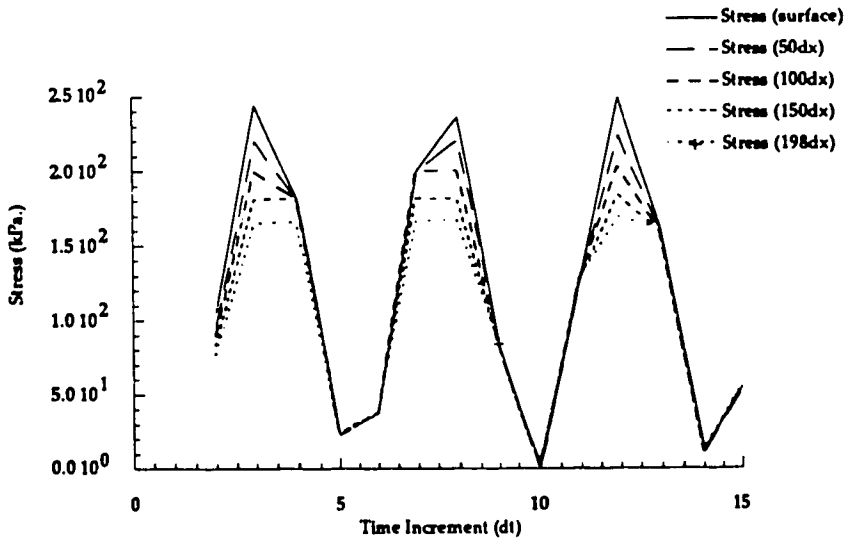

Figure 9.2 Plastic stress wave in soft clay, at the beginning of propagation (10 Hz., dt=0.01 sec.)

The rate of wave attenuation is more clearly seen in Fig. 9.3 where a slower stress cycle has been applied to the surface of the clay. The wave energy dissipation naturally increses as the distance of travel is farther. During the process viscoplastic strains are produced.

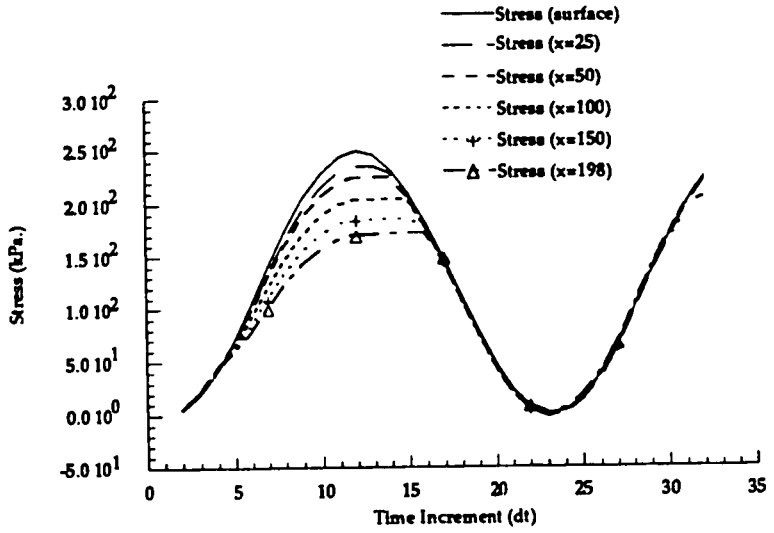

Figure 9.3 Plastic stress wave in soft clay at the beginning of propagation (3 Hz., dt=0.015)

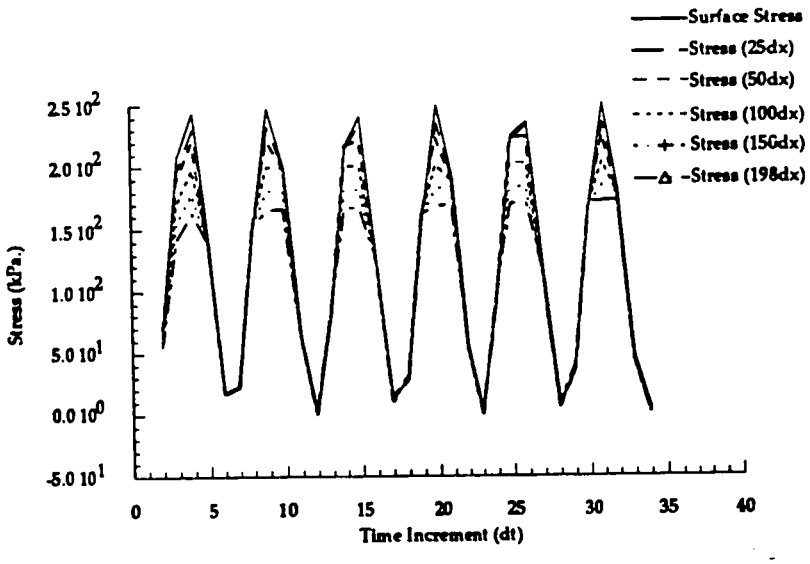

Figure 9.4 Plastic stress wave in soft clay, at the beginning of propagation (15 Hz. , dt= 0.0075)

The stress differences due to energy dissipation are time dependent and provided that the magnitude of the wave input is kept constant, the soil behaves elastically after a sufficient period of time has elapsed. Although the simulations have not been taken that far however the effect of time on the energy dissipation is clearly seen in Fig. 9.5 which is the tail end of the wave shown in Fig. 9.4.

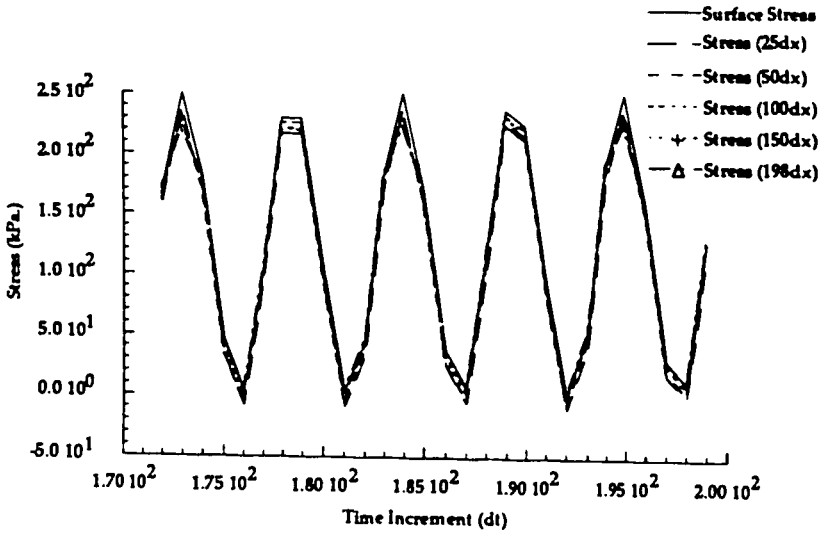

Figure 9.5 Plastic stress wave in soft clay approximately 50 cycles from start of propagation.

Differences between elastic and viscoplastic solutions decrease as vibration time increases. The behavior is elastic once the entire body has undergone plastic hardening.

The unloading has been assumed to be completely elastic and this fact may be a gross generalization of the cyclic clay behavior. Tests by Vey et al. (1967) have shown delayed elastic behavior and a more accurate analysis might be possible with a viscoelastic-viscoplastic model. Oka (1978) has proposed such a model and applied to the stress wave propagation problems. His constitutive model was based on the thermodynamic theory of mixtures and the viscoelastic behavior was represented by a linear dashpot-spring model previously studied by Akai et al. (1974).

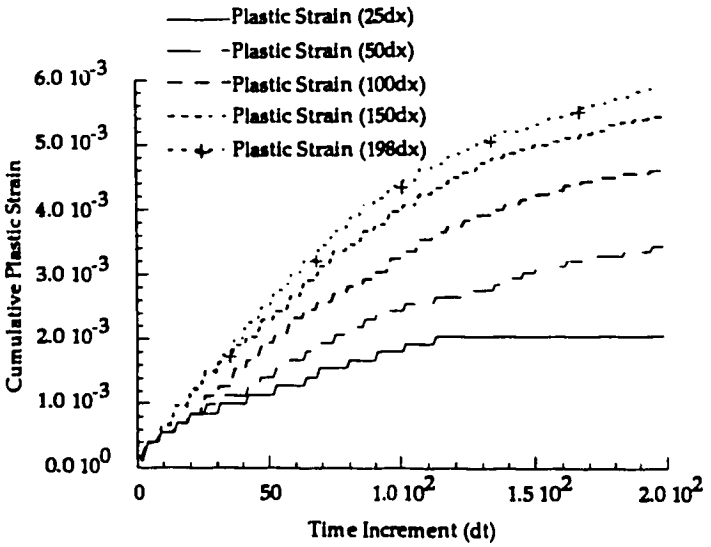

Figure 9.6 Stress strain curves for depths as indicated (15 Hz. , dt= 0.0075)

The plastic strains developed during the propagation of the waves are presented in Figure 9.6. The hardening of the clay is also apparent and it eventually results in an entirely hardened material where the behavior is purely elastic. The stress-strain relationships presented in Figures 9.7 and 9.8 show the hardening and the cyclic nature of the loads. The fact that the successive loading unoading lines (hysteresis loops) become closer indicate the dissipation of energy before a state of cyclic mobility is attained.

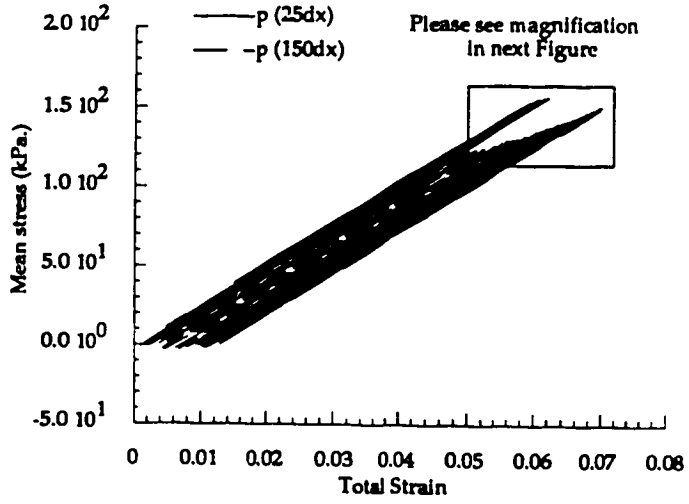

Figure 9.7 Stress strain curves for depths as indicated (15 Hz.)

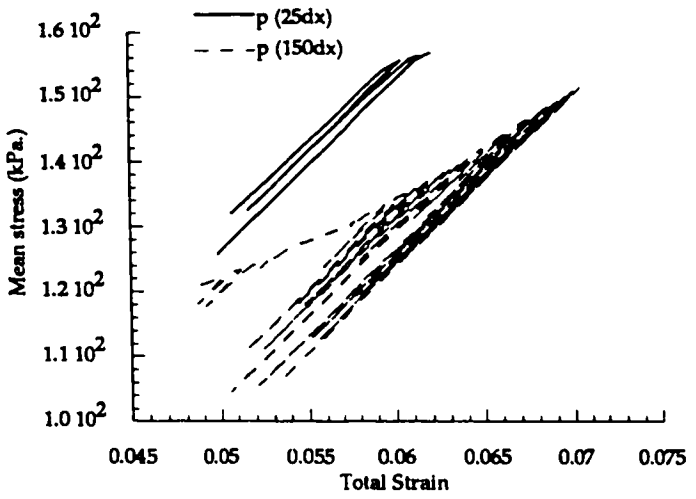

Figure 9.8 Magnified view from Fig. 9.7

In Figure 9.8, the hardening of the upper layers of the soil occurs fairly early (solid line) while deeper layers take considerably more time to undergo plastic hardening (dashed line). In effect, a hardened crust form close to the excited boundary and subsequent plastic deformation of the soil layer is due to the straining of the deeper layers. This conclusion agrees with the observed time lag in the distribution of stresses and strains in soft clays.

The effect of the boundary conditions cannot be overlooked in the foregoing analysis. It will be remembered that the stress at the free boundary of the elasto-viscoplastic body was used as a boundary condition, leading to the attenuation of the stress wave compared to the elastic solution. If on the other hand, the velocity of particle at the free boundary is specified the same analysis will show that the stress wave will be amplified compared to the elastic solution. This is the displacement approach and the stresses will tend towards the elastic stress from above while it was seen that the force approach will result in a solution tending towards the elastic solution from below.

The plastic strain rate behavior is shown in Fig. 9.9. It is interesting to note that although the same strain is reached at roughly the same number of increments, in reality the strain rates are dependent on frequency since the time increments for

each computation was different. In real time, the effect of frequencies on the total plastic deformation (Fig. 9.10) shows a frequency-time-strain surface similar to the experimental observations : while for low frequencies (3 Hz.) and higher frequencies (15 Hz.) the strains are comparable, the moderate vibrations (10 Hz.) cause more deformation. In fact, the differences in behavior are due to the actual rate of wave loading where there is a threshold frequency beyond which the soil is unable to respond immediately to the vibration and this response lag creates a behaviour similar to the ones obtained under lower frequencies (i.e. slower loading rates).

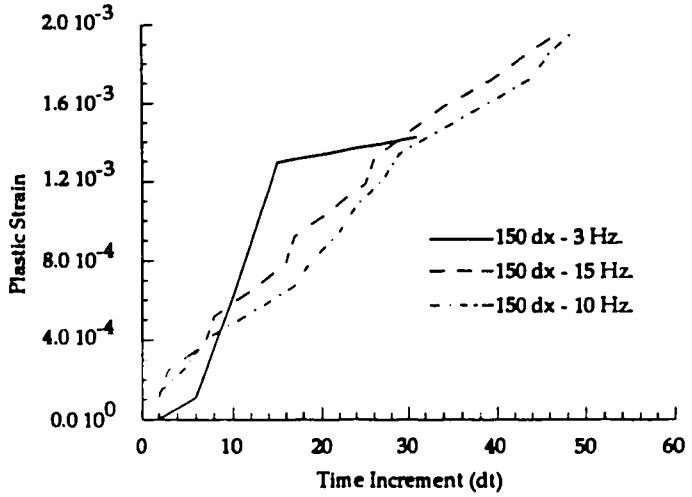

Figure 9.9 Plastic strain for various frequencies

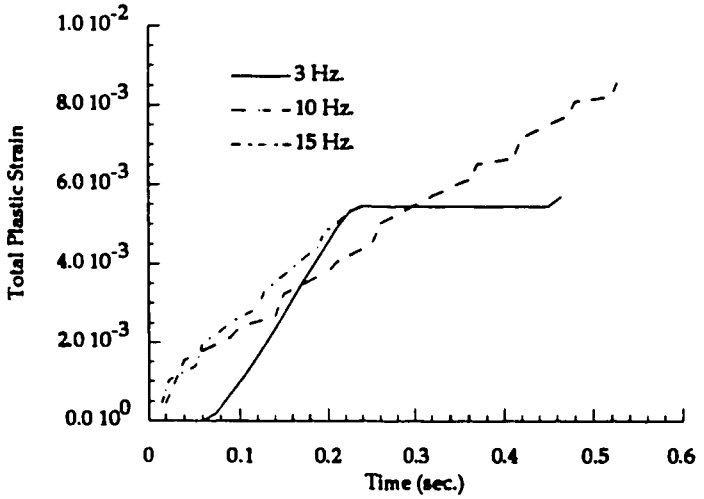

Figure 9.10 Total plastic strain for various frequencies

9.6. Conclusion

The wave propagation through cohesive soil has been described by the elasto-viscoplastic constitutive equation. The model predictions show that the dissipative nature of viscoplastic materials are well represented. It is seen that as time passes the vibrations cause plastic hardening of material and the wave propagation phenomena loses its rate and path dependence.

The decay of the waves and the relative speed with which loading is transferred to the soil implies that for the range of the frequencies considered in this study, the soft clay layer under vibratory loads approaches the instantaneous (elastic) response, as would be deduced from any rate type constitutive law.

When a stress pulse is applied to the boundary of the soil, the resulting stresses within the soil are lower than the elastic solution. The application of a displacement to the boundary will result in higher stresses than would be predicted by the elastic theory.

Although the final strains do not seem to depend on the frequency, the strain rates to attain a given strain magitude is clearly a function of the vibration frequency (note the slope of the lines in Fig. 9.10) . Based on the experimental results of the previous chapter, the stress controlled input has been shown to apply to the wave propagation through the soil. The calculated strain rate and the strain response show a distinct similarity to the responses observed in vibratory slump tests. Once again, it is seen that the effects of vibratory loading is felt the most for moderate frequencies (the vicinity of 10 Hz.) .

The final objective of the thesis will be the application of the elasto-viscoplastic constitutive model to boundary value problems in the light of the conclusions reached in Chapters 7, 8, and 9.

CHAPTER 10 : ANALYSIS OF BOUNDARY VALUE PROBLEMS

10.1. Introduction

The objective of this Chapter is the application of the ideas presented in previous sections to the analysis of soft clay foundations under static and vibratory loading conditions. The focus will be on the performance of land fills and subsequent land development on soft marine clays. The softening due to repeated loading [Fujiwara et al. (1990)] in the form of traffic vibrations will also be taken into account.

The predictions presented herein are validated against actual in situ measurements or trends concluded from in situ measurements. The following published data will be utilized:

Case	Author(s)	Published measurements
1	Shoji et al. (1990)	Vertical and horizontal displacements
2	Almeida et al. (1982)	Vertical and horizontal displacements
3	Mimura et al. (1990)	Vertical and horizontal displacements, pore pressures
4	Magnan et al. (1982)	Vertical and horizontal displacements
5	Western Japan Power Co. (1986)	Vertical and horizontal displacements under traffic load and construction activity

10.2. Methodology

The elasto-viscoplastic constitutive model is used in conjunction with the finite element method. The algorithm CRISP [Britto & Gunn (1987)] has been extended to allow the use of the viscoplastic constitutive equation. The new version has been named CRISPEX (CRISP-EXtended) and will be referred to as such in the following. The salient features of both programs will be outlined as the Chapter proceeds.

The finite element formulation is derived using the principle of virtual work (i.e., Gauss' theorem) which is expressed as

$$\int_v \{\Delta\varepsilon\}^T \{\Delta\sigma\}\, dv = \int_v \{\Delta u\}^T \{\Delta F_b\}\, dv + \int_s \{\Delta u\}^T \{\Delta T\}\, ds \qquad (1)$$

or

$$\int_v \{\Delta\varepsilon\}^T \{\Delta\sigma'\}\, dv + \int_v \{\Delta\varepsilon\}^T \{\Delta u_w\}\, dv = \int_v \{\Delta u\}^T \{\Delta F_b\}\, dv + \int_s \{\Delta u\}^T \{\Delta T\}\, ds \qquad (2)$$

In this equation Δu_w is the pore pressure increment vector, Δu is the displacement increment vector, ΔF_b is the body force increment vector and ΔT is the applied surface load increment vector. The displacements Δu in the element are expressed in terms of the interpolation functions N and the nodal displacement increments.

$$\{\Delta u\} = [N]\{\Delta \bar{u}\} \qquad (3)$$

The pore pressure Δu_w in the element are expressed in terms of

$$\{\Delta u_w\} = [\bar{N}]\{\Delta \bar{u}_w\} \qquad (4)$$

The strain increment vector and the volumetric strain increment are given as

$$\{\Delta\varepsilon\} = [B]\{\Delta u\} \qquad (5)$$

$$\Delta\varepsilon_{kk} = [C']^T \{\Delta u\} \qquad (6)$$

Where B is the strain-displacement compatibility matrix and [C'] is the volumetric strain nodal displacement matrix. A vector m is defined as m=<1,1,0> such that

$$\Delta\varepsilon_{kk} = [m]^T \{\Delta\varepsilon\} \qquad (7)$$

From which it can be deduced that

$$[C']^T = [m]^T [B] \qquad (8)$$

Substitution in the virtual work equation yields

$$[K]\{\Delta\bar{u}\} + \{K_v\}\Delta u_w = \{\Delta F\} \tag{9}$$

with

$$[K] = \int_v [B]^T [D][B]\, dv \tag{10}$$

$$[K_v] = \int_v [C'][\bar{N}]\, dv = \int_v [B]^T [m][\bar{N}]\, dv \tag{11}$$

The matrix [D] is the tangential material stiffness matrix. For elastic analyses, it represents the Hooke's Law in both CRISP and CRISPEX. For elasto-plastic analyses, the Original Cam Clay and the Modified Cam Clay relationships are included following the elastoplastic tangential stiffness matrix derivation by Zienkiewicz (1977). The new program has introduced an elasto-viscoplastic stiffness matrix proposed by Stolle et al. (1989). The integration in time is performed by an implicit scheme which takes full advantage of CRISP's solution algorithm (see section 10.3).

Including the contributions of the in situ stresses $\{\Delta\sigma_i\}$ the force vector is in equation (12). The first term on the right hand side of this equation includes self weight forces and gravity forces while the second term represents the effects of the element boundary pressures. The third term, as already stated, represents the stress state in the soil prior to load application. In the last term of this equation, the effect of the residual stress in excess of equilibrium is accounted for by the relaxation stress vector $\{\Delta\sigma_r\}$.

$$\{\Delta F\} = \int_v [N]^T \{\Delta F_b\}\, dv + \int_s [N]^T \{\Delta T\}\, ds + \int_v [B]^T \{\Delta\sigma_i\}\, dv + \int_v [B]^T \{\Delta\sigma_r\}\, dv \tag{12}$$

The description of the consolidation phenomena requires that the equation of continuity is also included in the formulation. The equation of continuity (eq. 13) will be discretized by the Galerkin weighted residuals method (eq. 14).

$$\frac{d\varepsilon_{kk}}{dt} = -\frac{k}{\gamma_w}\frac{\partial^2 u_w}{\partial x_i\,\partial x_i} \tag{13}$$

$$\int_v u_w^* \left[\frac{k}{\gamma_w}\frac{\partial^2 u_w}{\partial x_i\,\partial x_i} + \frac{\partial \varepsilon_{kk}}{\partial t}\right] dv = 0 \tag{14}$$

Where the scalar u^*_w is a virtual pore pressure.

The Zienkiewicz - Green theorem is applied to equation (14).

$$\int_v \left[\frac{k}{\gamma_w}\frac{\partial u_w^*}{\partial x}\frac{\partial u_w}{\partial x}\right] dv - \int_s u_w^* v_n\, dA + \int_v u_w^* \frac{\partial \varepsilon_{kk}}{\partial t}\, dv = 0 \tag{15}$$

The term v_n refers to the apparent flow velocity normal to the surface. It was previously assumed that the excess pore pressures vary over the finite element mesh according to the following interpolation functions :

$$\{\Delta u_w\} = [\overline{N}]\{\Delta \overline{u}_w\} \tag{4 bis}$$

It is then reasonable to assume that the virtual excess pore pressures are described by the same interpolation functions and hence the following can be written

$$\{\Delta u_w^*\} = [\overline{N}]\{\Delta \overline{u}_w^*\} \tag{16}$$

The pore pressure gradient is given by

$$\frac{\partial u_w}{\partial x} = \left[\frac{\partial}{\partial x}\overline{N}\right]\overline{u}_w^* \tag{17}$$

After substitution and elimination of the virtual excess pore pressure terms, the Galerkin weighted residual equation is obtained as a first order differential equation which is integrated over time from t to t+Δt (equation 18).

$$\left[\int_v [B]^T[m][\overline{N}]\right]^T \frac{d}{dt}[\overline{u}]\,dv - \int_v \left[\frac{\partial}{\partial x}[\overline{N}]\right]^T \frac{k}{\gamma_w}\left[\frac{\partial}{\partial x}[\overline{N}]\right]\overline{u}_w dv = \int_s [\overline{N}]^T v_n\, dA \quad (18)$$

Matrices [L] and [P] are defined as

$$[L] = \left[\int_v [B]^T[m][\overline{N}]\right] dV$$

$$[P] = \int_v \left[\frac{\partial}{\partial x}[\overline{N}]\right]^T \frac{k}{\gamma_w}\left[\frac{\partial}{\partial x}[\overline{N}]\right] dV$$

Therefore, equation (18) can be expressed in terms of [L] and [P]

$$\int_t^{t+\Delta t} [L]^T \frac{d}{dt}[\overline{u}]\,dt - [P]\int_t^{t+\Delta t} \overline{u}_w dt = \int_t^{t+\Delta t}\int_s [\overline{N}]^T v_n\, dA\, dt \quad (19)$$

The time integration is approximated in the following manner :

$$\int_t^{t+\Delta t} \overline{u}_w dt = \left[(1-\theta)\,\overline{u}_{w(t)} + \theta\,\overline{u}_{w(t+\Delta t)}\right]\Delta t \quad (20)$$

The value of θ determines the way the excess pore pressure u_w behaves during the time interval. The value $\theta=1$ is adopted in this analysis. A similar approximation made in the case of the apparent velocity v_n as well and the equation (21) is obtained with $\theta = 1$.

$$[L]^T\left(\overline{u}_{(t+\Delta t)}-\overline{u}_{(t)}\right) - [P]\left(\overline{u}_{w(t+\Delta t)}-\overline{u}_{w(t)}\right)\Delta t = [P]\left(\overline{u}_{w(t)}\right)\Delta t + \int_s [\overline{N}]^T v_{n(t+\Delta t)}\,\Delta t\, dA \quad (21)$$

The coupled solution is obtained by solving the system of equations (9) and (21) in the space-time domain. The equations are repeated here for convenience.

$$[K]\{\Delta\bar{u}\} + \{K_v\}\,\Delta u_w = \{\Delta F\}$$

$$[L]^T\{\Delta\bar{u}\} - [P]\{\Delta\bar{u}_w\}\,\Delta t = [P]\{\bar{u}_{w\,(t)}\}\,\Delta t + \int_s [\bar{N}]^T v_{n\,(t+\Delta t)}\,\Delta t\,dA$$

Note that the terms at time t are known from the initial conditions of the problem. This system of equations will result in the following matrix equation. The terms are as defined earlier, note the equality $[K_v] = [L]$.

$$\begin{bmatrix} [K] & [L] \\ [L]^T & -[P]\,\Delta t \end{bmatrix} \begin{bmatrix} \{\Delta\bar{u}\} \\ \{\Delta\bar{u}_w\} \end{bmatrix} = \begin{bmatrix} \{\Delta F\} \\ [P]\{\bar{u}_{w\,(t)}\}\,\Delta t + \int_s [\bar{N}]^T v_{n\,(t+\Delta t)}\,\Delta t\,dA \end{bmatrix} \qquad (22)$$

10.3. Numerical Aspects of Viscoplasticity

While stresses exceeding the yield are not permissible in elasto-plastic analyses, they are temporarily acceptable in viscoplastic formulations. The time during which stresses over yield are permitted results in creep strains. Mathematically speaking, this implies a non homogeneous differential equation since the creep strain are not dependent on the stress increment but the stress state. Computationally, the equilibrium equations are integrated in time and at each load increment viscoelastic strains are allowed to accumulate. This method corresponds to the initial stress method of plasticity analysis and the time integration is an explicit Euler formulation [Smith (1982)].

The explicit schemes suffer from limitations on the allowable time step imposed by numerical stability requirements [Cormeau (1975)]. The determination of the stability criteria is itself an expensive exercise as the flow rules become more involved in contrast to Cormeau's 1975 study where a non hardening, associated

flow rule was used. To provide more flexibility to CRISPEX, an unconditionally stable explicit time stepping scheme is adopted. The method is easily incorporated into the existing program and the overall performance suffers little. The determination of the relative efficiency of implicit and explicit algorithms is outside the scope of this work and will be omitted [see for example Hughes et al. (1978)].

Following the intuitive approach proposed by Stolle et al. (1989), the implicit time integration of the flow rule $\Phi(F)$ in equation (23) is deduced to be a monotonically decreasing function in time during initial creep or a monotonically increasing function in time during acceleration creep.

$$\dot{\varepsilon}_{ij}^{vp} = \Phi(F) \frac{\partial f_d}{\partial \sigma'_{ij}} \tag{23}$$

or with plasticity notation, and assuming that the solution to the next time step is given by

$$\dot{\varepsilon}_{ij}^{vp} = \lambda_{n+1} \frac{\partial f_d}{\partial \sigma'_{ij}} \tag{24}$$

The total strain increment is related to the stress increment by equation (9) which is rewritten as

$$\Delta\sigma_{ij\,(n)} = [D^e]\left(\Delta\varepsilon_{ij\,(n)} - \Delta\varepsilon_{ij\,(n)}^{vp}\right) \tag{25}$$

where the subscript (n) refers to the current time and $[D^e]$ is the elastic stiffness matrix. The viscoplastic strain increment is approximated as

$$\Delta\varepsilon_{ij\,(n)}^{vp} = \Delta t_{(n)}\, \dot{\varepsilon}_{ij\,(n+\theta)}^{vp} = \Delta t_{(n)}\left[(1-\theta)\, \dot{\varepsilon}_{ij\,(n)}^{vp} + \theta \dot{\varepsilon}_{ij\,(n+1)}^{vp}\right] \tag{26}$$

The decrease (or increase) of λ with time can be approximated by a truncated Taylor series.

$$\lambda_{n+1} = \lambda_n \pm \frac{\partial \lambda}{\partial F}\left[\left[\frac{\partial F}{\partial \sigma_{ij}}\right]^T \dot{\sigma}_{ij\,(n)} + \left[\frac{\partial F}{\partial k_d}\right]^T \dot{k}_{d\,(n)}\right] \tag{27}$$

The implicit form of equation (27) is used in equation (28).

$$\lambda_{n+1} = \frac{\lambda_n \pm \frac{\partial \lambda}{\partial F}\left[\left[\frac{\partial F}{\partial \sigma_{ij}}\right]^T \dot{\sigma}_{ij\,(n)} + \frac{\partial F}{\partial k_d}\dot{k}_{d\,(n)}\right][D^e]\,\Delta\varepsilon_{ij\,(n)}}{1 + \frac{\partial \lambda}{\partial F}\Delta t_{(n)}\left[\left[\frac{\partial F}{\partial \sigma_{kl}}\right]^T [D^e]\frac{\partial F}{\partial \sigma_{kl}} + \left[\frac{\partial F}{\partial k_d}\right]^T H_P \frac{\partial F}{\partial \sigma_{kl}}\right]} \tag{28}$$

The substitution of equations (24), (26) and (28) into equation (25) with θ=1 yields an expression similar to the tangential stiffness matrix used in elastoplastic analyses. H_p is a matrix relating changes in hardening parameters to incremental plastic strain.

$$\Delta\sigma_{ij\,(n)} = [D^{vp}]\,\Delta\varepsilon_{ij\,(n)} - \frac{\lambda_n\,\Delta t_{(n)}\,[D^e]\frac{\partial F}{\partial \sigma_{kl}}}{1 + \frac{\partial \lambda}{\partial F}\Delta t_{(n)}\left[\left[\frac{\partial F}{\partial \sigma_{kl}}\right]^T [D^e]\frac{\partial F}{\partial \sigma_{kl}} + \left[\frac{\partial F}{\partial k_d}\right]^T H_P \frac{\partial F}{\partial \sigma_{kl}}\right]} \tag{29}$$

and the viscoplastic tangential stiffness matrix is

$$[D^{vp}] = [D^e]\left[[I] - \frac{\Delta t_{(n)}\ \frac{\partial \lambda}{\partial F}\frac{\partial F}{\partial \sigma_{mn}}\left[\frac{\partial F}{\partial \sigma_{mn}}\right]^T [D^e]}{1 + \frac{\partial \lambda}{\partial F}\Delta t_{(n)}\left[\left[\frac{\partial F}{\partial \sigma_{kl}}\right]^T [D^e]\frac{\partial F}{\partial \sigma_{kl}} + \left[\frac{\partial F}{\partial k_d}\right]^T H_p \frac{\partial F}{\partial \sigma_{kl}}\right]}\right] \tag{30}$$

Note that when $\Delta t_{(n)} \rightarrow \infty$, the matrix $[D^{vp}]$ becomes the elastoplastic tangent stiffness matrix $[D^{ep}]$. This fact also suggests that the approach is a numerical reflection of Perzyna's overstress model which was shown to reduce to an elastoplastic law under the same conditions (see page 60).

It is now only necessary to derive the terms contained in the equation (30) and the procedure is ready to be implemented in a numerical routine. The constitutive equation is recapitulated here for convenience.

$$\dot{\varepsilon}_{ij} = \frac{\dot{s}_{ij}}{2G} + \frac{\kappa}{1+e}\frac{\dot{\sigma}'_m}{\sigma'_m}\frac{\delta_{ij}}{3} + \\ + C\exp\left[m'\left(\frac{\sqrt{2J_{2(d)}}}{M^*\,\sigma'_{m(d)}} + \ln\frac{\sigma'_{m(d)}}{\sigma'_{me}} - \frac{1+e}{\lambda-\kappa}\varepsilon^p_{kk}\right)\right]\left\langle\frac{s_{ij}}{\sqrt{2J_2}} + \left(M^* - \frac{\sqrt{2J_2}}{\sigma'_m}\right)\frac{\delta_{ij}}{3}\right\rangle \tag{31}$$

The the structure parameter C, elastic shear modulus G, and the permeability coefficient k are related to the stress state by the following relationships:

$$C = \exp\left(\frac{\delta}{\left(M^* - \frac{\sqrt{2J_2}}{\sigma'_m}\right)} - \xi\right) \tag{32}$$

$$G = G\sqrt{\frac{\sigma'_m}{\sigma'_{me}}} \tag{33}$$

$$k = k_o \exp\left(\frac{e - e_o}{C^*_k}\right) \tag{34}$$

Where C^*_k is a constant in the order of 0.1, δ and ξ are time dependent parameters and σ'_{me} is the preconsolidation pressure.

The derivation of the matrix $[D^{vp}]$ follows closely the derivation of the elastoplastic matrix $[D^{ep}]$. The associativity is now on the dynamic yield surface determined by the viscoplastic property function $\Phi(F)_{n+1} = \lambda_{n+1}$ .The formulation presented in equation (31) treats the static yield surface as a reference and thus relegates it to a position akin to a hardening parameter position. The term required for the numerical code is the derivative of λ with respect to its variables.

$$\frac{\partial\lambda}{\partial F} = \frac{\partial\,\Phi(F)}{\partial F} \tag{35}$$

Since

$$\Phi(F) = C\,M^*\,\sigma'_m \exp[m'\,F] \tag{36}$$

The differential is

$$\frac{\partial\lambda}{\partial F} = \frac{\partial\,\Phi(F)}{\partial F} = C\,M^*\,\sigma'_m\,m'\,F'\exp[m'\,F] \tag{37}$$

F is the overstress function whose partial derivatives with respect to stress state and volumetric plastic strain state have been already accounted for in equation (28) and presented in equation (38).

$$\frac{\partial F}{\partial \sigma'_{ij}} = \frac{1}{M^* \sigma'_m}\left[\frac{s_{ij}}{\sqrt{2J_2}} + \left(M^* - \frac{\sqrt{2J_2}}{\sigma'_m}\right)\frac{\delta_{ij}}{3}\right] \qquad (38)$$

The elasto-viscoplastic tangential stiffness matrix is thus completely defined. The implementation of this new stiffness matrix has been carried out in the program CRISPEX.

Drained, undrained and Biot consolidation analyses are provided under plane strain or axisymmetric conditions. With the added soil model, elastic, anisotropic elastic, elasto plastic (Cam Clay and Modified Cam Clay), and elasto-viscoplastic constitutive equations are implemented. The choice of elements can be made between linear strain or cubic strain triangles.

10.4. Analyses of Soft Clay Foundations

The most elusive aspect of the prediction and subsequent design of foundations on soft clays is the accurate calculation of lateral deformations [Tavenas et al. (1979, 1980)]. The assumption of initial undrained behaviour has been demonstrated to lead to erroneous lateral movement profiles and consequently the consolidation must be assumed to occur simultaneously with loading. It will be remembered from page 6 that the excessive lateral deformations can lead to important delays and increase the cost of the project in question. In the light of the previous chapters, the following analyses will demonstrate that not only a reasonable estimate of progressive and long term horizontal displacements can be made but also that the existence of vibratory loading increases the magnitude of lateral flow.

The case studies that were mentioned on page 131 are summarized in Table 10.1 through Table 10.7. The finite element mesh is similar in each case and the standard element used is a 6 noded linear strain triangle with 15 degrees of freedom (see section 10.5).

Table 10.1 Summary of Problem analyzed by Shoji et al. (1990)

CASE 1.1 Instrumented embankment (residential zoning)	
Foundation soil	Highly organic soil (0 - 5.8 m) Silty clay (5.8 - 20 m)
Foundation geometry and dimensions	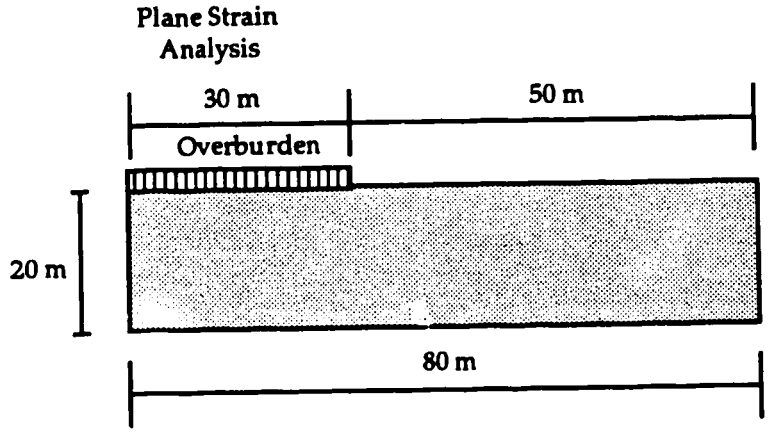
Unconfined compressive strength	organic soil : 15.5 kPa. silty clay : 36 kPa.
Plastic Limit	organic soil : 127.7 silty clay : 34.5
Liquid Limit	organic soil : 404 silty clay : 66.1
Water content	organic soil : 315 silty clay : 80.8
In situ stresses	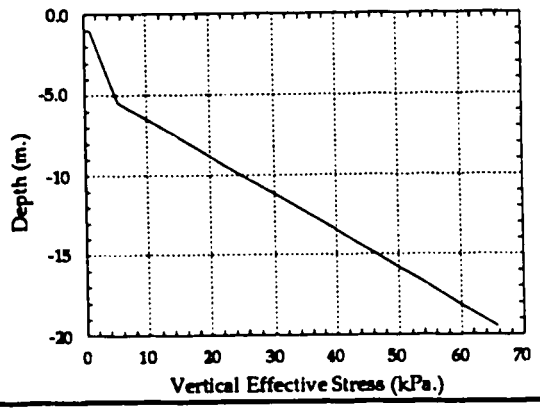

Table 10.1 cont.

Loading	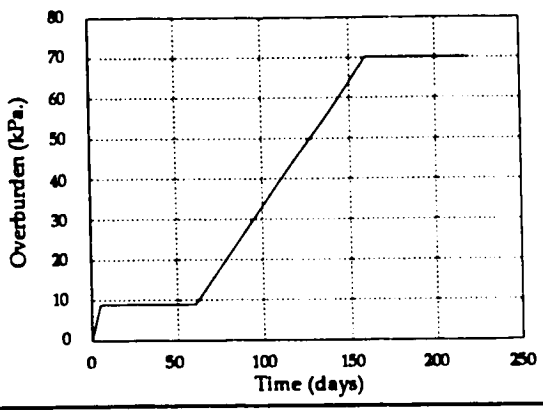

CRISPEX viscoplastic material parameters for case 1.1:

Depth	λ	κ	M	e_o	G_o	k_h	k_v	C	m'	p'_o
0-5.8	0.740	0.080	1.50	4.25	250	3 e-9	10 e-10	6 e-5	15.5	8
5.8-20	0.372	0.054	1.28	1.28	1000	3 e-9	10 e-10	4.5 e-6	21.5	100

In the above G_o and p'_o are in kPa., k_h and k_v are in m/sec., and C is in $sec.^{-1}$

The field measurements presented by Shoji et al. (1990) are in the context of finite element back analysis of two dimensional consolidation for the determination of the optimum locations for measurement instrumentation. Since an elastic model was used for back analysis, the soil parameters used herein are assumed values (see Crispex parameters in Table 10.1, 10.2, 10.3).

Whenever the analyses involve the construction of an embankment, the loading has been applied as surface stresses with due consideration of the embankment slope. In all cases, the slope has been assumed to have a 1:3 ratio and the effects of the slope have not been included.

Table 10.2 Summary of Problem analyzed by Shoji et al. (1990)

CASE 1.2 Instrumented embankment (residential zoning)	
Foundation soil	Highly organic soil (0 - 7.5 m) Soft clay (7.5 - 12 m)
Foundation geometry and dimensions	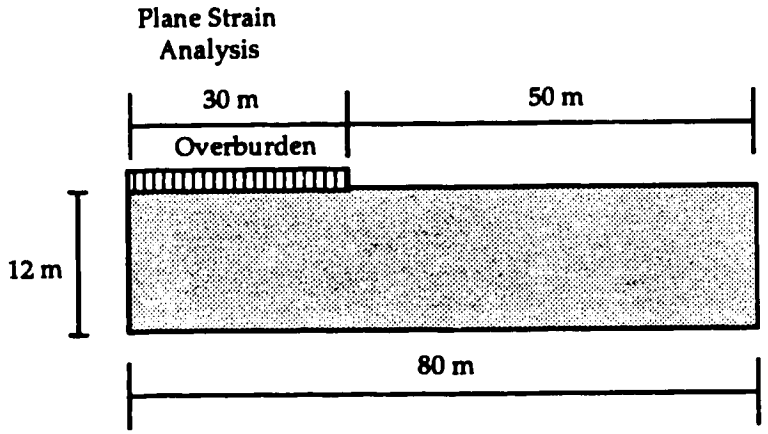
Plasticity Index	organic soil : 180 clay : 17
Water content	organic soil : 211.5 clay : 64.6
In situ stresses	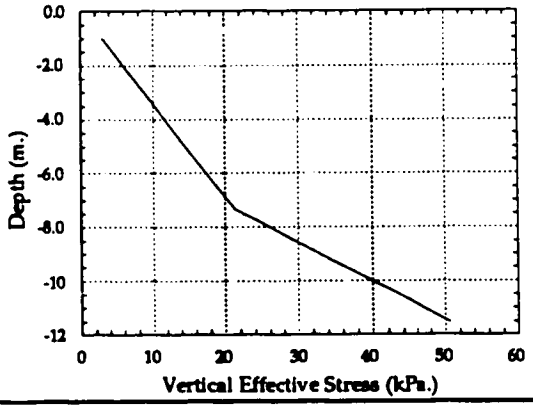

Table 10.2 cont.

Loading	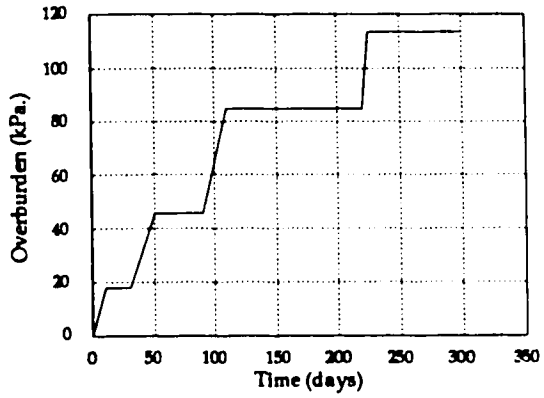

CRISPEX viscoplastic material parameters for case 1.2:

Depth	λ	κ	M	e_o	G_o	k_h	k_v	C	m′	p'_o
0-7.5	0.74	0.08	1.5	4.25	350	3 e-9	10 e-10	1 e-5	10	8
7.5-12	0.344	0.047	1.5	1.78	4000	3 e-9	10 e-10	1 e-7	15.5	80

In the above G_o and p'_o are in kPa., k_h and k_v are in m/sec., and C is in $sec.^{-1}$

Table 10.3 Summary of Problem analyzed by Shoji et al. (1990)

CASE 1.3 Instrumented embankment (industrial zoning)	
Foundation soil	Highly organic soil (0 - 1.75 m) Soft clay (1.75 - 12 m)
Foundation geometry and dimensions	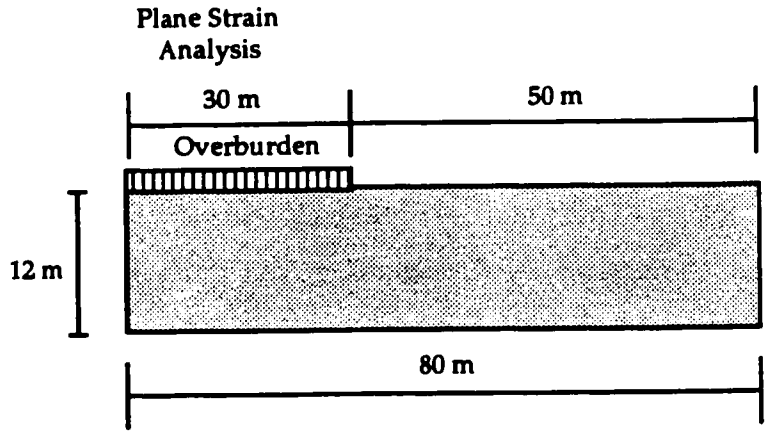
Unconfined compressive strength	organic soil : 18 kPa. clay : 37 kPa.
Plastic Limit	organic soil : 193 clay : 52
Liquid Limit	organic soil : 489 clay : 116.5
Water content	organic soil : 347 clay : 103
In situ Stresses	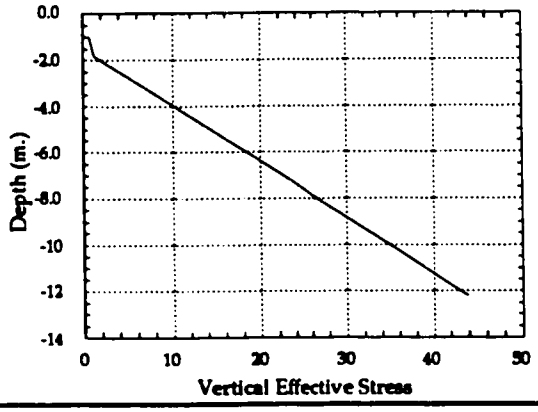

Table 10.3 cont.

Loading	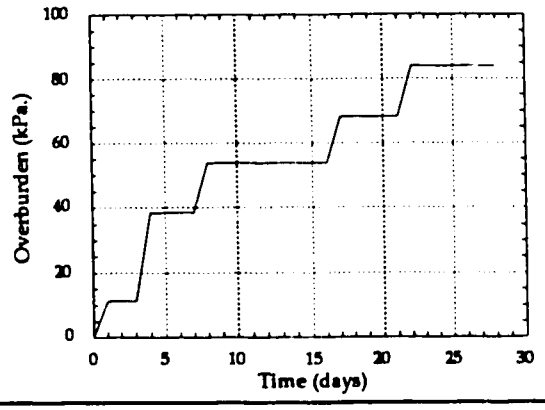

CRISPEX viscoplastic material parameters for case 1.3:

Depth	λ	κ	M	e_o	G_o	k_h	k_v	C	m'	p'_o
0-1.75	0.74	0.08	1.5	4.25	350	3 e-9	10 e-10	1 e-5	10	8
1.75-12	0.344	0.047	1.5	1.78	4000	3 e-9	10 e-10	1 e-7	15.5	80

In the above G_o and p'_o are in kPa., k_h and k_v are in m/sec., and C is in $sec.^{-1}$

Table 10.4 Summary of Problem analyzed by Almeida et al. (1982)

CASE 2 Instrumented embankment construction by the Brazilian Highway Research Institute and the Federal University of Rio de Janeiro, Brazil.	
Foundation soil	Soft grey Rio de Janeiro clay
Foundation geometry and dimensions	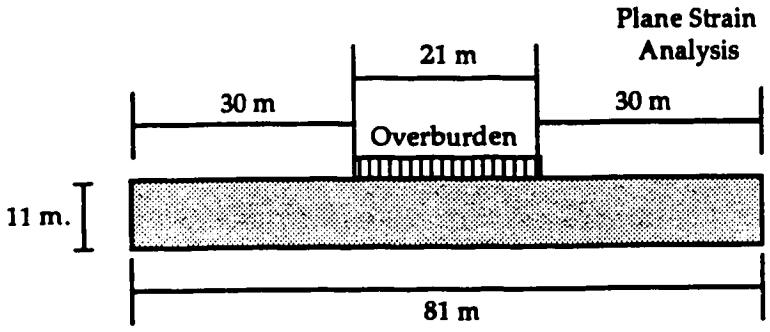
Average undrained strength	10 kPa.
Average Plastic Limit	50
Average Liquid Limit	130
Average water content	145
In situ stresses	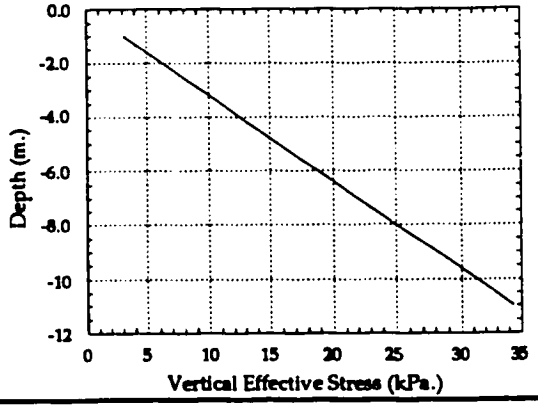

Table 10.4 cont.

Loading	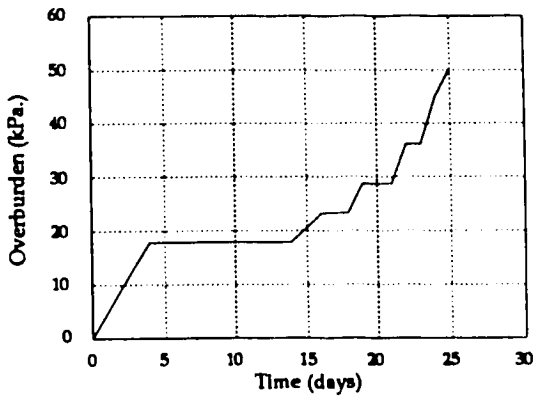

CRISPEX viscoplastic material parameters for case 2:

Depth	λ	κ	M	e_o	G_o	k_h	k_v	C	m'	p'_o
0-5	0.90	0.13	1.14	5.8	350	3 e-9	10 e-10	1 e-5	8	20
5-7.5	0.83	0.13	1.14	5.8	700	3 e-9	10 e-10	1 e-6	11	26
7.5-11	0.70	0.10	1.14	4.6	900	3 e-9	10 e-10	1 e-7	15.5	40

In the above G_o and p'_o are in kPa., k_h and k_v are in m/sec., and C is in $sec.^{-1}$

The measurements presented by Almeida et al. (1982) involve the study of the predictive capabilities of two computer algorithms, one of which is an earlier version of CRISP. The assumptions concerning the drainage have also been studied and the general behavior of a soft clay foundation loaded to failure by an embankment is deduced. Since the Cam Clay parameters for the soil are given, only the viscoplastic parameters are assumed as per Table 10.4.

Table 10.5 Summary of Problem analyzed by Mimura et al. (1990)

CASE 3 Instrumented reclamation embankment in Osaka Bay (Koshien reclamation)	
Foundation soil	Soft alluvial marine clay
Foundation geometry and dimensions	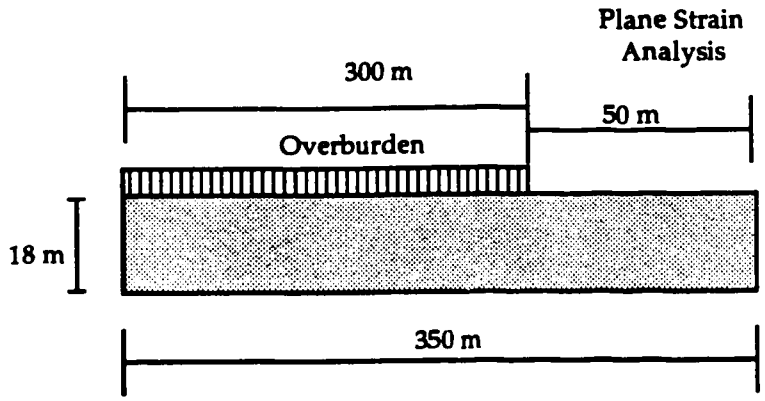
In situ stresses	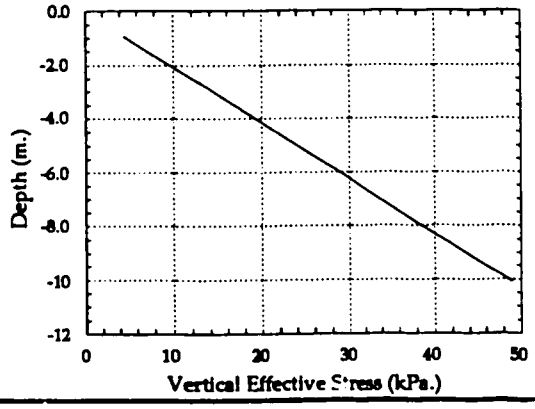
Loading	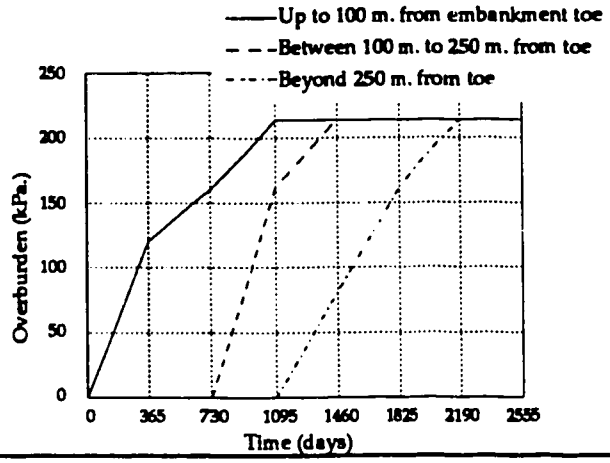

Table 10.5 cont.

CRISPEX viscoplastic material parameters for case 3:

Depth	λ	κ	M	e_o	G_o	k_h	k_v	C	m'	p'o
0-18	0.37	0.05	1.4	2.7	80	3.5 e-9	1.8 e-9	4.6 e-5	5.6	20

In the above G_o and p'_o are in kPa., k_h and k_v are in m/sec., and C is in $sec.^{-1}$

Table 10.6 Summary of Problem analyzed by Magnan et al. (1982)

CASE 4 Instrumented test embankment by the Laboratoires des Ponts et Chaussées at Cubzac-les-Ponts in Gironde, France.	
Foundation soil	Overconsolidated clay (top layer) and lightly overconsolidated soft organic clay
Foundation geometry and dimensions	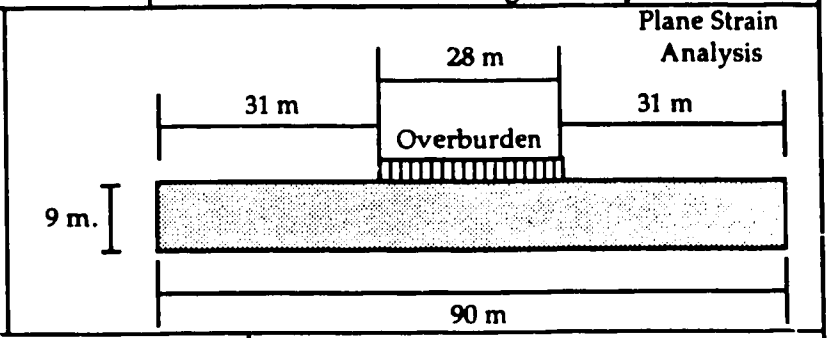
Unconfined compressive strength	50 kPa.
In situ stresses	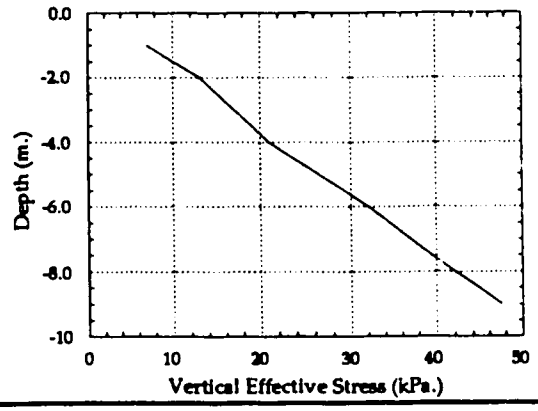

Table 10.6 cont.

Loading	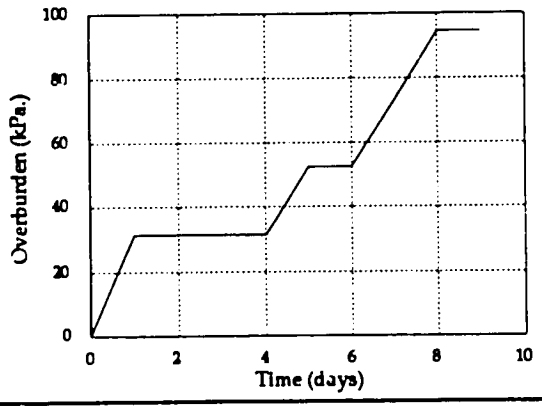

CRISPEX viscoplastic material parameters for case 4:

Depth	λ	κ	M	e_o	G_o	k_h	k_v	C	m'	p'_o
0-1	0.13	0.013	1.2	1.1	1000	3 e-9	10 e-10	1 e-5	4.5	80
1-4	0.35	0.035	1.2	2.75	700	3 e-9	10 e-10	1 e-6	11	80
4-9	0.30	0.030	1.2	2.75	700	3 e-9	10 e-10	1 e-7	11	80

In the above G_o and p'_o are in kPa., k_h and k_v are in m/sec., and C is in $sec.^{-1}$

Mimura et al. (1990) presented a viscoplastic analysis of long term deformations of a soft clay soil under a land reclamation project. They have considered the deformation of the deeper layers of harder diluvial clays over a period of 7 years. It must be said that the field measurements have been confined to a small area of the reclamation and consequently this study is mainly a numerical one which nevertheless provides very reasonable predictions in light of the limited field data. Again, the time dependent parameters are assumed.

The field measurements of Magnan et al. (1982) have been used in conjunction with an elasto-plastic model and in this sense the study is similar to the one presented by Almeida et al. (1982)

Table 10.7 Summary of Problem analyzed by West Japan Power Co. (1986)

CASE 5 Instrumented land reclamation project in Okayama prefecture, Japan.	
Foundation soil	Alluvial marine clay
Foundation geometry and dimensions	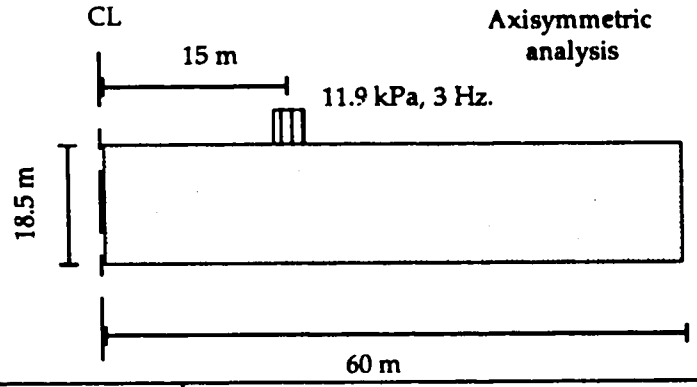
Unconfined strength	40 kPa.
In situ stresses	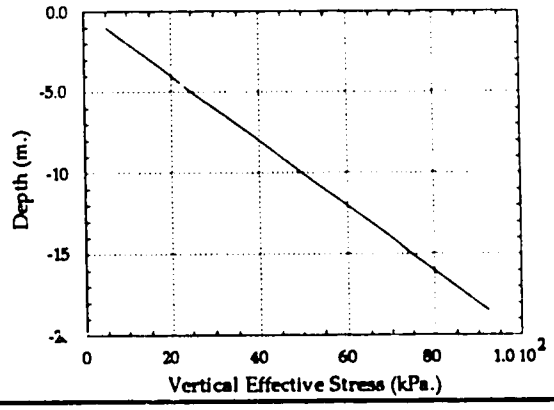
Loading	25.5 t. truck with a foot print of 7x5 m. : 11.9 kPa. Travel trajectory : circular with a radius of 15 m. Width of travel path : 5 m. Travel speed : 9 - 10 km/h Dominant frequency of induced vibrations : 3 Hz. Maximum acceleration on surface beneath truck : 0.3 g Duration of travel : 170 days

Table 10.7 cont.

CRISPEX viscoplastic material parameters for case 5:

Depth	λ	κ	M	e_o	G_o	k_h	k_v	C	m'	p'_o
0-5	0.80	0.08	1.05	4.25	250	3 e-9	10 e-10	7.5 e-5	1.0	5
5-10	0.75	0.08	1.05	4.0	400	3 e-9	10 e-10	1 e-5	2.0	15
10-18.5	0.75	0.08	1.05	4.0	600	3 e-9	10 e-10	1 e-6	2.0	25

In the above G_o and p'_o are in kPa., k_h and k_v are in m/sec., and C is in $sec.^{-1}$

10.5. Details of the Analysis Procedure

The mesh shown in Fig. 10.1 has been used (with appropriate dimensions and soil parameters) in all prediction analyses. There is a total of 110 linear strain triangle elements with three pore water pressure nodes at the vertices. Since the variation of the pore pressure across the element is linear, rather large time increments are required for the total distribution of excess pore water pressures during consolidation. The reason for which the viscoplastic tangential stiffness matrix was formed implicitly can now be appreciated. The soil is assumed to start consolidation as soon as the initial load increment has been applied. The field loading rates (as shown in Table 10.1 through Table 10.7) have been followed in all analyses.

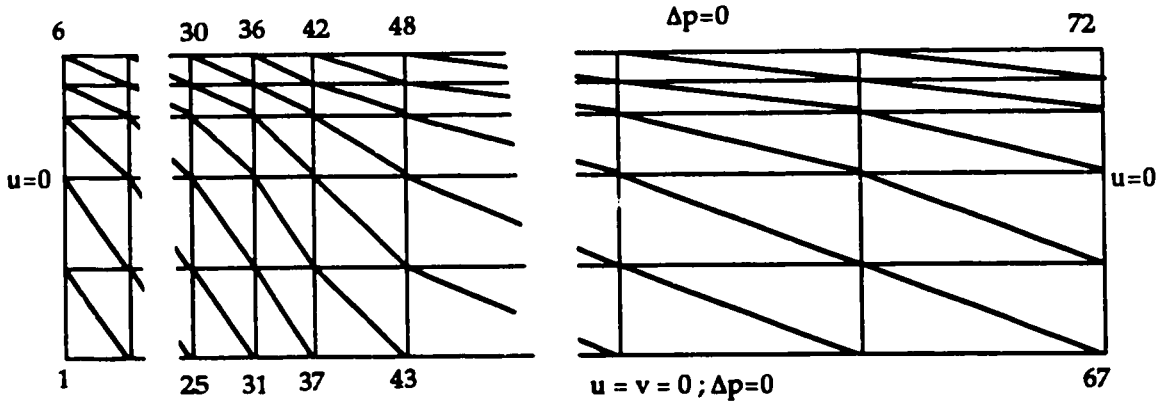

Figure 10.1 Typical Finite element mesh used in the analyses of cases 1 through 5; node numbers as indicated.

The load is applied over the smaller elements closer to the left boundary of the mesh (Fig. 10.1) which also represents the axis of symmetry for both axisymmetric and plane strain analyses. Wherever applicable, more than one material type have been considered. These can be found at the end of each case summary in the preceding pages (see *"CRISPEX viscoplastic material parameters"* for each case).

The vibration of the surface load has been broken into a sinusoidal wave whose amplitude is a percentage of the static load. To capture the peaks of a frequency of 3 Hz. , the time unit has been reduced to milli-seconds for the viscoplastic parameters, permeability coefficients, and all variables involving the acceleration of gravity. In short, unit consistency has been maintained.

The determination of the load increments for each case has been carried out by successive trials to ensure that the expansion of the yield surface (in those elements which are yielding) is not excessive, in general a 3% increase in the current yield locus has been considered to be satisfactory.

The focus being on the deformation behavior of soft clays, the results of the predictions are presented in terms of vertical and horizontal displacements and compared to the published field measurements. The effects of vibration loading have been investigated and a series of analyses have been run by assuming that the loading case 5 is also applied on some of the other cases to simulate traffic activity over these embankments as they are being built or developed.

The field measurements for the case 5 indicate that there is a marked correlation between the construction activity on the fill and the observed lateral deformations. It is clear that the vibratory nature of the surface loads effect the rate dependent deformation of the clay foundation since neither consolidation nor the sheer weight of the machinery alone can account for the magnitude of the lateral displacements. The prediction of deformations must therefore include the susceptibility of soft clays to behave softer under traffic vibrations.

10.6. Finite Element Analysis Results

10.6.1. Case 1.1

The embankment in this instance is built over two main layers of soft soil. The upper layer consists of highly organic soil which in this analysis has been modeled as a very soft clay layer. The lateral deformations (Fig. 10.2) indicate that the top layer of 6 m. is in fact partly drained. The use of a relatively strong surface crust has been found to be satisfactory in obtaining the following predictions.

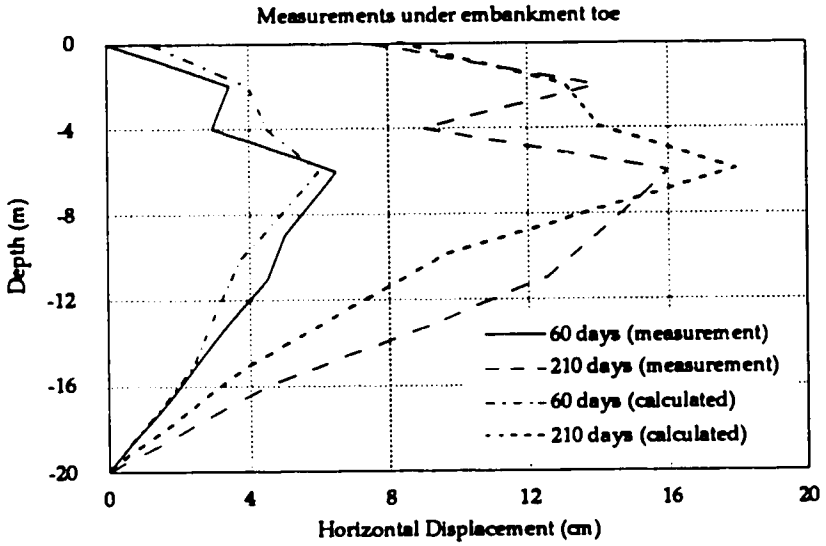

Figure 10.2 Lateral deformations under the toe of embankment in the case 1.1

If a load simulating traffic activity on the surface is imposed as construction proceeds, the lateral deformation profile (Fig. 10.3) is changed and thus deviates from the measured values. The upper portion of the soil show a quasi-undrained behavior, eliminating the effects of the surface crust. It is deduced from analysis results that while the lateral deformations are increased in the upper layers of soil, the pore pressures are either constant or on the rise.

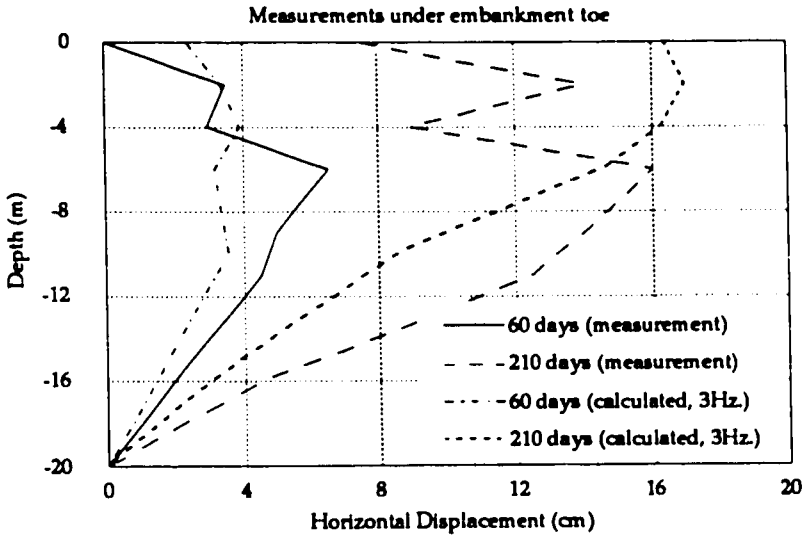

Figure 10.3 Lateral deformations under the toe of embankment including traffic loading effects in the case 1.1

The zigzag pattern of the measured deformations are probably due to a thin layer of high permeability layer between the organic soil and the soft clay. Due to the lack of a comprehensive soil profile information, this aspect was not simulated in the finite element input.

10.6.2. Case 1.2

The fact that the surface of the organic deposits behaved in a partially drained way is very apparent in all of the cases presented by Shoji et al. Here, it is seen that the relatively thick layer of soft organic material contributes to a typical partially drained profile (Fig. 10.4) . This is to be expected since the permeability of the top soils in cases 1.1, 1.2, and 1.3 are two to three orders of magnitude higher than the soft underlying clays. It must also be stated that the surface of the organic top soil is itself covered with a sandy soil, the thickness of which was left unspecified in the above mentioned paper.

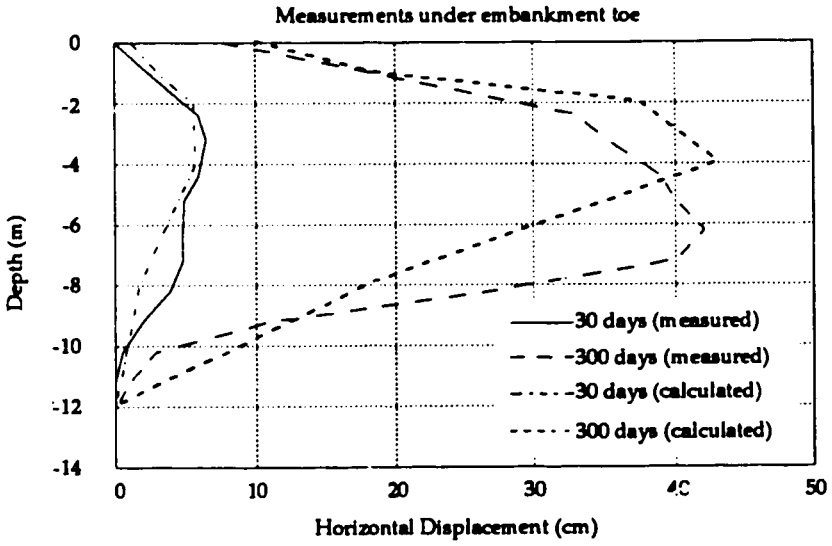

Figure 10.4 Lateral deformations under the toe of embankment in the case 1.2

10.6.3. Case 1.3

The third embankment is founded on mainly soft clay, the organic soil extending to only about 2 m. in depth. This may have led to the over-prediction of the early response of the lateral deformation (Fig. 10.5). The construction schedule being relatively fast (see Table 10.3), the viscoplastic model predicts an extended undrained phase, while the drainage conditions in situ might have been different than assumed in the analysis. It is believed that the effects of the drainage conditions on the finite element analysis results are increased when the analysis is carried out in real time as opposed to load increments. One must remember that real time increments are actually involved in the calculation of the incremental tangential stiffness matrix as well as the calculation of stresses.

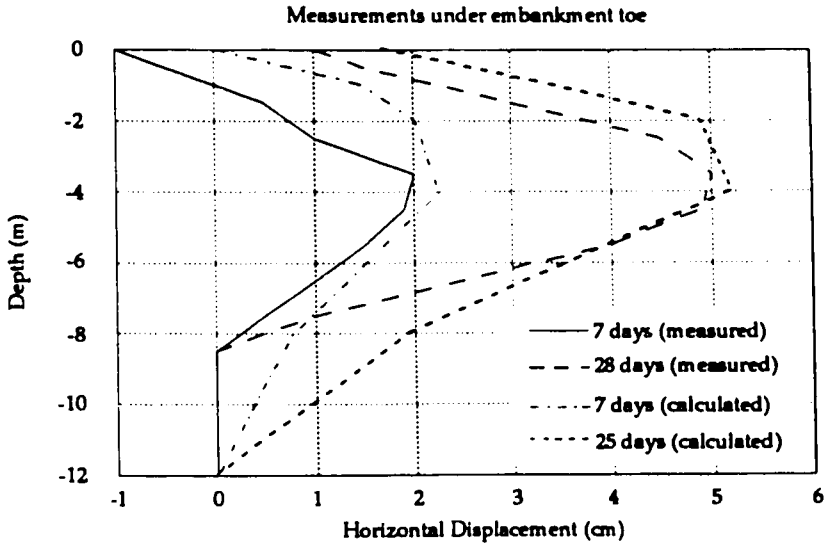

Figure 10.5 Lateral deformations under the toe of embankment for the case 1.3

The long term response of the foundation is predicted much better since the effects of the drainage are now replaced by time effects and both the elastic shear modulus and the permeability coefficient are evolving with the stress path (equations 32, 33, page 139).

It is generally concluded that a consolidation analysis is highly sensitive on the prescribed drainage conditions at its undrained limit and can produce divergent results, especially when time is implicitly involved in the stiffness matrix formation.

10.6.4. Case 2

This analysis is particularly interesting since the computer simulations for it have already been performed using CRISP and the Modified Cam Clay model. In the present analysis, a more crude layering of the soil profile has been adopted, however the agreement between the field measurements and the computed values is quite remarkable (Figs. 10.6, 10.7, 10.8, 10.9).

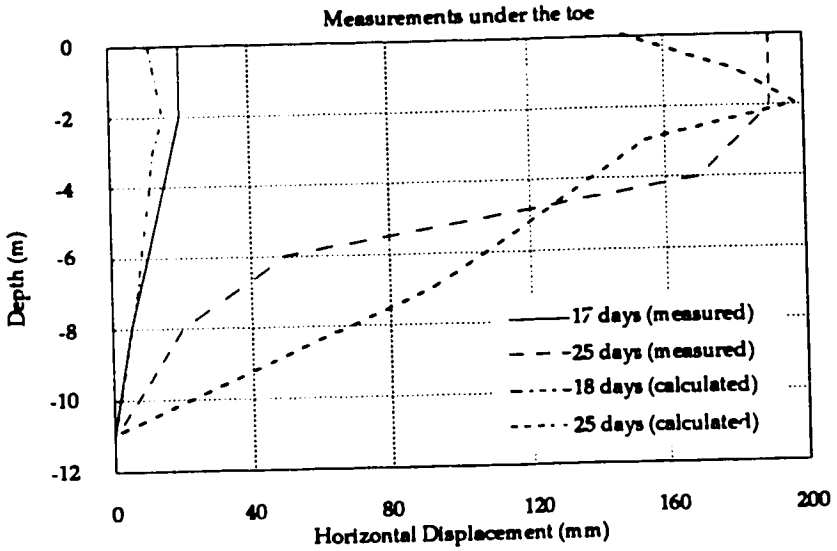

Figure 10.6 Lateral deformations under the toe of embankment for the case 2

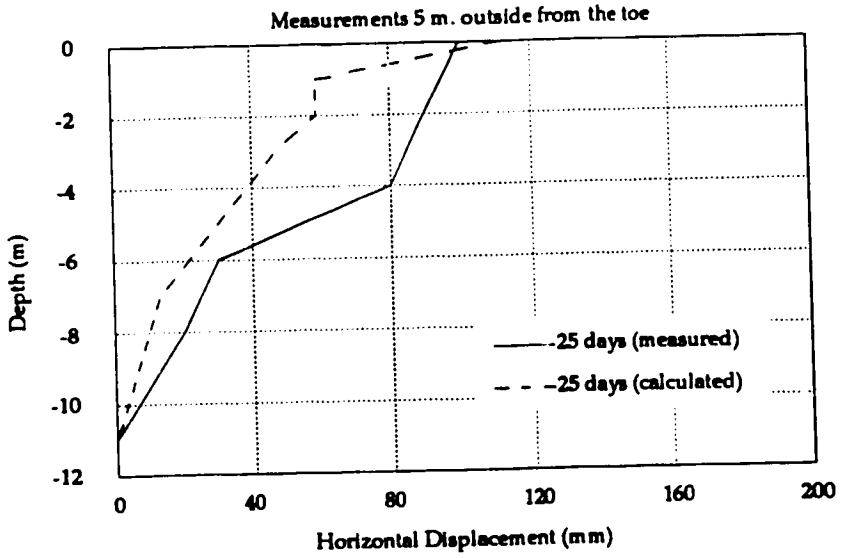

Figure 10.7 Lateral deformations 5 m. from the toe of embankment for the case 2

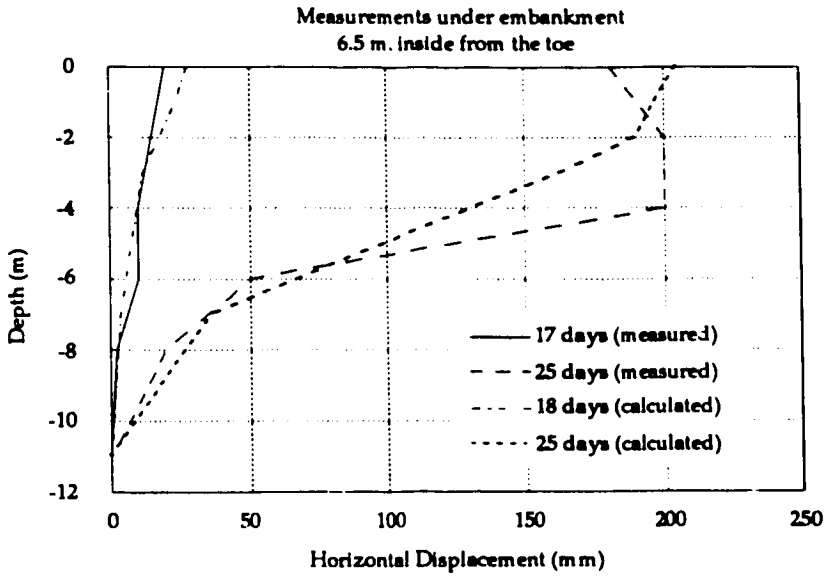

Figure 10.8 Lateral deformations under the embankment 6.5 m. from the toe for the case 2

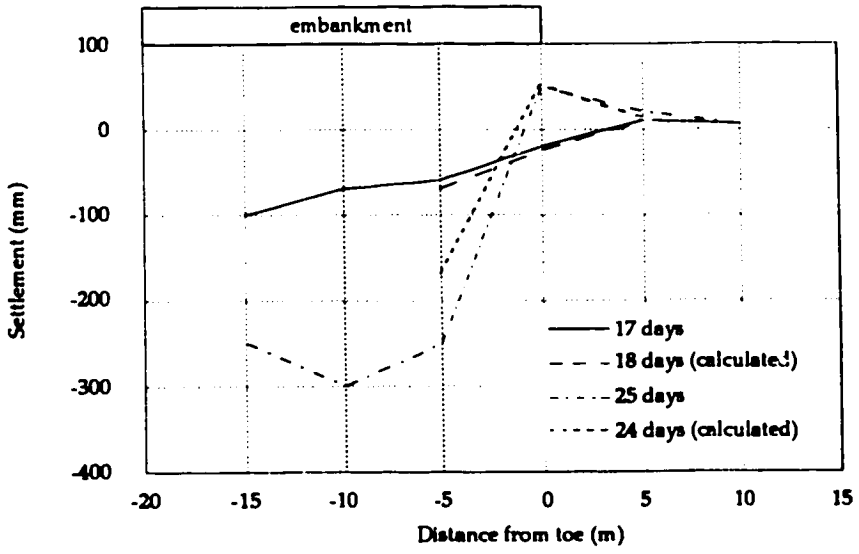

Figure 10.9 Settlement for the case 2

The effects of a stronger surface layer can be seen in Fig. 10.6 and Fig 10.8. Although this can be a detrimental predictive feature, it can be handled by increasing the loading increments and decreasing the initial time increments. As was previously discussed, the determination of the load and time increments to suit the problem and the model can be the single most important determining factor in the correctness of the analysis outcome. There is no single rule of thumb that has been used for the analyses presented in this chapter. Rather, each case was considered separately in its duration in time and extent of the loading with respect to the undisturbed in situ conditions.

Although the Cam Clay parameters were available for the problem [Almeida et al. (1982)], the predictions were obviously made to fit the measurements by manipulating the viscoplastic parameters C and m', following the guidelines established in the previous chapters. In effect, this exercise is one of back analysis where the viscoplastic parameters for the soil profile given by Almeida et al. have been identified.

10.6.5. Case 3

Among all the analyses presented in this section, case 3 is perhaps the most roughly simulated and the lateral deformation profiles (Fig. 10.10) show this. The foundation has been limited to the uppermost layer of soft clay, and the underlying harder clays have been completely disregarded. The size and the duration of this project and the difficulties in analysis and even output file handling have been only some of the reasons for this over approximation of the field conditions. The main objective in choosing this comparison is that the stress level which is applied on the surface of the deposit is higher than the previous cases. Under the circumstances, the predictions are quite satisfactory, even though the movement towards the sea which has been measured under the embankment is not represented. This shortcoming is obviously associated with the fact that the deformation of the underlying stiffer clay has been disregarded in the analysis.

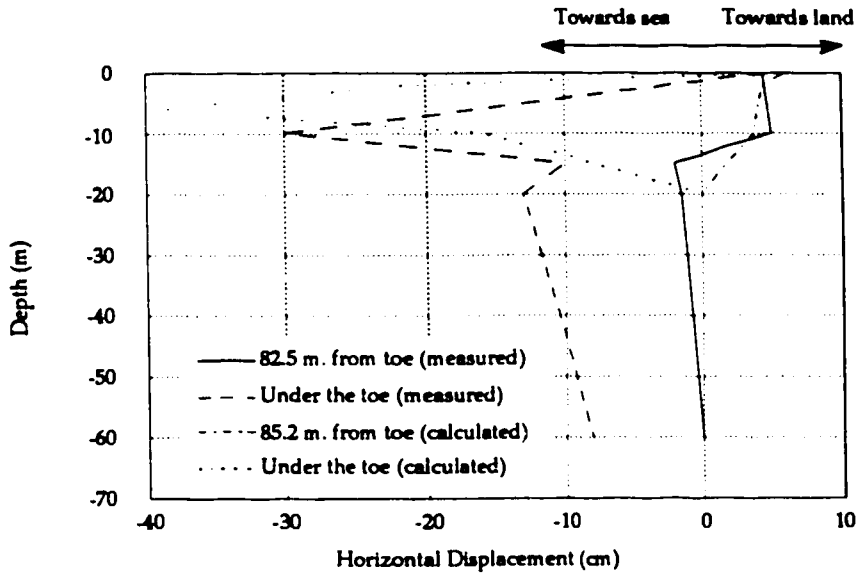

Figure 10.10 Lateral deformations under land reclamation on soft marine clay

10.6.6. Case 4

The Cam Clay parameters for this soil have also been provided by the Authors (see Table 10.6) and the viscoplastic parameters have been identified through a series of trial analyses. It is again seen that the agreement between the measured and computed lateral deformation profiles are quite satisfactory.

The main issue in this case as in the others is the correlation of the deduced viscoplastic parameters with the ones that would have been obtained through laboratory testing. It is quite reasonable to assume that the values assumed for c and m′ already contain the effects of the construction activity since they have been made to fit the field measurements. It is therefore impossible to differentiate between static effects and vibratory ones. One way of making such a distinction is the separate measurement of traffic load effects after all construction (i.e. embankment loading) activity has ceased (see section 10.6.7).

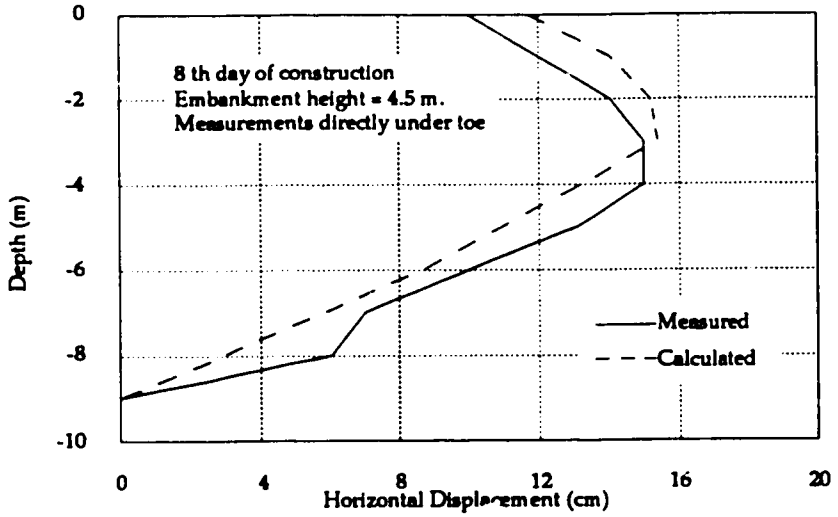

Figure 10.11 Lateral deformations under the embankment toe for the case 4

10.6.7. Case 5

Field measurements where the effect of traffic on the deformation of the clay deposit are available. The analysis of case 5 is undertaken as follows. First, the deformation of the foundation under its own weight and the static weight of construction equipment has been analyzed. Second, the vibration induced by the construction equipment has been simulated in real time by applying a sinusoidal load vibration along with the weight of the equipment. The magnitude of this vibrating load has been determined from the vertical accelerations (typically in the order of 0.3g directly under a moving truck) induced on the surface by the moving vehicle. Third, a static analysis is performed with modified viscoplastic parameters along the findings of the vibrational slump test results.

The geometry of the site is shown in Fig. 10.12 with the locations of the measurement probes indicated by the numbers in circles. Essentially, the surface movement is measured by standard electronic surveying methods, while the flow of soil below the surface is recorded by inclinometers.

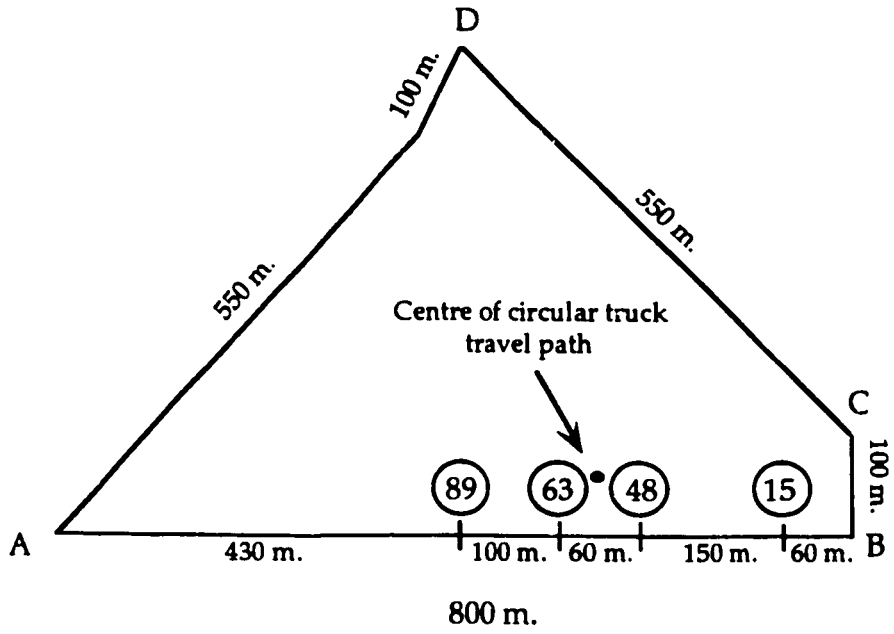

Figure 10.12 The site geometry and the measurement locations for the Yorishima land reclamation project

The land reclamation extends beyond the borders shown in Fig. 10.12, the borders here being made up of sheet piles separating adjacent fill zones. The instrumentation was mainly placed along the A-B side since it is in the vicinity of corner B that large unexpected deformations were observed. The correlation between horizontal deformations and the construction activity (in the form of trucks carrying fill material over the reclaimed land) is well illustrated in Fig. 10.13. There seems to be 20 mm. of surface lateral movement for each 1000 trucks that have travelled close to the sheet pile along A-B.

The lateral flow of the soft clay layer is mainly concentrated in the upper 4 to 5 meters of the deposit and this observation suggests that the surface of the fill consists of an extremely soft, muddy clay. Visual observation of the site indicates that the water table is at the surface and there is no crust to speak of whatsoever. The centre of the assumed (circular with a radius of 15 m., see Table 10.7) truck travel path is 20 meters from the sheet pile. The distance of this point to the four measurement points is 36.05 m. to stations 48 and 63, 131.53 m. and 181.1 m. to stations 89 and 15 respectively (see Fig. 10.14).

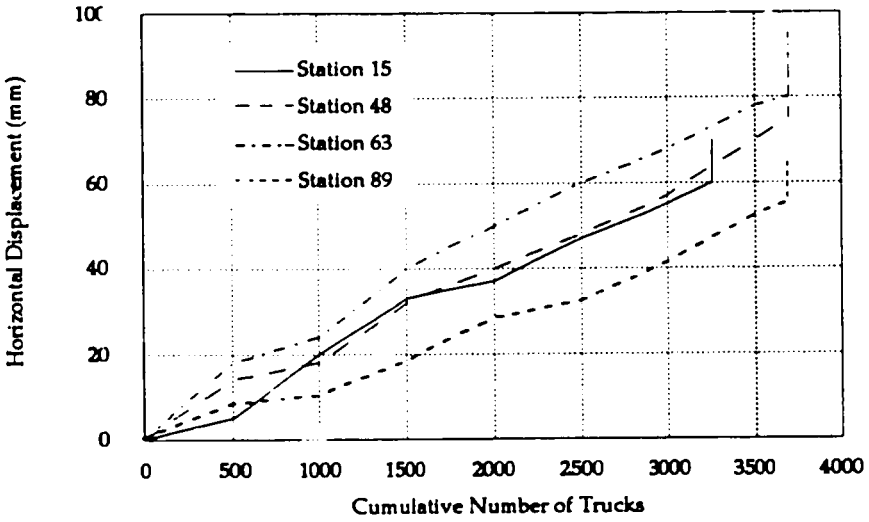

Figure 10.13 Correlation of surface horizontal deformation with the amount of construction activity on the landfill

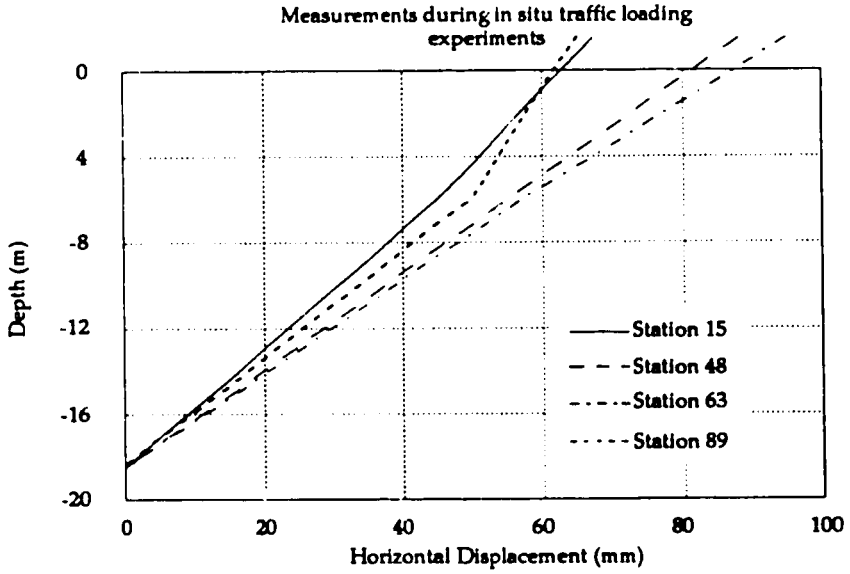

Figure 10.14 Horizontal displacements after 160 days of observations

The horizontal displacements presented in Fig. 10.14 suggest a relatively uniform distribution of the horizontal displacements with respect to the distance from the area of loading. The straight line profiles are somewhat indicative of the lack of more elaborate instrumentation. The calculations which will be presented in the following relate to deformations measured at stations 48 or 63 where maximum displacement of the sheet pile has been observed.

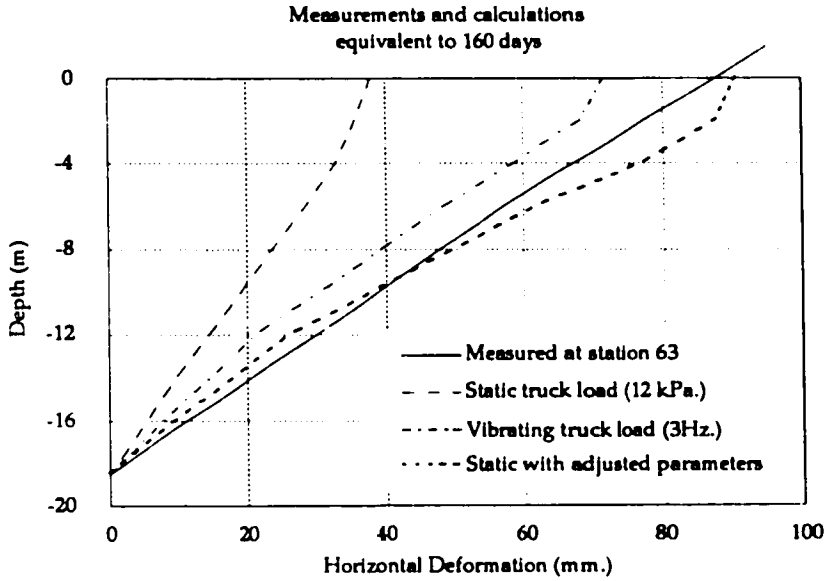

Figure 10.15 Calculated horizontal deformations at 20 meters from the centre of the circular truck path

The finite element analyses show (Fig. 10.15) that the effect of the vibrations is confined within a depth of 4 to 5 meters from the surface while the radius of the affected area is comparatively larger. The double curvature of the lateral deformations profiles indicate partially drained conditions where the top of the layer is in a quasi-undrained phase. The overall displacement patterns for the static and dynamic loading conditions are given in Figure 10.16 and 10.17 respectively. The slightly improbable shape of the displacements pattern after 150 days is due to the exaggeration of the displacements by a factor of 100. Again, the deformations in the upper layers are seen to exceed their respective values under static consolidation.

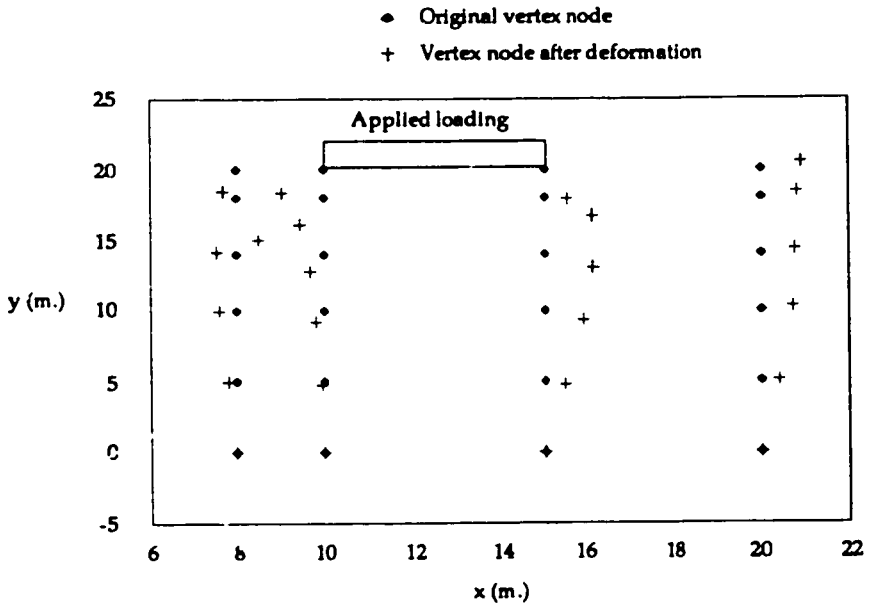

Figure 10.16 Deformation pattern for finite element nodes after 150 days of static loading; the displacements have been exaggerated 100 times

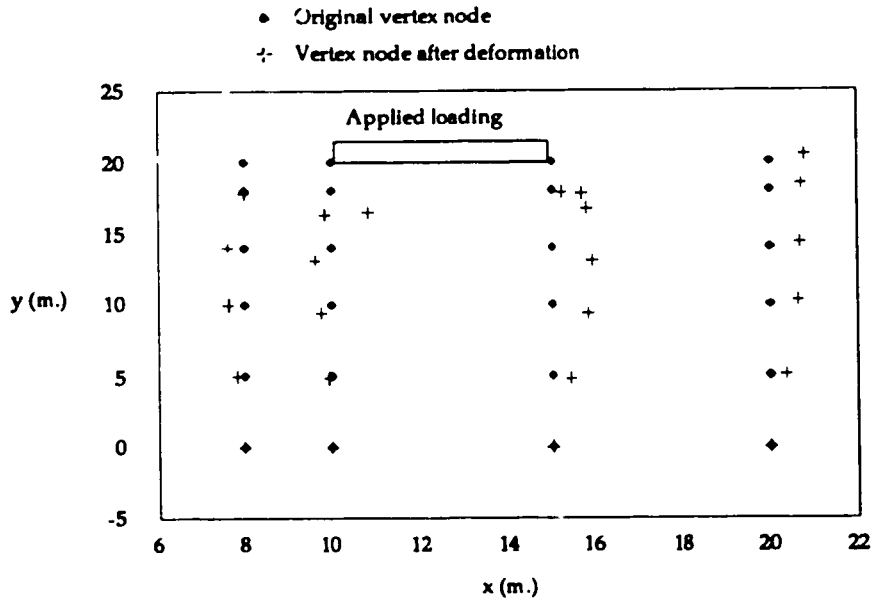

Figure 10.17 Deformation pattern for finite element nodes after 150 days of dynamic loading; the displacements have been exaggerated 100 times

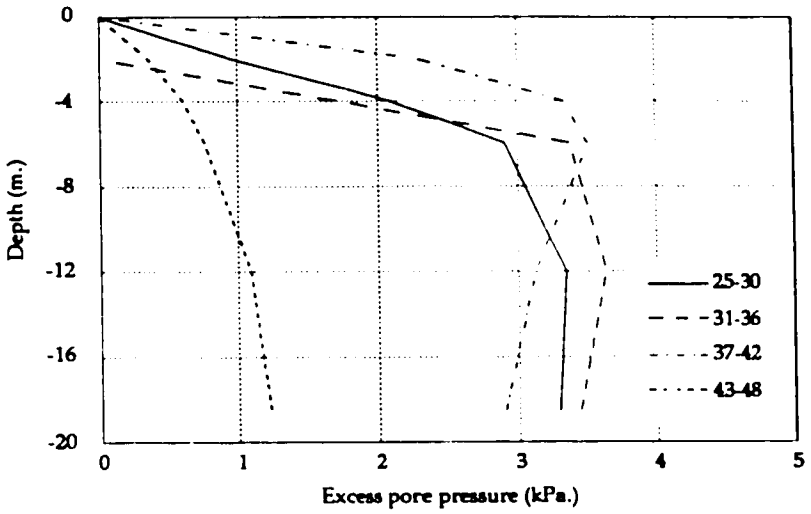

Figure 10.18 150 day isochrones for calculated excess pore pressures for static loading conditions

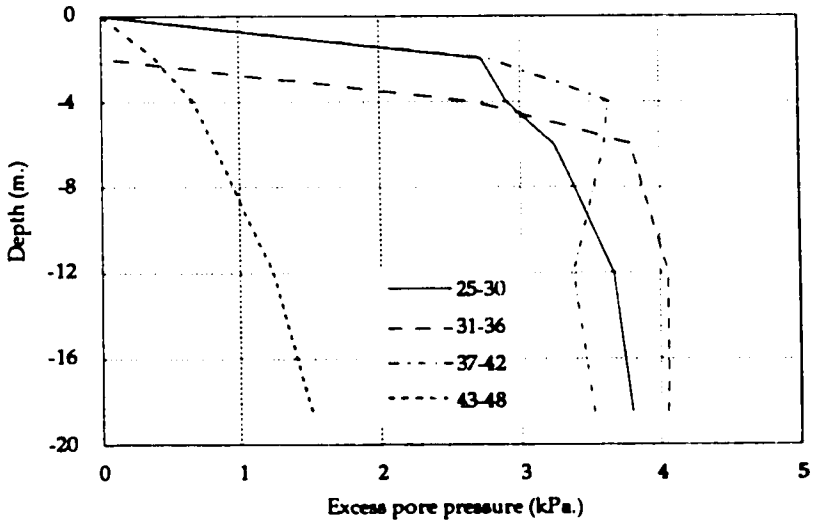

Figure 10.19 150 day isochrones for calculated excess pore pressures for dynamic loading conditions

In the upper layers of the deposit, pore pressures are higher and dissipation rates are slower. Compared to the static loading case (Fig. 10.18) , the isochrones for the vibrational loading case (Fig. 10.19) show that the surface load conditions do in fact affect the consolidation behavior of the deeper layers. This is seen in Fig. 10.18 and 10.19 where the pore pressures in deeper layers in Fig. 10.19 are higher than those shown in Fig. 10.18. The legend in both figures indicate nodal numbers as shown in Fig. 10.1.

When the information from displacement patterns and excess pore pressure distributions are combined, the behavior of the soft clay foundation under vibration load is found to demonstrate a typical rate dependent phenomenon. It was established earlier in this thesis that vibrations promote the inherent rate dependency of soft clays and the finite element analysis results also show evidence of this behaviour.

10.7. Conclusion

The mechanical behaviour of soft clays under vibration loading requires the proper description of time dependent characteristics of the soil. In the light of the previous chapters, the computer program CRISPEX presented in Chapter 10 has proven to be an adequate predictive tool for the analysis of soft clay foundations. It is seen that the calculations agree well with the measured field data and the mechanical behaviour of the foundation corresponds to the fundamental characteristics of highly viscous plastic soils (e.g., strong dependency on time, length of time required for the full propagation of surface agents, deformation and pore pressure patterns within the clay mass).

The details of the CRISPEX results can be found in Appendix A where further interpretation of the calculations is included.

In soft clay foundations, the pore pressures have been observed to increase even after the end of the loading period [Almeida et al. (1982), Leroueil et al. (1988)]. This is obviously the result of time dependent deformations under constant stresses which actually act against the consolidation process.

The effect of considering traffic vibration on the soil is softer deformation response which retards the dissipation of pore water pressures (since at this stage the deformation of the soil is not entirely due to expelled pore water) and as the construction proceeds, a sustained quasi-undrained situation is created [Choa et al. (1979)]. The existence of vibratory loads contributes and prolongs this stage of the embankment behaviour, consequently the "back-pressure effect" is enhanced. The calculations thus imply a behaviour that is in agreement with the conclusions of the vibrational slump test results.

This point is important for both short and long term stability concerns: in the case of the former, unexpected undrained failure may occur due to slower consolidation rates and in the case of the latter, damage to land development projects may be caused (e.g., via differential settlements) by under-estimated primary consolidation periods. It is the hope of the author that the ideas put forward in this thesis along with the proposed analysis tools will assist the Geotechnical Engineer in addressing these concerns.

SUMMARY AND RECOMMENDATIONS

Summary of Contributions

The mechanical behaviour of soft clays under vibration loads has been studied from experimental and analytical perspectives. The findings contained in this thesis can be summarized as follows:

1- Vibration loads on soft clays result in a softer response characterized by an increase in strain rates compared to non vibrational loads. This finding has been confirmed through laboratory tests, stress wave propagation calculations and finite element analyses.

2- The deformation behaviour of an unsupported soft clay sample under its own weight and a horizontal vibration at its base is governed by a surface in the *Time-Strain rate-Frequency* domain.

3- The predictive ability of the Adachi-Oka viscoplastic model is established for the time dependent loading conditions such as vibration loads. Through this finding, and a careful examination of the evolution of the model's rate dependent variables during straining, it has been confirmed that the influence of vibrations is akin to rate effects.

4- A comparison of the Adachi-Oka model (and more generally the Perzyna overstress model) with an Arrhenius type rate process model has revealed that the rate dependent parameters of the former correspond to the physical internal state variables of the latter. As a corollary, it has been established that the phenomenological nature of the overstress type model implicitly accounts for the physical processes that are expressed by internal state variables.

5- A comprehensive Finite Element program has been developed using the Adachi-Oka elasto-viscoplastic constitutive model. As the first to use this model, this computer program provides a new analytical tool for the analysis of static as well as dynamic boundary conditions and steady and acceleration creep phenomena.

Recommendations for Further Research

1- A rigorous definition of the Time-Strain Rate-Frequency surface as a state surface is likely to provide improved description of the frequency effects on the deformation of soft clays.

2- To accomplish this goal, further laboratory testing, involving vertical vibrations for instance, is needed to ascertain the uniqueness of the relationships presented in this thesis.

3- The quantitative comparison of the phenomenological rate dependent parameters as they relate to the physical variables in thermodynamically founded theories will surely be useful in the understanding of the mechanical behaviour of soft clays.

REFERENCES AND BIBLIOGRAPHY

ADACHI, T., MIMURA, M., OKA, F., 1985, "Descriptive Accuracy of Several Existing Constitutive Models for Normally Consolidated Clays," Proc. 5th Intl. Conf. on Num. Meth. in Geomech. Nagoya, Japan, 259.

ADACHI, T., OKA, F., 1982, "Constitutive Equations for Normally Consolidated Clay Based on Elasto-Viscoplasticity," Soils and Foundations, v.22, no.4, 57.

ADACHI, T., OKA, F., 1984, "Constitutive Equations for Normally Consolidated Clays and Assigned Works for Clay," Proc. Symp. on Sedimentation and Consolidation, Predictions and Validation, Ed. R. N. Yong, F. C. Townsend, San Francisco, 123.

ADACHI, T., OKA, F., MIMURA, M., 1987, "Mathematical Structure of an Overstress Elasto-Viscoplastic Model for Clay," Soils and Foundations, v.27, no.3, 31.

ADACHI, T., OKA, F., TANGE, Y., 1982, "Finite Element Analysis of Two-dimensional Consolidation using an Elasto-Viscoplastic Constitutive Equation," Proc. 4th Intl. Conf. on Numerical Meth. in Geomech., Edmonton, v.2, 287.

ADACHI, T., OKANO, M., 1974, "A Constitutive Equation for Normally Consolidated Clay," Soils and Foundations, v.14, no.4, 55.

AHMAD, S. A., PEAKER, K. R., 1977, "Geotechnical Properties of Soft Marine Singapore Clay," Proc. of the Intl. Symp. on Soft Clay, 3.

AKAI, K., ADACHI, T., ANDO, N., 1975, "Existence of a Unique Stress-Strain-Time Relation of Clays," Soils and Foundations, v.15 no.1, 1.

AKAI, K., HORI, M., 1974, "Considerations of Wave Characteristics in Soil Assumed as a Viscoelastic Material," Proc. JSCE, no.221, 81.

AKAI, K., YAMAMOTO, J., OZAWA, Y., 1962, "On the Behavior of Pore Pressure During Shear of Saturated Clay," Trans. of JSCE (in Japanese), no.85,1.

ALMEIDA, M. S. S., RAMALHO-ORTIGAO, J. A., 1982, "Performance and finite Element Analyses of a Trial Embankment on Soft Clay," Intl. Symp. on Numerical Models in Geomechanics, Zurich, 548.

ANDERSEN, K. H., 1975, Repeated Loading on Clay, NGI Internal Report, in WOOD, D. M., 1982, "Laboratory Investigations of the Behaviour of Soils Under Cyclic Loading: A Review," Soil Mechanics-Transient and Cyclic Loads, Ed. G. N. Pande and O. C. Zienkiewicz, John Wiley & Sons, 513.

ARAI, K., 1985, "Representation of Soft Clay Behavior Based on Minimization of Dissipated Energy," Proc. 5th Intl. Conf. on Num. Meth. in Geomech., Nagoya, Japan, v.1, 277.

ARAI, K., HASHIBA, S., KITAGAWA, K., 1988, "A Unified Approach to Time Effects in Anisotropically Consolidated Clays," Soils and Foundations, v.28, no.4, 147.

BARDEN, L., 1969, "Time Dependent Deformation of Normally Consolidated Clays and Peats," Proc. ASCE, SM1, 1.

BAZANT, Z. P., 1978, "Endochronic Inelasticity and Incremental Plasticity," Intl. J. of Solids and Structures, v.14, 691.

BEEN K., SILLS, G. C., 1981, "Self Weight Consolidation of Soft Soils: an Experimental and Theoretical Study," Géotechnique, v.31, no.4, 519.

BERGADO, D. T., MIURA, N., PANICHAYATUM, B., SAMPOCO, C. L., 1988, "Reinforcement of soft Bangkok Clay Using Granular Piles," Proc. of the Intl. Geotechnical Symp. on Theory and Practice of Earth Reinforcement, 179.

BINGHAM, E. C., 1922, Fluidity and Plasticity, McGraw Hill, New York.

BIOT, M. A., 1941, "General Theory of Three Dimensional Consolidation," J. Appl. Physics, v.12, 155.

BIOT, M. A., 1955, "Theory of Elasticity and Consolidation for a Porous Anisotropic Solid," J. Appl. Physics, v.26, 182.

BIOT, M. A., 1956, "Theory of Propagation of Elastic Waves in a Fluid Saturated Porous Solid, Parts I&II," J. Acoustics Soc. of America, v.28, 168.

BIOT, M. A., 1962, "Mechanics of Deformation and Acoustic Propagation in Porous Media," J. Appl. Physics, v.33, 1483.

BIOT, M. A., 1963, "Theory of Stability and Consolidation of a Porous Medium Under Initial Stress," J. Math. and Mech., v.12, 521.

BISHOP A. W., 1966, "The Strength of Soils as Engineering Materials," Géotechnique, v.16, 91.

BISHOP, A. W., HENKEL, D. J., 1962, The Measurement of Soil Properties, E. Arnold Pub., London.

BJERRUM , L., 1967, "Engineering Geology of Norwegian Normally Consolidated Clays as Related to Settlements of Buildings," Géotechnique, v.17, no.2, 81.

BJERRUM , L., 1972, "Embankments on Soft Ground," Proc. of the Specialty Conf. on Performance of Earth and Earth Supported Structures, Purdue, Indiana, ASCE Publishers, v.2, 1.

BLÜMEL W., TAMMINGA, P. G., 1987, "Water Permeability of Dredged Mud," Proc. of the 9th European Conference on SMFE, Dublin, Ireland.

BOWEN, R. M., 1982, "Compressible Porous Media by the Use of a Theory of Mixtures," Intl. J. Engineering Science, v.20, no.6, 697.

BRENNER, R. P., NATULAYA, P., CHILINGARIAN, G. V., ROBERTSON, J. O., 1981, Chapter 2, Soft Clay Engineering, Eds. E. W. Brand and R. P. Brenner, Elsevier, Amsterdam.

BREWER, J. H., 1972, The Response of Cyclic Stress in a Normally Consolidated Saturated Clay, Ph. D. Thesis, N. C. State University, in WOOD, D. M., 1982, "Laboratory Investigations of the Behaviour of Soils Under Cyclic Loading: A Review," Soil Mechanics-Transient and Cyclic Loads, Ed. G. N. Pande and O. C. Zienkiewicz, John Wiley & Sons, 513.

BRITTO, A. M., GUNN, M. J., 1987, Critical State Soil Mechanics via Finite Elements, Ellis Horwood Ltd., Chichester.

BROMS, B. B., 1987, "Soil Improvement in South East Asia for Soft Soils," Proc. of the 8th Asian Regional Conf. on Soil Mechanics and Foundation Engineering, Guest Lecture preprint.

BROWN, S. F., LASHINE, A. K. F., HYDE, A. K. L., 1975, "Repeated Load Triaxial Testing of a Silty Clay," Géotechnique, v.25, no.1, 95.

BURLAND, J. B., 1965, "The Yielding and Dilation of Clay," Correspondence, Géotechnique, v.15, 211.

CALLADINE, C. R., 1963, "The Yielding of Clay," Géotechnique, v.13, no.3, 250.

CASAGRANDE, A., 1949, Discussion on "Binger And Thompson, Symposium on the Panama Canal - The Sea Level Project," Trans. ASCE, v.114, 870.

CASAGRANDE, A., WILSON, S. D., 1951, "Effects of Rate of Loading on the Strengths of Clays and Shales at Constant Water Content," Géotechnique, v.2, no.2, 251.

CHADWICK, P., COX, A. D., HOPKINS, H. G., 1964, "Mechanics of Deep Underground Explosions," Philosophical Transactions of the Royal Society, London, v.287A, 235.

CHEN, W. F., SALEEB, A. F., 1986, Constitutive Equations for Engineering Materials, Volume II: Plasticity and Modeling, Wiley-Interscience, New York.

CHOA, V., VIJARATHAM, A., KARUNARATNE, G. P., RAMASWAMY, S. D., LEE, S. L., 1979, "Consolidation of Changi Marine Clay of Singapore Using Flexible Drains," Proc. 7th European Regional Conference, Brighton, U.K., v.3, 29.

CHRISTOULAS, S., KALTEZIOTIS, N., TSIAMBAOS, G., SBATAKAKIS, N., 1987, "Engineering Geology of Soft Clays. Examples from Greece", Embankments on Soft Clays, Special Publication, Bulletin of the Public Works Research Center, Athens, Greece, 1.

COLLINS, K., MCGROWN, A., 1974, "The Form and Function of Microfabric Features in a Variety of Natural Soils," Géotechnique, v.24, 223.

CORMEAU, I., 1975, "Numerical Stability in Quasi-Static Elasto/Viscoplasticity," Intl. J. for Num. Meth. in Eng., v.9, 109.

COURANT, R., HILBERT, D., 1962, Partial Differential Equations, Methods of Mathematical Physics, v.2, Interscience, New York.

CRAWFORD, C. B., BOZOZUK, M., 1990, "Thirty Years of Secondary Consolidation in Sensitive Marine Clay," Canadian Geotechnical Journal, V.27, no.3, 315.

CRISTESCU, N., 1967, Dynamic Plasticity, North Holland, Amsterdam.

CRISTESCU, N., SILICIU, I., 1976, Viscoplasticity, Martinus Nijhoff, The Hague.

DEESWASMONGKOL, N., NOPPADOL, P., AREEPITAK, C., 1988, "Major Slope Stability Problems in Dam Constructions in Thailand", Proc. of the Intl. Geotechnical Symp. on Theory and Practice of Earth Reinforcement, 265.

DESAI, C. S., KREMPL, E. KIOUSIS, P.D., KUNDU, T., Editors, 1987, Proc. 2nd Intl. Conf. on Constitutive Laws for Engineering Materials : Theory and Applications, Tucson, AZ., Elsevier.

DESAI, C. S., SIRIWARDANE, H. J., 1984, Constitutive Laws for Engineering Materials with Emphasis on Geologic Materials, Prentice-Hall, New York.

DIMAGGIO , F. L., SANDLER, I. S., 1971, "Material Model for Granular Soils," Journal of the eng. Mechanics Div., ASCE, v.97, EM3, 935.

DRUCKER, D. C. , 1951, "A More Fundamental Approach to Plastic Stress-Strain Relations," Proc. of the 1st National Congress on Applied Mechanics, ASME, 487.

DRUCKER, D. C. , 1953, "Limit Analysis of Two and Three Dimensional Soil Mechanics Problems," Journal of Mech. and Phys. of Solids, v.1, 217.

DRUCKER, D. C. , 1959, "A Definition of Stable Inelastic Material," Journal of Applied Mechanics, v.26, 101.

DRUCKER, D. C. , 1964a, "On the Postulate of Stability of Material in the Mechanics of Continua," Journal de Mécanique, v.3, no.2, 235.

DRUCKER, D. C. , 1964b, "Stress-Strain-Time Relations and Irreversible Thermodynamics," Proc. Intl. Symposium on Second Order Effects in Elasticity, Plasticity and Fluid Dynamics, Haifa, Israel, 1962, Pergamon Press, Oxford, 331.

DRUCKER, D. C. , GIBSON, R. E., HENKEL, D. J., 1957, "Soil Mechanics and Work Hardening Theories of Plasticity," Transaction of the ASCE, v.122, 338

DRUCKER, D. C. , PRAGER, W., 1952, "Soil Mechanics and Plastic Analysis or Limit Design," Quarterly Journal of Applied Mechanics, v.10, 157.

EIDE, O., 1967, "Geotechnical Problems with Soft Bangkok Clay on the Nakhon Sawan Highway Project," Proc. of the 1st Engineering Conference, Engineering Institute of Thailand, Bangkok, Thailand, NGI Pub. No. 74.

ERINGEN, A. C., INGRAM, J. D., 1967, "A Continuum Theory of Chemically Reacting Media, Part II," Intl. J. Engineering Science, v.5 , 289.

EROL, O., DEMIREL, T., LOHNES, R. A., 1977, "Rate Process Theory Applied to Soils," Proc. Intl. Symp. on Soft Clay, Bangkok, 117.

FARUQUE , M. O., 1986, "Modeling of Undrained Creep of Normally Consolidated Clays," Journal of Engineering Mech., ASCE, v.112, no.10, 1007.

FLODIN, N., BROMS, B., 1982, "Historical Development of Civil Engineering in Soft Clay," Chapter 1 in Soft Clay Engineering, Ed. E. W. Brand and R. P. Brenner, Elsevier, Amsterdam.

FREUDENTHAL, A. M., 1958, "The Mathematical Theories of Inelastic Continuum,", Handbuch der Physik, v.6, Spring Verlag, Berlin.

FUJIWARA, H., UE, S., 1990, "Effect of Preloading on Post-Construction Consolidation Settlement of Soft Clay Subjected to Repeated Loading," Soils and Foundations, v.30, no.1, 76.

GOLAIT, Y. S., KATTI, R. K., 1987, "Stress-Strain Idealization for Bombay High Calcareous Soils," Proc. of the 8th Asian Regional Conf. on Soil Mechanics and Foundation Engineering, 177.

HAMPTON, D, WEZEL, R. A., 1967, "Stress Wave Propagation in Confined Soils," Proc. Intl. Symp. on Wave Propagation and Dynamic Properties of Earth Materials, New Mexico, 433.

HEIERLI, W., 1962, "Inelastic Wave Propagation in Soil Columns," Proc. ASCE, v.88, SM6, 33.

HIGHT, D. W., GENS, A., JARDINE, R. J., 1985, "Evaluation of Geotechnical Parameters from Triaxial Tests on Offshore Clay," Society of Underwater Tech. Conf. on Offshore Site Investigations, London.

HILL, R., 1950, The Mathematical Theory of Plasticity, Clarendon Press, London.

HOHENEMSER, K., PRAGER, W., 1932, "Über die Ansätze der Mechanik isotroper Kontinua," ZAMM, v.12, 216.

HORI, M., 1974, Fundamental Study of Wave Propagation Characteristics Through Soils, Ph.D. Thesis, Kyoto University, (in Japanese).

HUGHES, T. J. R., TAYLOR, R. L., 1978, "Unconditionally Stable Algorithms for Quasi-Static Elasto/Viscoplastic Finite Element Analysis," Computers and Structures, v.8, 169.

HVORSLEV, M. J., 1937, "Uber die Festigkeitseigenschaften gestörter bindiger Böden," Ingeniorvidenskabelige Skrifter, A. No. 45, Copenhagen.

ISHIHARA, K., 1967, "Propagation of Compression Waves in a Saturated Soil," Proc. Intl. Symp. on Wave Propagation and Dynamic Properties of Earth Materials, U. of New Mexico, 451.

ISHIHARA, K., 1976, Fundamentals of Soil Dynamics, Kajima Publishing Co., Tokyo, (in Japanese).

IWAN, I. W., 1967, "On a Class of Models for the Yielding Behavior of Continuous and Composite Systems," J. Appl. Mech., v.34, 612.

KALIAKIN, V. N., DAFALIAS, Y. F., 1990, "Theoretical Aspects of the Elastoplastic-Viscoplastic Bounding Surface Model for Cohesive Soils," Soils and Foundations, v.30, no.3, 11.

KAMEI, T., HIRAI, H., 1990, "An Elasto-Viscoplastic Model with Combined Hardening of Anisotropically Consolidated Cohesive Soils," Soils and Foundations, v.30, no.2, 89.

KAO, T. C., WANG, C. H., MOH, Z. C., 1987, "Construction Failures of Excavation in Soft Clay Studies," Proc. of the 8th Asian Regional Conf. on Soil Mechanics and Foundation Engineering, 297.

KARMAN, T., DUWEZ, P., 1950, "The Propagation of Plastic Deformation in Solids." J. of Appl. Physics, v.21, 987.

KARUNARATNE, G. P., TAN, S. A., LEE, S. L., CHOA, V., 1989, "Analysis of flexible Drains in Changi Reclamation," Canadian Geotechnical Journal, v.26, no.3, 401.

KATTI, R. K., HUMAD, S., DEWAIKAR, D. M., KULKARNI, S. K., KHADILKAR, B. S., CHANDRASEKARAN, V. S., SUNDARAM, P. N., 1977, "Characteristics of Bombay Marine Clay in Twin City Area," Proc. of the Intl. Symp. on Soft Clay, 27.

KENNEY, T. C., 1964, "Sea-level movements and the Geologic Histories of Boston, Nicolet, Ottawa, and Oslo," Géotechnique, v.14, no.3, 203.

KONDNER, R. L., HO, M. M. K., 1965, "Viscoelastic Response of a Cohesive Soil in the Frequency Domain," Transactions of the Soc. of Rheology, v.9, part 2, 329.

KÖITER, W. T., 1953, "Stress-strain Relations, Uniqueness and Variational Theorems for Elastic-Plastic Materials with Singular Yield Surface," Q. App. Math., v.2, 350.

LACASSE, S., BERRE, T., LEFEBVRE, G., 1985, "Bloc Sampling of Sensitive Clays," Proc. of the 11th Intl. Conf. on SMFE, San Fransisco, v.2, 887.

LADE, P. V., 1977, "Elasto-plastic Stress-Strain Theory for Cohesionless Soil with Curved Yield Surfaces," Intl. J. of Solids and Structures, v.13, 1019.

LADE, P. V., 1979, "Stress-Strain Theory for Normally Consolidated Clay," Proc. 3rd Intl. Conf. on Num. Methods in Geomech., Aachen, Germany, v.4, 1325.

LAMB, H., "On the Propagation of Tremors over the Surface of an Elastic Solid," Philosophical Transactions of the Royal Soc., v.203, 1.

LAMBE, T. W., WHITMAN, R. V., 1969, Soil Mechanics, J. Wiley & Sons, New York.

LEE, S. L., KARANURATNE, G. P., YONG, K. Y., CHOW, Y. K., CHEW, S. H., 1988, "Consolidation of Dredged Clay in Reclamations," Soils and Foundations, v.28, no.2, 1.

LEFEBVRE, G., LANGLOIS, P., LUPIEN, C., LAVALÉE, J., 1984, "Laboratory Testing on In Situ Behavior of Peat as Embankment Foundation," Canadian Geotechnical Journal, v.21, 332.

LEONARDS, G. A., 1979, "Stability of Slopes in Soft Clays," Proc. of the the Pan American Conference on SMFE, Lima, Peru, Special Lecture, v.2, 225.

LEROUEIL, S., KABBAJ, M., TAVENAS, F., 1988, "Study of the Validity of a σ'_v-ε_v-$d\varepsilon_v$ Model in In Situ Conditions," Soils and Foundations, v.28, no.3, 13.

LEROUEIL, S., KABBAJ, M., TAVENAS, F., BOUCHARD, R., 1985, "Stress-Strain-Strain Rate Relation for the Compressibility of Sensitive Natural Clays," Géotechnique, v.35, no.2, 159.

LEROUEIL, S., TAVENAS, F., MIEUSSENS, C., PEIGNAUD, M., 1978, "Construction Pore Pressures in Clay Foundations Under Embankments. Part II: Generalized Behaviour," Can. Geotech. J., v.15, no.1, 66.

LOCAT, J., LEFEBVRE, G., 1985, "The Compressibility and Sensitivity of Artificially Sedimented Clay Soil: The Grande Baleine Marine Clay, Quebec, Canada," Marine Geotechnology, v.6, no.1, 1.

LUMB, P., 1977, "The Marine Soils of Hong Kong and Macau," Proc. of the Intl. Symp. on Soft Clay, 45.

MA, S. D., 1987, "Actual Behaviour of the Mucky Clay Foundation under a Breakwater," Proc. of the 8th Asian Regional Conf. on Soil Mechanics and Foundation Engineering, 469.

MAGNAN, J. P., HUMPERT, P., MOURADIS, A., 1982, "Finite Element Analysis of Soil Deformations with Time under an Experimental Embankment at Failure," Intl. Symp. on Numerical Models in Geomechanics, Zurich, 601.

MALVERN, L. E., 1951a, "The Propagation of Longitudinal Waves of Plastic Deformation in a Bar of Metal Exhibiting Strain Rate Effect," J. Appl. Mech., v.18, 203.

MALVERN, L. E., 1951b, "Plastic Wave Propagation in a Bar of Metal Exhibiting Strain Rate Effect," Q. Appl. Math., v.8, 405.

MASSARSCH, K. R., BROMS, B. B., SUNDQUIST, O., 1975, "Pore Pressure Deformation with Multiple Piezometers," Proc. of the ASCE Specialty Conf. on In situ Measurement of Soil Properties, Raleigh, NC., v.1, 260.

MATSUI, T., 1988, "A Constitutive Model for Cyclic Viscoplasticity of Soils," Soils and Foundations, v.28, no.4, 19.

MATSUI, T., ABE, N., 1982, "Application of Elasto-plastic and Elasto-viscoplastic Models to multi-dimensional Consolidation Analysis," Proc. Intl. Symp. on Num. Models in Geomech., Zurich, 711.

MAYNE, P. W., KULHAWY, F. H., 1982, " K_o- OCR Relationships in Soils," ASCE Journal of Geotechnical Engineering, v.106, GT11, 1219.

MIMURA, M., SEKIGUCHI, H., 1986, "Bearing Capacity and Plastic Flow of Rate Sensitive Clay Under Strip Loading," Bulletin of the Disaster Prevention Research Institute, Kyoto University, v.36, 99.

MIMURA, M., SHIBATA, T., NOZU, M., KITAZAWA, M., 1990, "Deformation Analysis of a Reclaimed Marine Foundation Subjected to Land Construction," Soils and Foundations, v.30, no.4, 119.

MITCHELL, J. K., 1976, Fundamentals of Soil Behavior, J. Wiley & Sons, New York.

MITCHELL, J. K., CAMPANELLA, R. G., SINGH, A., 1968, "Soil Creep as a Rate Process," J. Soil Mech. and Foundations Div., ASCE, SM1, 231.

MITCHELL, J. K., 1960, "Fundamental Aspects of Thixotropy in Soils," Proc. ASCE, Journal of SMFE, v.8, 19.

MOHAN, D., BHANDARI, R. K., 19 , " Analysis of Some Indian Marine Clays," Proc. of the Intl. Symp. on Soft Clay, 59.

MROZ, Z., 1967, "On the Description of Anisotropic Hardening," J. of the Mechanics and Physics of Solids, v.15, 163.

MURAYAMA, S., SHIBATA, T., 1961, "Rheological Properties of Clays," Proc. 5th. Intl. Conf. on SMFE, v.1, 269.

MURAYAMA, S., SHIBATA, T., 1964, "Flow and Stress Relaxation of Clays," Proc. IUTAM Symp. on Rheology and Soil Mechanics, 99.

NAGHDI, P. M., 1960, "Stress-Strain Relations in Plasticity and Thermoplasticity," Plasticity, Eds. E. H. Lee, P. S. Symonds, Pergamon Press, London, 121.

NAGHDI, P. M., MURCH, S. A. 1963, "On the Mechanical Behavior of Viscoelastic/Plastic Solids," J. of Appl. Mech., v.30, 321.

NAKASE, A., 1987, "Kansai International Airport - Construction of Man-Made Island," Proc. of the 8th Asian Regional Conf. on Soil Mechanics and Foundation Engineering, Guest Lecture preprint.

NAKASE, A., KIMURA T., SAITOH K., TAKEMURA J., HAGIWARA T., 1987, "Behaviour of Soft Clay with a Surface Crust," Proc. of the 8th Asian Regional Conf. on Soil Mechanics and Foundation Engineering, 401.

NOVA, R., 1982, "A Viscoplastic Constitutive Model for Normally Consolidated Clay," Proc. IUTAM Symp. on Deformation and Failure of Granular Materials, 287.

ODA, Y., MITACHI, T., 1988, "Stress Relaxation Characteristics of Saturated Clays," Soils and Foundations, v.28, no.4, 69.

OKA, F. , 1978, Constitutive Theory of Cohesive Soil and its Application to Stress Wave Propagation, Ph.D. Thesis, Kyoto University.

OKA, F., 1979, "Constitutive Theory for Solid-Fluid Mixture and its Application to Stress Wave Propagation Through Cohesive Soil," Proc. JSCE, no.272, 117.

OKA, F., 1981, "Prediction of Time Dependent Behaviour of Clay," Proc. 10th. Intl. Conf. on SMFE, v.1, 215.

OKA, F., 1982, "Elasto-Viscoplastic Constitutive Equation for Overconsolidated Clay," Proc. Intl. Symp. on Numerical Meth. in Geomech., Zurich, 147.

OKA, F., 1985, "Elasto-Viscoplastic Constitutive Equations with Internal State Variables," Computers and Geomechanics, v.1, 59.

OKA, F., ADACHI, T., OKANO, Y., 1986, "Two-Dimensional Consolidation Analysis Using an Elasto-Viscoplastic Constitutive Equation," Intl. J. of Numerical and Analytical Meth. in Geomech., v.10, 1.

OSAKI, T., 1974, "Review of Dynamic Analyses," Tsuchi & Kiso, v.22, no.3, 1, (in Japanese).

PARKIN, B. R., 1962, "Theory Compared with Experiments on Soil Column," Discussion: Implications of an Elementary Theory, Symp. on Impact Waves in Sand, Trans. ASCE, v.127, 1270.

PERZYNA, P., 1963, "The Constitutive Equations for Rate Sensitive Plastic Materials," Q. of Applied Mathematics, v.20, 321.

PERZYNA, P., 1963, "The Constitutive Equations for Work Hardening and Rate Sensitive Plastic Materials," Proc. Vibrational Problems, Warsaw, v.4, no. 3, 281.

PERZYNA, P., 1964, "The Constitutive Equations for Work Hardening and Rate Sensitive Plastic Materials,", Proc. Vibration Problems, v.4, 281.

PERZYNA, P., 1966, "Fundamental Problems in Viscoplasticity," Advances in Applied Mechanics, v.9, 243.

POOROOSHASB, H. B., ROSCOE, K. H., 1961, "The Correlation of the Results of Shear Tests with Varying Degrees of Dilatation," Proc. 5th Intl. Conf. on Soil Mechanics, Paris, v.1, 297.

PRAGER, W., 1937, "Mécanique des Solides Isotropes au delà du Domaine Elastique," Memorial Scientifique et Mathématique, v.87, Paris.

PRAGER, W., 1954, "Discontinuous Fields of Plastic Stress and Flow," Proc. 2nd U.S. National Congress of Applied Mechanics, 21.

PREVOST, J. H., 1977, "Mathematical Modeling of Monotonic and Cyclic Undrained Clay Behaviour," Intl. J. of Numerical and Analytical Methods in Geomechanics, v.1, 195.

PREVOST, J. H., 1980, "Mechanics of Continuous Porous Media," Intl. J. Engineering Science, v.18, no.5, 787.

PREVOST, J. H., CUNY, B., HUGHES, T. J. R., SCOTT, R. F., 1981, "Offshore Gravity Structures : Analysis," Journal of the Geotech. Div., ASCE, v.107, GT2, 143

PUSCH, R., 1973, "Physico-chemical Processes which Affect Soil Structure and Vice-Versa," Proc. Intl. Symp. Soil Structure, Göthenburg, Sweden, Appendix, 27.

QUINLAN, P. M., 1956, "The Elastic Theory of Soil Dynamics," Special Technical Publication no.156, ASTM, 3.

RAKHMATULIN, H. A., 1945, Prikl. Mat. Mekh., v.9, 91, (in Russian, in Cristescu, N., 1967, Dynamic Plasticity, North Holland)

RAYMOND G. P., GASKIN, P. N., ADDO-ABEDI, F. Y., 1979, "Repeated Compressive Loading of Leda Clay," Can. Geotech. J., v.16, no.1, 1.

REISSNER E., 1937,1936, in "Prakash, S., 1981, Soil Dynamics," McGraw-Hill, New York, 367.

RICHARDSON, A. M., WHITMAN, R. V., 1963, "Effect of Strain Rate upon Undrained Shear Strength of Saturated Remoulded Fat Clay," Géotechnique, v.13, no.4, 310.

ROSCOE, K. H., SCHOFIELD, A. N., WROTH, C. P., 1958, "On the Yielding of Soils," Géotechnique, v.11, no.1, 22.

ROSCOE, K. H., BURLAND, J. B., 1968, "On the Generalized Stress-Strain Behaviour of 'Wet' Clay," Engineering Plasticity, Cambridge University Press, 535.

ROSCOE, K. H., POOROOSHASB, H. B., 1963, "A Theoretical and Experimental Study of Strains in Triaxial Compression Tests on Normally Consolidated Clays," Géotechnique, v.13, 12.

ROSCOE, K. H., SCHOFIELD, A. N., THURAIRJAH, A., 1963, "Yielding of Clays in States Wetter than Critical," Géotechnique, v.13, no.3, 211.

SALVADORI, M. G., SHALAK, R., WEIDLINGER, P., 1960, "Waves and Shocks in Locking and Dissipative Media," Proc. of ASCE, v.86, EM2, 77.

SCHOFIELD, A. N., WROTH, C. P., 1968, Critical State Soil Mechanics, McGraw-Hill, London.

SEAMAN , L., 1966, "One Dimensional Stress Wave Propagation in Soils," Stanford Research Inst., AD-632106, DASA 1757, 19.

SEKIGUCHI, H., 1977, "Rheological Characteristics of Clays," Proc. 9th Intl. Conf. on SMFE, v.1, 289.

SEKIGUCHI, H., 1984, "Theory of Undrained Creep Rupture of Normally Consolidated Clay Based on Elasto-Viscoplasticity," Soils and Foundations, v.24, no. 1, 129.

SHIBATA, T., 1963, "On the Volume Changes of Normally Consolidated Clays," Annuals of the Disaster Prevention Research Institute, Kyoto University, v.6, 128.

SHOJI, M., OHTA, H., ARAI, K., MATSUMOTO, T., TAKAHASHI, T., 1990, "Two-Dimensional Consolidation Back Analysis," Soils and Foundations, v.30, no.2, 60.

SINGH, A., MITCHELL, J. K., 1968, "General Stress-Strain-Time Function for Soils," Proc. ASCE, SM1, 21.

SKEMPTON, A. W., 1970, "The Consolidation of Clays by Gravitational Compaction," J. of the Geological Soc. of London, v.125, 373.

SKEMPTON, A. W., BISHOP, A. W., 1954, "Soils," Chapter 10 in Building Materials: their Elasticity and Inelasticity, Ed. M. Reiner, North-Holland, Amsterdam.

SKEMPTON, A. W., NORTHEY, R. D., 1952, "The Sensitivity of Clays," Géotechnique, v.3, no.1, 30.

SMITH, I. M., 1982, Programming the Finite Element Method with Application to Geomechanics, John Wiley & Sons, Chichester.

SOKOLOVSKI, V. V., 1948, "Propagation of Elasto-viscoplastic Waves in bars," (in Russian), Prikl. Mat. Mekh., v.12, 261. (in Cristescu, N., 1967, Dynamic Plasticity, North Holland)

STOLLE, D. F. E., HIGGINS, J. E., 1989, "Viscoplasticity and Plasticity - Numerical Stability Revisited," Numerical Methods in Geomechanics, NUMOG III, Eds. S. Pietruszczak, G. N. Pande, Elsevier.

SUNG, T. Y., 1953, "Vibrations in Semi-Infinite Solids due to Periodic Surface Loading," Special Technical Publication no.156, ASTM, 35.

SUZUKI, O., 1988, "The Lateral Flow of Soil Caused by Banking on Soft Clay Ground," Soils and Foundations, v.28, no.4, 1.

SUZUKI, O., 1988, "The Lateral Flow of Soil Caused by Banking on Soft Clay Ground," Soils and Foundations, v.28, no.4, 1.

TAN, S. B., LEE, K. W., 1977, "Engineering Geology of the Marine Member of the Kallang Formation in Singapore," Proc. of the Intl. Symp. on Soft Clay, 75.

TAVENAS, F., BLANCHETTE, G., LEROUEIL, S., ROY, M., LA ROCHELLE, P., 1975, "Difficulties in the In situ Determination of K_o in Soft Sensitive Clays," Proc. of the ASCE Specialty Conf. on In situ Measurement of Soil Properties, Raleigh, NC., v.1, 450.

TAVENAS, F., JEAN, P., LEBLOND, P., LEROUEIL, S. 1983, "The Permeability of Natural Soft Clays Part II: Permeability Characteristics," Can. Geotech. Journal, v.20, no.4, 645.

TAVENAS, F., LEROUEIL, P., LA ROCHELLE, P., ROY, M., 1978, "Creep Behaviour of an Undisturbed Lightly Overconsolidated Clay," Can. Geotech. J. v.15, no.3, 402.

TAVENAS, F., LEROUEIL, S., 1977, "Effects of Stresses and Time on Yielding of Clays," Proc. of the 9th. Intl. Conf. on SMFE, Tokyo, Japan, v.3, 261.

TAVENAS, F., LEROUEIL, S., 1980, "The Behaviour of Embankments on Clay Foundations," Can. Geotech. J., v.17, no.2, 236.

TAVENAS, F., MIEUSSENS, C., BOURGES, F., 1979, "Lateral Displacements in Clay Foundations Under Embankments," Can. Geotech. J., v.16, no.3, 532.

TAYLOR, G. I., 1958, Scientific Papers, Ed. G. K. Bachelor, Cambridge University Press, v.2, 467.

UEHARA, H., YOSHIZAWA, M., KOHAGURA, S., 1988, "Experimental Studies to Improve the Surface Land Reclaimed From the Sea," Proc. of the Intl. Geotechnical Symp. on Theory and Practice of Earth Reinforcement, 239.

VALANIS, K. C., 1971, "A Theory of Viscoplasticity without a yield Surface, Part I & II," Arch. of Mechanics, v.23, 517,535.

VALANIS, K. C., 1975, "On the Foundations of the Endochronic Theory of Viscoplasticity," Arch. of Mechanics, v.27, 857.

VEY, E., STRAUSS, L. V., 1967, "Stress-Strain Relationships in Clay due to Propagating Stress Wave," Proc. Intl. Symp. on Wave Propagation and Dynamic Properties of Earth Materials, New Mexico, 575.

VIALOV, S. S., SKIBITSKY, A. M., 1961, "Problems of Rheology of Soils," Proc. 5th. Intl. Conf. on SMFE, v.1, 387.

WALKER, L. K., 1969, "Secondary Compression in the Shear of Clays, " Proc. ASCE, SM1, 167.

WEI, R. L., 1987, "Theoretical and Practical Problems of Soft Clay," Proc. of the 8th Asian Regional Conf. on Soil Mechanics and Foundation Engineering, 121.

WHITMAN, R. V., 1957, "The Behavior of Soils under Transient Loadings," Proc. of the 4th Intl. Conf. on SMFE, v.1, 207.

WROTH, C. P., 1979, "Correlations of Some Engineering Properties of Soils," Proc. of the 2nd Intl. Conf. on Behavior of Offshore Structures, London, v.1, 121.

WROTH, C. P., WOOD, D. M., 1978, "The correlation of Index Properties with Some Basic Engineering Properties of Soils," Can. Geotech. J., v.15, no.2, 137.

WU, T. H., DOUGLAS, A. G., GOUGHNOUR, R., 1962, "Friction and Cohesion of Saturated Clays," Proc. ASCE, v.88, SM3, 1.

YANG, Q. S., POOROOSHASB, H. B., YONG, R. N., 1987, "The General Formulations of Plasticity in Stress-Space and Strain-Space," Proc. 2nd Intl. Conf. on Constitutive Laws for Engineering Materials : Theory and Applications, Tucson, AZ., v.1, 353.

YE, B. R., ZHANG, J., ZHANG, X., 1988, "Improvement of Very Soft Ground," Proc. of the Intl. Geotech. Symp. on Theory and Practice of Earth Reinforcement, 257.

YONG, R. N., SHEERAN, D.E., 1973, "Fabric Unit Interaction and Soil Behavior," Proc. International Symposium on Soil Structure, Göthenburg, Sweden, 176.

YOUNGER, J. S., BALASUBRAMANIAM, A. S., LEE H. J., ANSHUMALI, M., 1987, "A lime Column Model Study on Bangkok Clay," Proc. of the 8th Asian Regional Conf. on Soil Mechanics and Foundation Engineering, 221.

ZIENKIEWICZ, O. C., 1977, The Finite Element Method, McGraw Hill, London.

ZIENKIEWICZ, O. C., 1984, "Coupled Problems and Their Numerical Solution," Chapter 1 in Numerical Methods in Coupled Systems, Ed. R. W. Lewis, P. Bettes, and E. Hinton, John Wiley & Sons Ltd.

APPENDIX 1

DETAILS OF THE FINITE ELEMENT ANALYSIS RESULTS

A.1. Hardware Specification

All analyses presented in this thesis have been performed on a VAX/VMS with a 8550 CPU by the Digital Equipment Corporation. The communications with this machine and all pre/post processing of the files associated with the finite element analysis have been handled by a Macintosh SE.

A.2 Mesh Geometry and Element Specification

The finite element mesh that was used in the analyses has been based on the sample presented in Fig. 10.1. Needless to say, the appropriate dimensioning of the elements has been problem specific but the overall number of elements have been kept constant (Fig. A.1).

Consolidation analyses have been performed using a 6 noded (15 degrees of freedom) linear strain triangle. Since the stress variations are linear across this element, 110 elements were used to model the problems shown in Table 10.1 through 10.7. Efficiency and accuracy constraints would dictate the use of about 40 cubic strain triangles for the same problems. In the present study, the 22 noded cubic strain triangle (30 and 40 degrees of freedom for drained/undrained and consolidation analyses respectively) is used in the modeling of the laboratory tests (see section A.6).

A.3. Material Zones and In Situ Conditions

Wherever possible, the soil deposit has been considered to be made up of a number of layers (maximum of 10 different material zones). Each of the zones can have its own constitutive relationship, therefore a more realistic description of the material is possible.

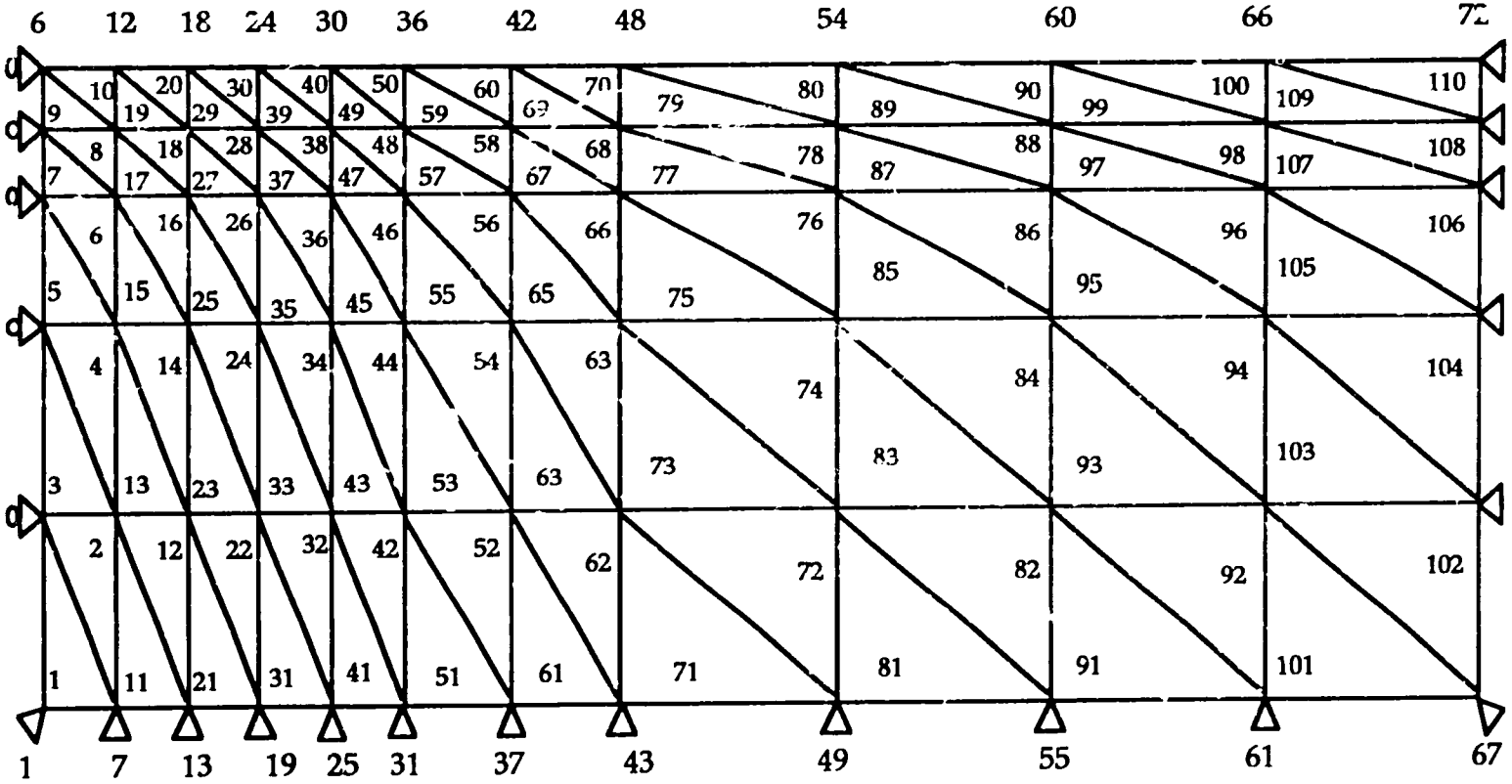

Figure A.1. Finite Element Discretization and Displacement Fixities

The in situ stresses need to be assigned in the case of plasticity analyses (Cam Clay, Modified Cam Clay, and Overstress Viscoplasticity models) and for each case analyzed, the available published site history has been adopted. The general lack of reliable and definitive data on these points meant that the conditions prevailing in the soil before the start of construction were considered to be entirely due to the self weight of the soil and the position of the water table.

The modeling of the top soil is also an important aspect in these analyses since the mechanical behavior of this layer influences deeper layers. Although the problems solved herein are well defined as to the strength of the surface soil, it is numerically tricky to analyse a soil deposit in the absence of a surface crust: when the calculated deformations at the surface become large, equilibrium in the deformed state suffers. On the other hand, for situations such as the case 5 where it is known that there is no surface crust to speak of, the use of an artificial crust does not seem to be adequate. To circumvent these opposing constraints, the load increments are applied very slowly in the beginning of the analysis (load increments of typically 0.5 to 1 % of the total load to be applied) to allow the "numerical" soil to strengthen sufficiently (through yielding) so that subsequent load increments do not cause the excessive expansion of the yield surface.

A.4. Deformation Patterns

The post-processing of the finite element analysis output is performed by a graphing software (Kaleidagraph™). Although this method suffers from a certain lack of practicality, it produces an acceptable representation of the output.

The program has numerous output options (stresses and deformations at integration points, reactions at restrained nodes, boundary conditions, in situ conditions, etc.) and even when the output is kept to a minimum, the data files that are produced are usually larger than what most text editors can handle (in the range of 900 - 1000 kbytes for a typical consolidation analysis). Under these circumstances, the interpretation of the output data becomes a complicated process whereby the editor of the VAX and various word processing, spreadsheet, and plotting applications on the Macintosh must be integrated.

The analyzed configuration of case 1.1 (see Chapter 10) is shown in Fig. A.2. It will be noted that the aspect ratio (width/depth) of the geometry is rendered faithfully and the points correspond to the vertex nodes in Fig. A.1.

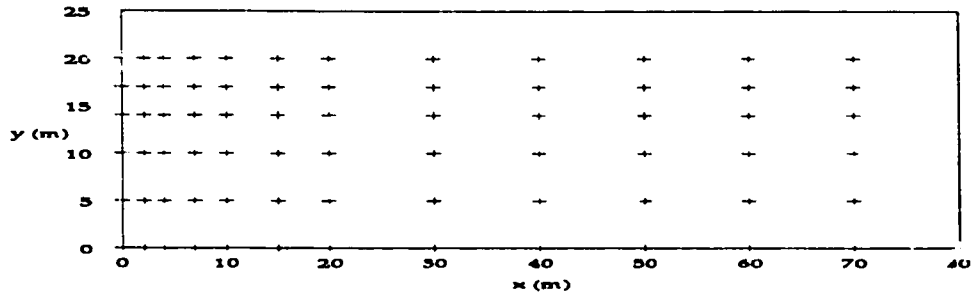

Figure A.2. Vertex nodes and their coordinates in the undeformed state for the analysis of case 1.1 (see Chapter 10)

For a clear representation of the deformations a magnification factor of 20 or 50 is used as indicated in figures A.3. through A.6. The deformation patterns indicate that the maximum horizontal displacements occur just inside the toe of the embankment (x=15 m.). The maximum settlement also occurs here and the heave of the soil beyond the loaded region is captured as well.

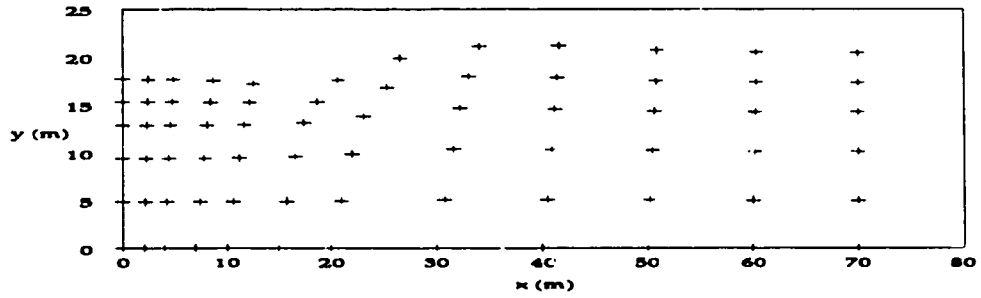

Figure A.3. Vertex nodes and their coordinates at 1 day (x and y displacements are magnified 50 times)

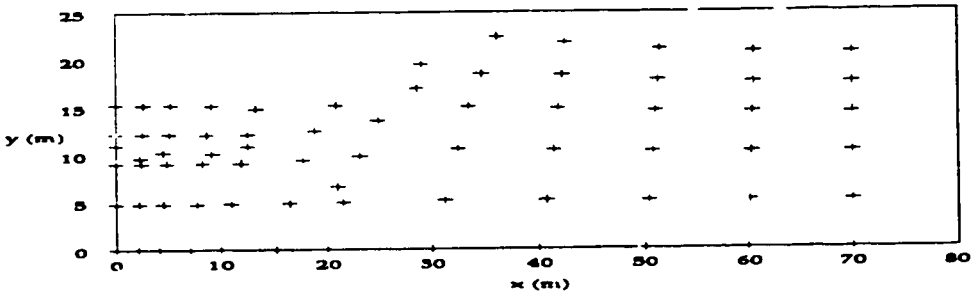

Figure A.4. Vertex nodes and their coordinates at 61 days (case 1.1); (x and y displacements are magnified 50 times)

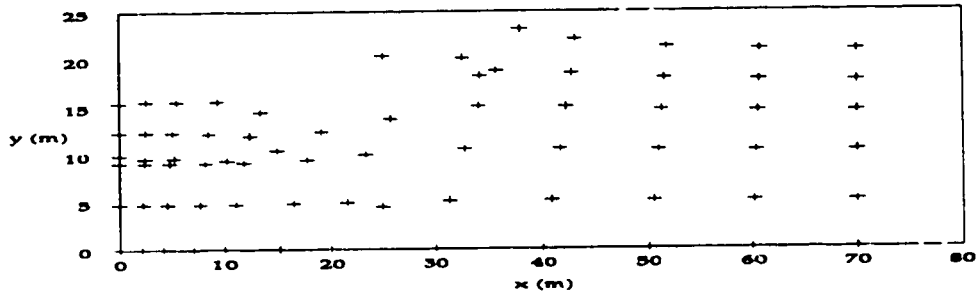

Figure A.5. Vertex nodes and their coordinates at 128 days (case 1.1); (x and y displacements are magnified 20 times)

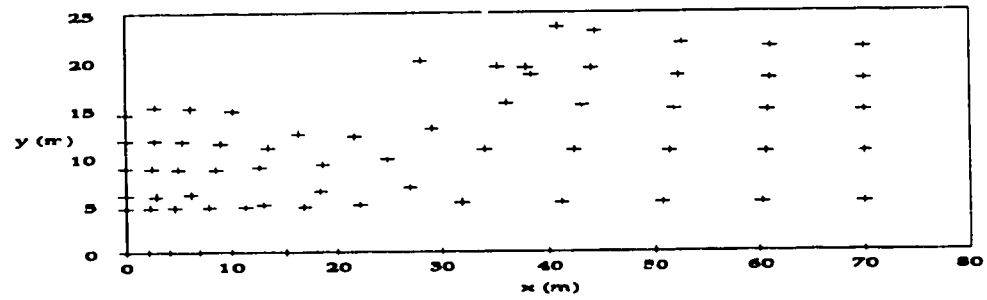

Figure A.6. Vertex nodes and their coordinates at 228 days (case 1.1); (x and y displacements are magnified 20 times)

The initial geometry of the landfill project described in case 5 is presented in Figure A.7. This is an axisymmetric analysis simulating a truck following a circular path whose center corresponds to the line (x=0) and the width of the loading is confined to the region bounded by ($10 \leq x \leq 15$).

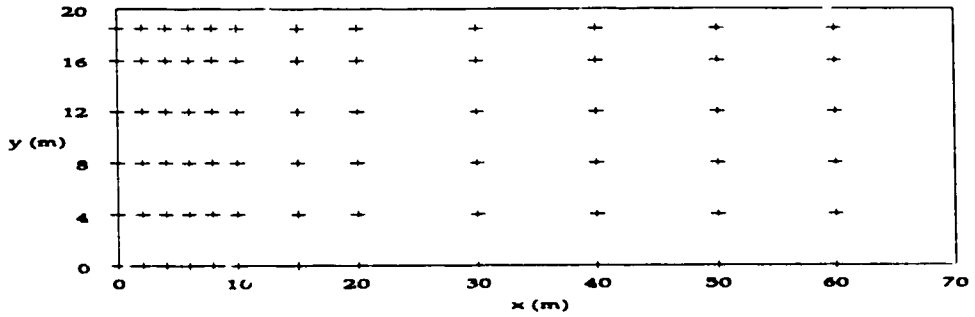

Figure A.7. Vertex nodes and their coordinates in the undeformed state for the analysis of case 5 (see Chapter 10)

The deformation fields for 10 days and 155 days after the start of the load are shown in Figures A.8 and A.9. It is seen that the overall pattern remains very similar and the differences are only in the magnitudes of the displacements as shown in Chapter 10. As previously stated, the deformations are confined to the immediate vicinity of the truck path (both in x and y directions). It is therefore likely that for practical purposes, the deformations caused by vibrational loads can be predicted from short term measurements through extrapolation.

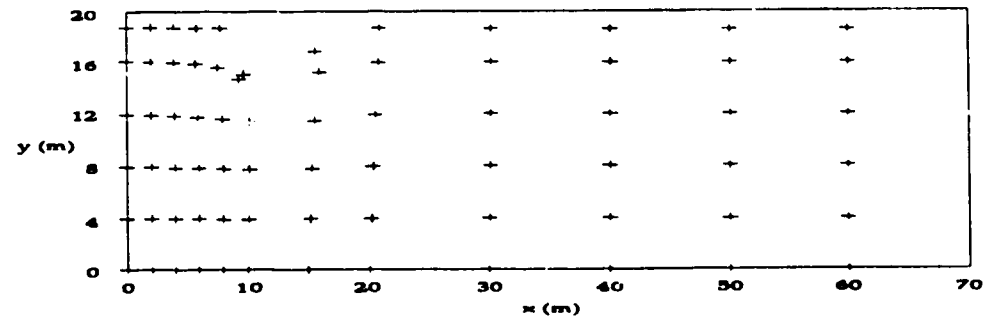

Figure A.8. Vertex nodes and their coordinates at 10 days (case 5); (x and y displacements are magnified 50 times)

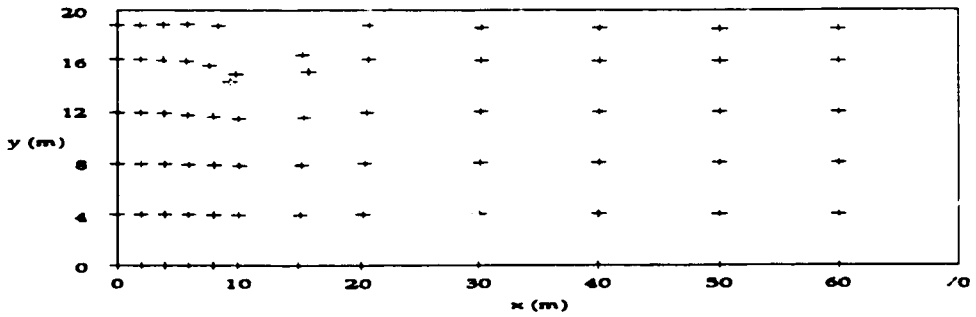

Figure A.9. Vertex nodes and their coordinates at 155 days (case 5); (x and y displacements are magnified 50 times)

A.5. Excess Pore Water Pressure Distribution Patterns

The excess pore pressures calculated during the construction of the embankment of case 1.1 are presented in Figures A.10. through A.13. The continuous increase in the excess pore pressure is readily observed although the construction proceeds in a stepwise fashion as was shown in Table 10.1.

The continuous increase of the excess pore pressure is likely to be an indication of the time that the clay mass needs to respond to external agents. As construction proceeds, excess pore pressures travel deeper into the layer even though consolidation has started. In this sense, the soil is behaving in a quasi-undrained manner. It is also important to note that while in true undrained behavior, the overburden stresses are transmitted instantaneously to the soil-water mass, the quasi-undrained behaviour observed here shows a time lag in the transfer of the overburden stresses to the soil-water mass. The said time lag acts in opposition to the ongoing consolidation process and creates the so called back-pressure effect.

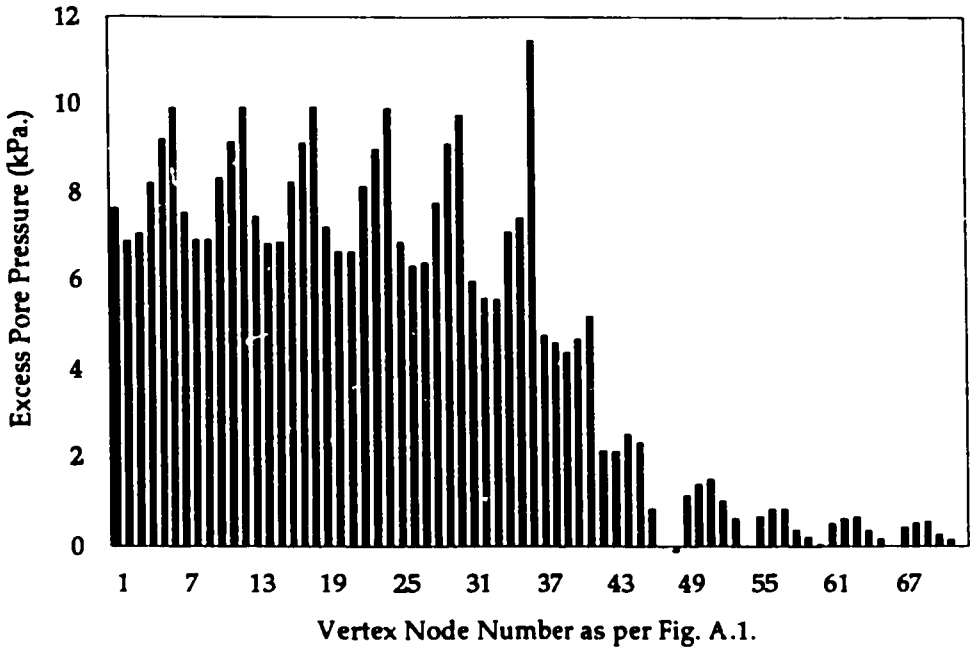

Figure A.10. Excess pore pressure at vertex nodes at 1 day for case 1.1 (please refer to Fig. A.1. for the location of nodes)

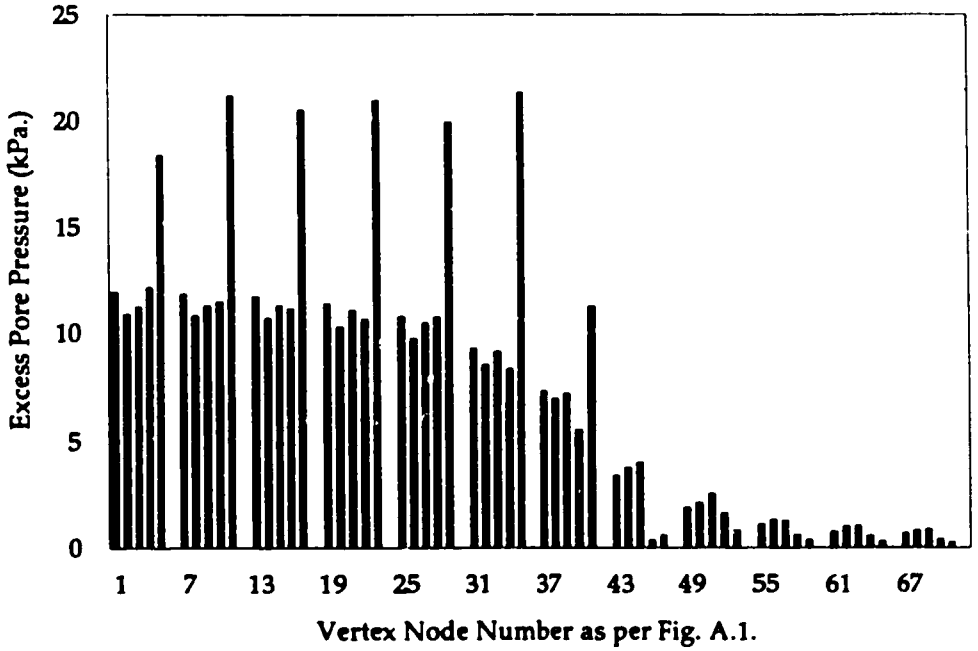

Figure A.11. Excess pore pressure at vertex nodes at 61 days for case 1.1 (please refer to Fig. A.1. for the location of nodes)

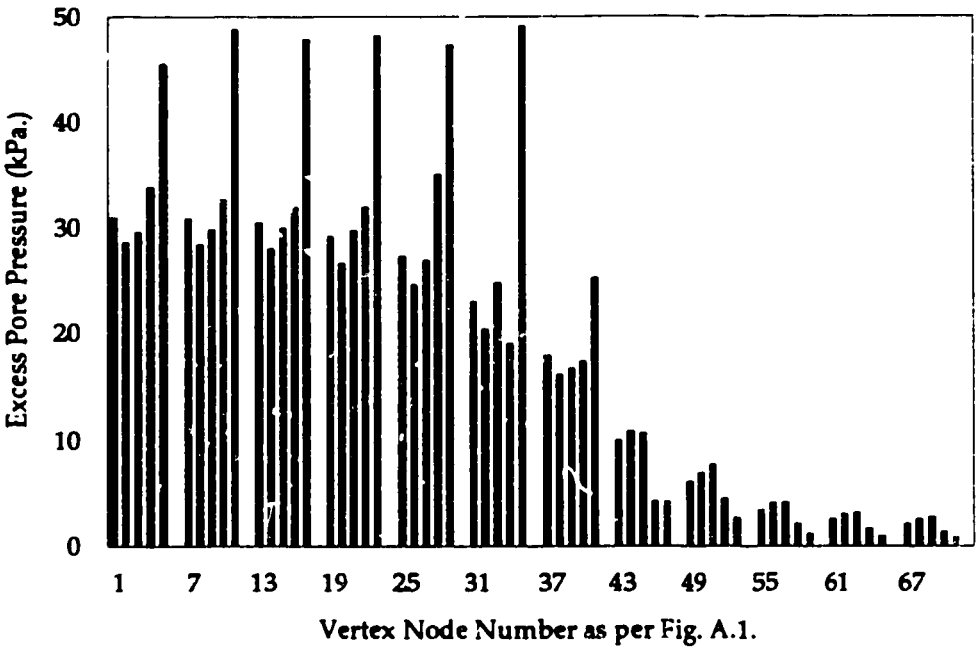

Figure A.12. Excess pore pressure at vertex nodes at 128 days for case 1.1 (please refer to Fig. A.1. for the location of nodes)

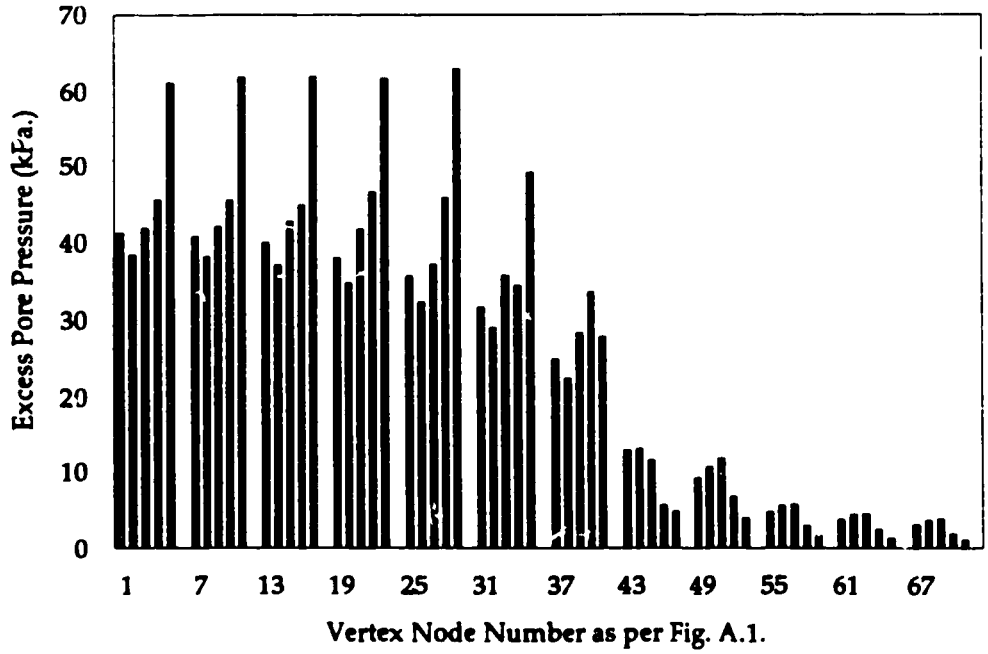

Figure A.13. Excess pore pressure at vertex nodes at 228 days for case 1.1 (please refer to Fig. A.1. for the location of nodes)

The excess pore pressures created by the vibrational truck load (case 5) are presented in Figures A.14 and A.15. The region of excess pore pressure is again seen to propagate through the clay mass with considerable retardation. Herein may lie the reason for the deformation patterns maintaining a similar pattern throughout the loading process. Once excess pore pressures are created and consolidation has begun, a displacement pattern emerges. If the back-pressure effect balances the consolidation however, there is no reason why there should be a change in the initial displacement pattern. The time lag that was mentioned earlier could then counteract the time required for pore pressure dissipation and a quasi-undrained equilibrium condition is possible. It is reasonable that any further increase in the magnitudes of the displacements are due to quasi-undrained creep of the soft clay. Further supporting evidence is the fact that the surface stresses due to traffic activity are generally too low to create significant excess pore pressure gradients to ensure consolidation.

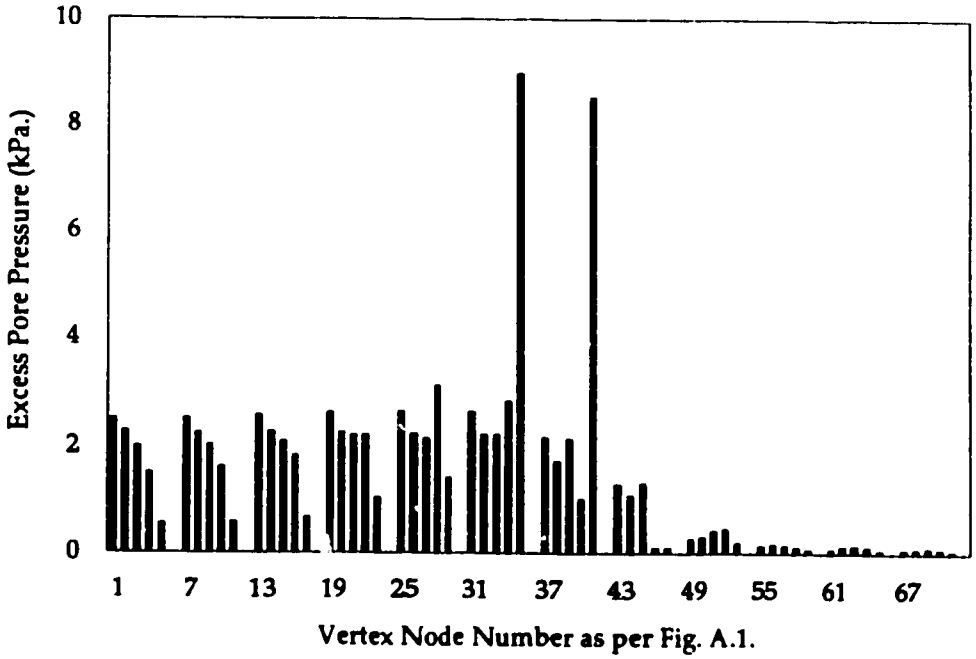

Figure A.14. Excess pore pressure at vertex nodes at 10 days for case 5 (please refer to Fig. A.1. for the location of nodes)

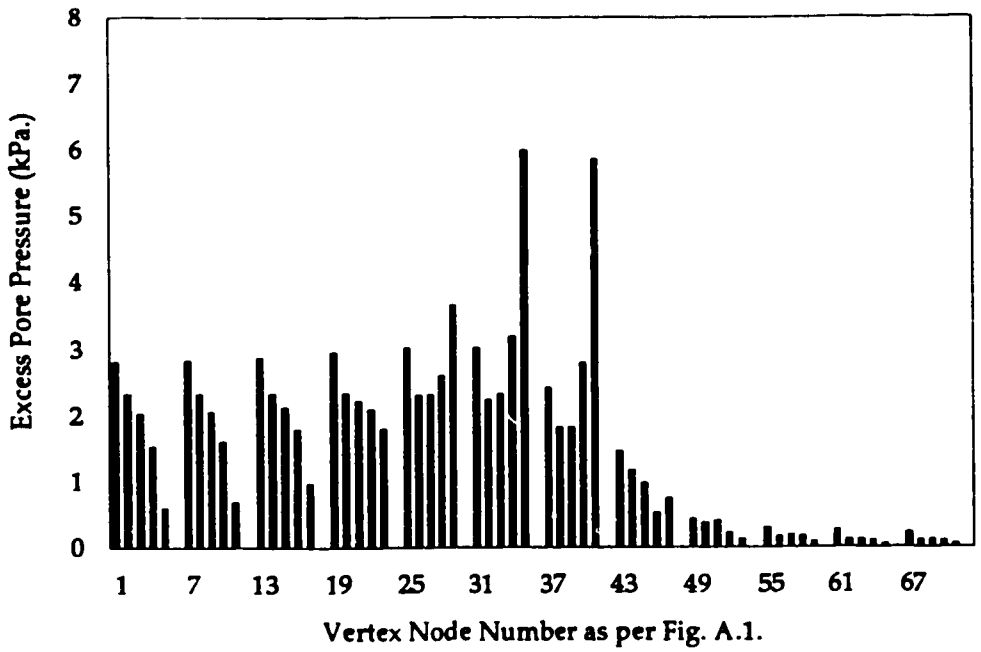

Figure A.15. Excess pore pressure at vertex nodes at 155 day for case 5 (please refer to Fig. A.1. for the location of nodes)

A.6. Simulation of Laboratory Tests

The program CRISPEX has also been used to simulate the vibrational slump tests described in Chapter 8. A cylindrical clay sample of diameter 50 mm. and height 50 mm. is subjected to a *vertical* vibration with the same characteristics as the ones used in the *horizontal* vibration slump tests. The use of vertical vibrations in the numerical analysis is purely based on the fact that the axial symmetry requirements had to be satisfied.

The finite element discretization of the clay sample is presented in Figure A.16. The elements are 15 noded cubic strain triangles with 30 degrees of freedom each. The total number of degrees of freedom in the problem is 90 and each analysis is carried out to simulate 10 minutes of vibration. The soil parameters are the same as in case 5 (see Table 10.7). These parameters have been previously obtained for a series of remoulded Osaka Clay samples, which happens to be the same soil used for the vibrational slump tests.

The sample is modeled to be free standing and is only acted upon by its own weight. The excitation is due to the up-and-down acceleration of the sample with a given frequency. The acceleration of the sample is directly controlled while the frequency is imposed by specifying the time between each acceleration reversal. The calculated results have been obtained for an acceleration of ±0.02g. (±0.2 gal.) and at frequencies of 0 Hz., 1 Hz., and 10 Hz.

Although the actual vibrational slump tests have been conducted without drainage control, it is reasonable to assume that during the test (70 minutes), a thin dry shell is likely to form on the exposed surfaces of the sample thus creating a barrier for the pore water. Furthermore, the accelerations imposed on the sample are not likely to create an important pressure gradient sufficient to expel the pore water. It is therefore assumed that the sample essentially behaves in a drained fashion.

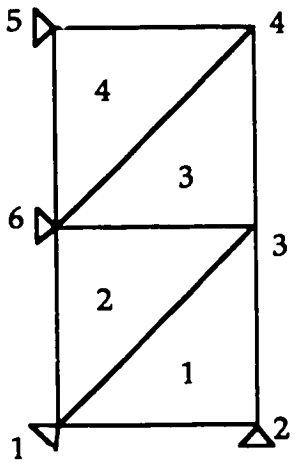

Figure A.16. Finite element discretization of the vibrational slump test sample

On the other hand, the assumption of undrained behaviour leads to the creation of relatively low magnitude pore pressures: at their highest, they are calculated to be 0.5% of the total stress within the sample. The clay sample having such low permeability, it is unlikely that the pore water can in fact travel towards the exposed surfaces. Indeed, in none of the 41 tests was there any observable water on the surface of the samples.

Under these conditions, a soil sample has been numerically put trough the vibrational slump test. The deformation of the specimen is graphically presented in Figures A.17 to A.20. The points represent the numbered vertex nodes in Figure A.16. and the displacements are magnified 500 times. The deformations obtained here can be compared with the tests presented in Chapter 8 where typical values are in the range of approximately half a millimeter.

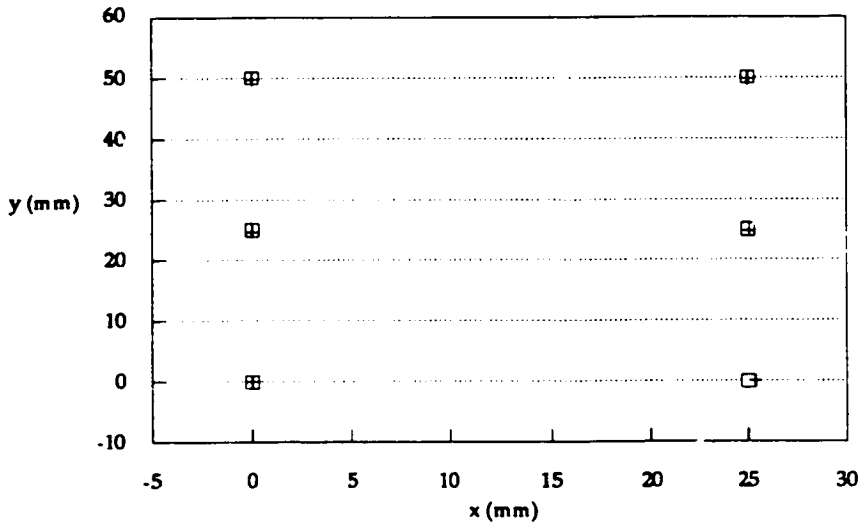

Figure A.17. Deformed shape of the slump test specimen after 5 minutes (squares denote original shape as per Fig. A.16.)

The results for the vibrational slump tests have been obtained using exactly the same material properties and thus reflect the change in the behaviour of the sample as a response to the external agents. This is a very important feature of the present analysis tool in that the varying response of the same material under different loading conditions are captured without adjusting the material parameters describing the material.

Figures A.18 and A.19 show that the deformation response of the sample is definitely influenced by the frequency content and in the range of the frequencies considered herein, a remarkable softening behaviour is observed (cf. Fig. A.17 for static slump at the end of 5 minutes).

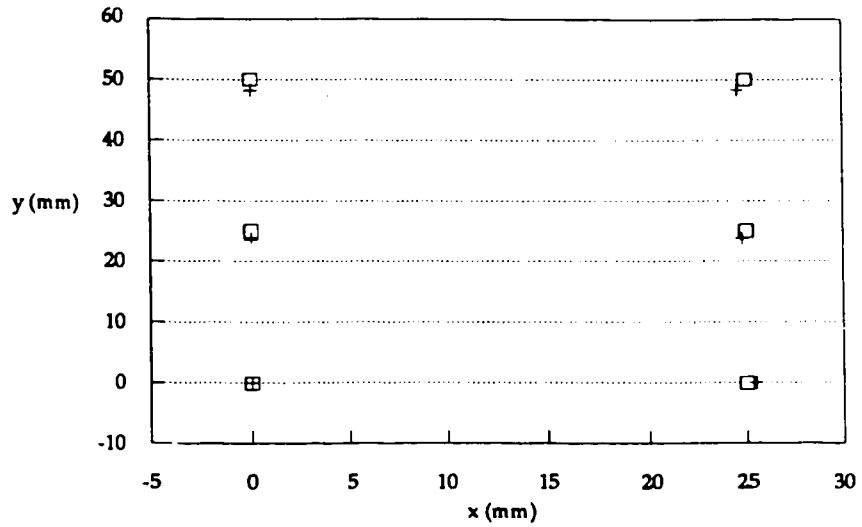

Figure A.18. Deformed shape of the slump test specimen under vertical vibration of 1 Hz., with 0.02 G acceleration for 5 minutes (squares denote original shape as per Fig. A.16.)

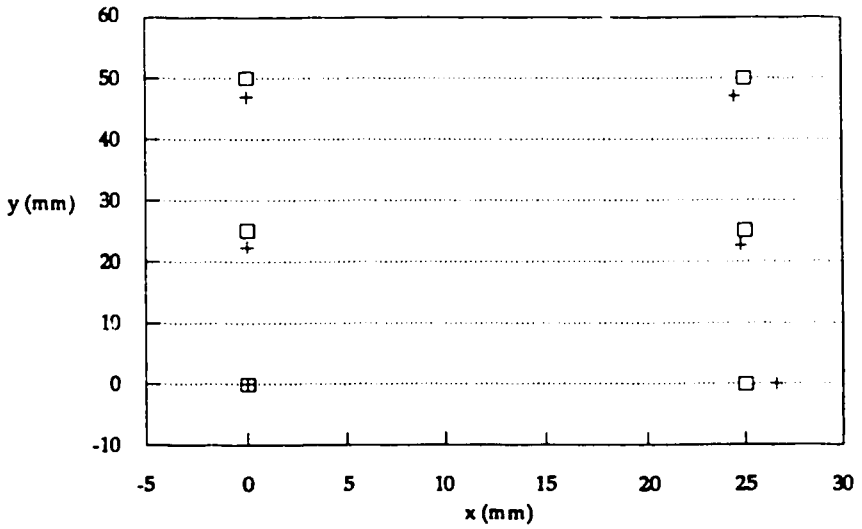

Figure A.19. Deformed shape of the slump test specimen under vertical vibration of 20 Hz., with 0.02 G acceleration for 5 minutes (squares denote original shape as per Fig. A.16.)

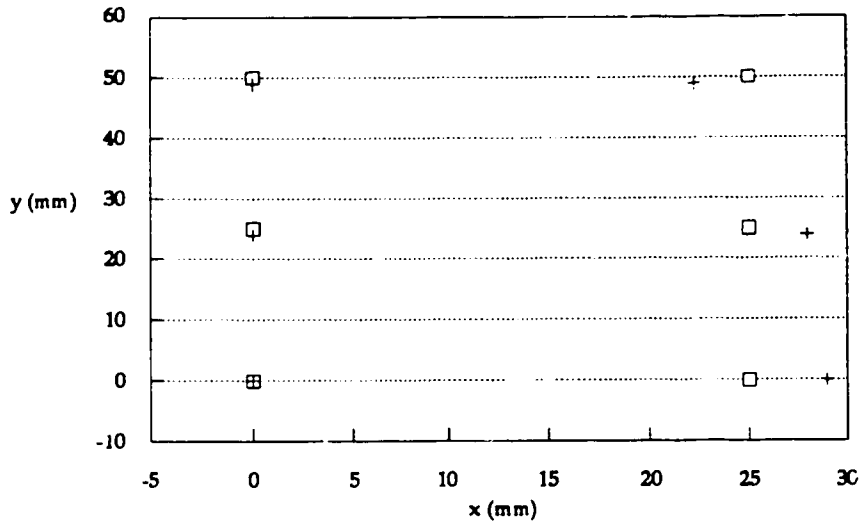

Figure A.20. Deformed shape of the slump test specimen after 70 minutes (squares denote original shape as per Fig. A.16.)

When the static slump test is carried to its full duration, the deformations shown in Figure A.20 are obtained. It is noted that the lateral bulging of the sample is quite considerable however a quantitative assessment of this result cannot be made at the present time since the slump test does not measure lateral deformations. As an indication of behaviour however, the calculated bulging is most likely due to the fact that the material has been assumed to be homogeneous, while during testing, the surface might have dried out, thus creating an envelope capable of reducing lateral deformations. Another point that must be kept in mind is that the calculations involve vertical vibrations while the measurements have been made for horizontal vibrations.